Alma Mater Studiorum – Università di Bologna

MOLECULAR MECHANISMS DRIVING ABERRANT ACTIVATION OF EGFR PATHWAY: IMPLICATIONS FOR CANCER TREATMENT

Presentata da: **Valerio Gelfo**

Coordinatore Dottorato

Prof.ssa Emanuela Ferracin

Supervisore

Prof. Andrea Ardizzoni

Co-Supervisore

Dott.ssa Mattia Lauriola

TABLE OF CONTENTS

1. Introduction

1.1. ERBB receptor family

ERBB receptor family, originally named because of their homology to the erythroblastoma viral gene product, v-erb, forms the subclass I of the receptor tyrosine kinase (RTK) superfamily composed by four members namely ErbB1 (EGFR or HER1) ErbB2 (HER2/neu), ErbB3 (HER3) and ErbB4 (HER4)[1] and 13 polypeptides extracellular ligands, with a conserved Epidermal Growth Factor (EGF)-like domain[2].

The ERBB family is expressed in several tissues but primarily include those of epithelial, mesenchymal and neuronal origin. Indeed, in normal cells the ERBB axes serves a crucial role in development, proliferation and organogenesis[3].

ERBB family members are structurally related and shares the same structural features. Each receptor is composed of three functional domains: an extracellular domain responsible for ligand-binding (domain I-IV), the α-helical transmembrane segment and the intracellular protein tyrosine kinase domain that also contains motifs and residues that mediate interactions with intracellular signalling molecules (Fig. 1A).

Under homeostatic conditions, receptor activation is tightly regulated by the availability of ligands. The family of ligands that bind ERBB receptors, is divided into three distinct groups. The first includes epidermal growth factor (EGF), transforming growth factor alpha (TGFα) and amphiregulin (AR), which all bind specifically to EGFR. The second group includes betacellulin (BTC), heparin-binding EGF (HB-EGF) and epiregulin (EPR), which bind to both EGFR and HER4. The third group is composed of the neuregulins (NRG1-4) and subdivided on their ability to bind both HER3 and HER4 (NRG1 and NRG2) or only HER4 (NRG3 and NRG4)[4].

Upon ligands binding all members of ERBB family are able to form heterodimers with other members, while only ERBB1 and ERBB4 can form active homodimers (Fig. 1B).

Two members of the family, ERBB2 and ERBB3, are non-autonomous. ERBB2 lacks the capacity to interact with a growth factor ligand[5], whereas the kinase activity of ERBB3 is defective [6]. Nevertheless, both ERBB2 and ERBB3 form heterodimeric complexes with the other members of ERBB receptor family and activate strong cellular signals.

Although ERBB2 does not bind to EGF-like ligands, it functions as the preferred heterodimeric partner of the other three ERBB members[7]. Furthermore, ERBB2-containing heterodimers are characterized by a higher affinity and broader specificity for various ligands than the other heterodimeric receptor complexes, owing to slow rates of growth-factor dissociations. Also, ERBB2-containing heterodimers undergo slow endocytosis, and they more frequently recycle back to the cell surface[8]. These features translate to potent mitogenic signals owing to the simultaneous and prolonged recruitment of multiple signalling pathways.

ERBB3, the kinase-defective receptor binds to four ligands, and forms three functional heterodimers. On the heterodimerization, the cytoplasmic domain of ERBB3 undergoes tyrosine phosphorylation and can recruit PI3K to six distinct sites and Shc to one site. Although there is no site for GRB2. This segregation enables ERBB3 to evade ligand-induced degradation[9].

ERBB4 shares recognition and signaling with ERBB1. They both bind to a large and distinct group of ligands i.e., betacellulin and the heparin-binding ligand, HB-EGF, as well as the two low-affinity ligands, epiregulin and epigen. Like ERBB1, ERBB4 recruits GRB2, Shc and STAT5. Although ERBB4 might not be able to directly recruit Cbl, and therefore downregulation of this receptor is slow, a proteolytic cleavage product of the cytoplasmic domain of ERBB4 translocate to the nucleus and might possess transcriptional activity[10]. Cellular response to ErbB pathways ranges from cell division and migration to adhesion, differentiation, and apoptosis. Output depends on cellular context, as well as specific ligand and ERBB dimers formation (Fig. 1B). For example, homodimeric receptor formation are less mitogenic and transforming than the corresponding heterodimeric combination; ErbB2 containing heterodimers are the most potent complex, i.e. ErbB2-ErbB3 heterodimer induces a potent mitogenic signal[11,12].
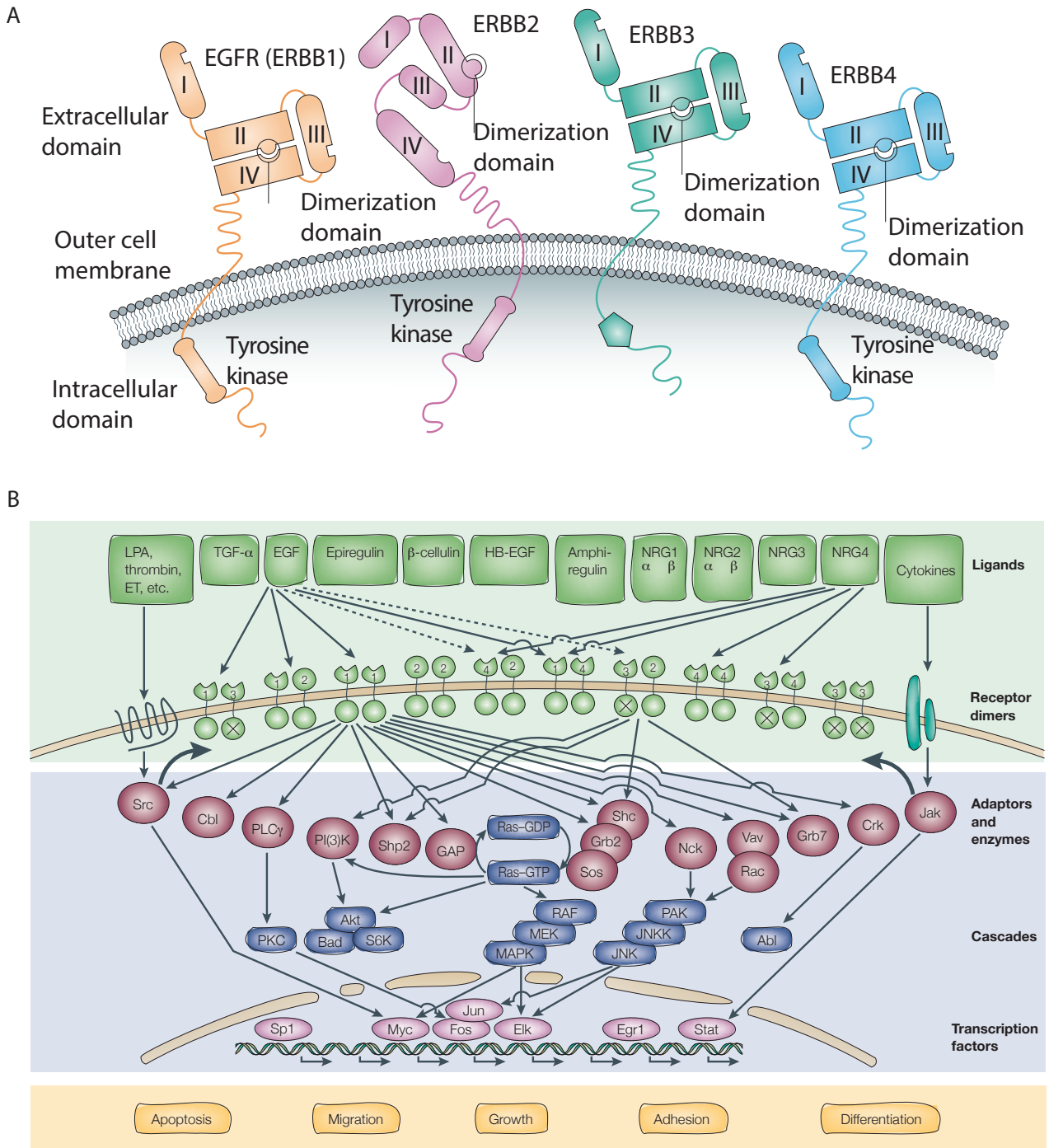
Figure 1: ErbB receptor family structure and signaling network. (**A**) Epidermal Growth factor receptor (EGFR), ERBB3 and ERBB4 exist in a tethered conformation in which the dimerization domain is not available to interact with partner ErbB moieties in the absence of ligand. There is no known ligand for ERBB2 and this receptor exists in an active extended conformation permanently available for dimerization. Adapted from J. Baselga, Nature review, 2000. (**B**) Ligands binding to ErbB receptor induces a conformational change in the folded structure exposing the dimerization domain. This step allows dimerization formation and functional activation of EGFR, ERBB3 and ERBB4. Through adaptor/enzymes molecules and transcription factors extracellular inputs are translated into several specific cellular responses such as apoptosis, migration, growth, adhesion and differentiation. Adapted from Y. Yarden, Nature Review 2001.

1.2. ERBB signalling network

For decades ErbB pathway has been studied as a linear pathway: binding of the ligand to the monomeric receptor promotes receptor dimerization and self-phosphorylation on tyrosine residues in the catalytic domain. The issue of signalling specificity, along with the existence of non-autonomous RTKs and the broad range of EGF-induced biological outcomes, motivated a paradigm shift a decade ago; the view of simple pathways connecting ERBB protein to enzymatic processes and biological outcomes has given way to a web of interconnected pipelines, called the EGFR/ERBB network [1]. In higher eukaryotes, this linear pathway has evolved into a richly interactive, multi-layered network conferring selective gains in terms of adaptation, tolerance to mutations and signal diversification [13].

From a system-biology view, several functional features of the ERBB network contribute to the robustness of the signalling, sharing traits with complex biological and engineered systems[14]. The robustness of biological system is an inherent system property, which enables normal performance despite external and internal perturbation[15]. Several attributes are shared by robust systems of eukaryotic and prokaryotic organisms, as well as by engineering systems, and they might collectively function as the framework that underlies robustness[14], namely network architecture, modularity, system controls, redundancy and buffering.

The network architecture is characterized by a layered structure, that interfaces with the input of multiple growth factors, functioning through eight potential receptors, hetero- or homodimers, activates common signalling cascades collectively defined as core process.

This core process results in the specific activation of transcription factors that lead to the selected cell fate, characterized of interconnected subnetwork that modify signals in a highly reproducible manner unlike, the diverse sources of input and different output, the core is conserved. The input layer displays remarkable redundancy. For example, betacellulin can bind to and activates both ERBB1 and ERBB4, whereas epiregulin binds to ERBB1, ERBB3 and ERBB4. The multiplicity of ERBB ligands feeds into the combinatorial nature of the ERBB network, in which homo- or heterodimeric receptors can be formed, thus establishing

a high level of complexity. Each ligand-driven receptor dimer possesses distinct functional properties in terms of binding affinity, endocytic routing and effector activation.

Modularity, with a hierarchical configuration is divided into quasi-autonomous sub-system. This configuration enables a system to locally contain inflicted damage and promote heritable phenotypic variation (evolvability).

The system control level of positive and negative feedbacks helps to maintain dynamic relationship between inputs and outputs, within defined limits. In this regards, positive-feedback loops enhance the amplitude and prolong the active state of signalling pathways to convey robustness in the face of variable inputs. In the case of ERBB ligand binding to the primary receptor is tuned by the identity of the secondary receptor. ERBB2 can be considered as an important positive regulator as it functions as preferred secondary receptor and ERBB2-containing heterodimers evade negative regulation[8]. Also Ras-MAPK pathway ERBB-mediated activation strongly induce the transcription of ERBB ligands including TGFa and HB-EGF[16]. A vast cellular effort is also invested for mechanisms of signal attenuation including post-translational modifications, compartmentalization, catalytic inactivation and steric hindrance. One of the most effective, irreversible process that robustly attenuates signalling, by targeting surface receptors, is receptor internalization coupled to degradation in lysosomes. Also, dephosphorylation is another mechanism of signal attenuation. For example, density-enhanced phosphates-1 (DEP1) dephosphorylate EGFR as well as other RTKs and protein tyrosine phosphatase-1B (PTPB1) which dephosphorylates RTKs in endosomes[17,18]. Newly synthetized attenuator defines the window of active signalling as their expression reach a peak after one hour. For example suppressor of cytokine signalling-5 (SOCS5) leads to a marked reduction in the levels of the receptor by promoting EGFR degradation, possibly via proteasome[19]. Two other newly synthetized attenuators, with a lower activation kinetics, are adaptor protein sprout (SPRY) and leucine-rich repeats and immunoglobulin-like domains-I (LRIG1) acting through Cbl, while mitogen-inducible gene-6 (MIG6) functions directly on the receptor[20–22].

Redundancy is a functional degeneracy of individual components or whole modules which are non-identical, offers different ways to generate an output in the face of severe perturbations, thereby increasing functional plasticity. The ERBB network displays redundancy at each layer of the network, at the input level as well as in the core of the network. For example, in the pathway that leads to activation of Raf1 by son of sevenless (SOS), ERBB1 can recruit SOS through either GRB2 or Shc, whereas GRB2 can associate with the receptor either directly or through Shc[23,24].

Buffering is a protective mechanism that enables damaged components to maintain (to some extent) proper functioning, i.e. HSP90 is the main chaperon that refold mutated or otherwise perturbed proteins enabling normal activity. By contrast to other ERBB receptors, ERBB2 is the most prominent kinase target of HSP90 that stabilize ERBB2 at the plasma membrane; notably HSP90 is able to restrain ERBB2 kinase activity limiting the capacity of ERBB2 to recruit ligand-bound receptor such as ERBB3 into the active heterodimer[25].
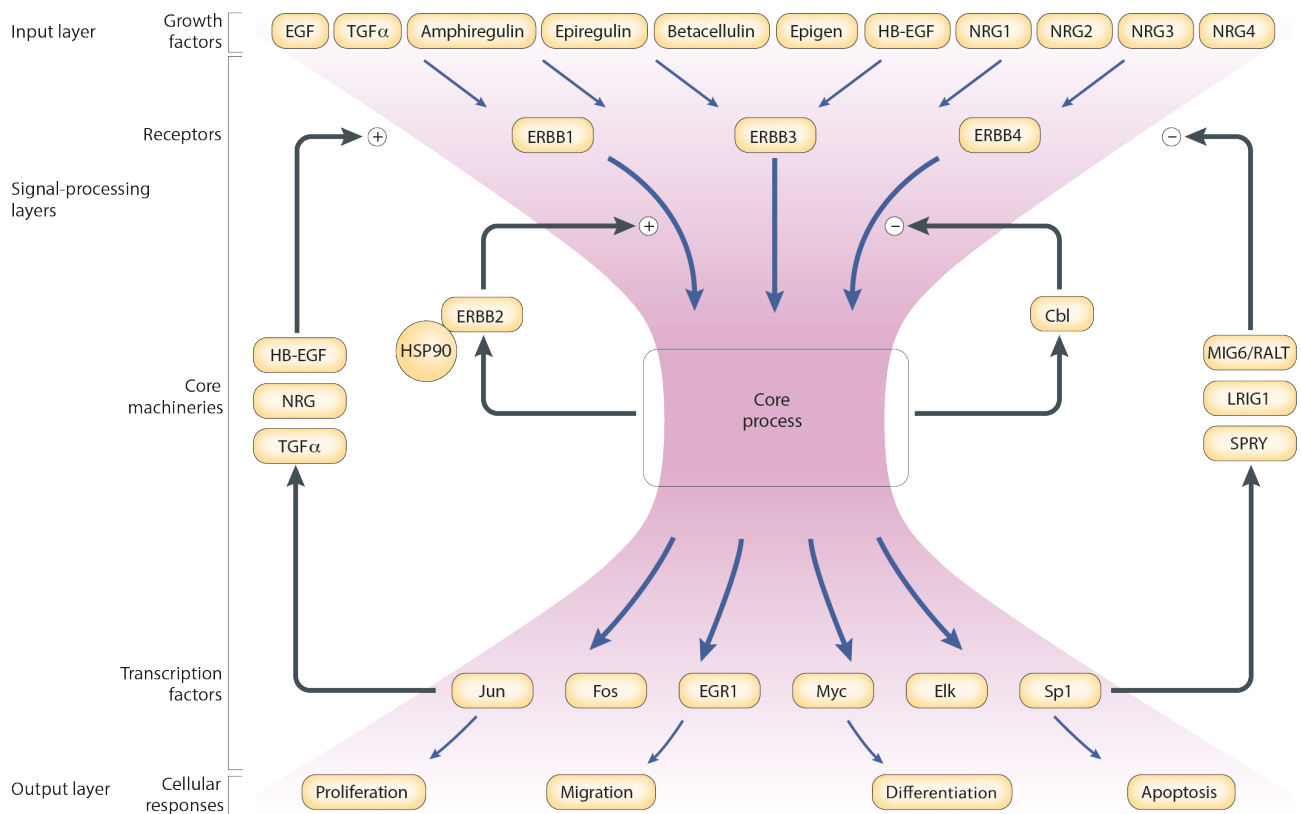
Figure 2: a system prospective of ERBB network. The ERBB network is characterized by three distinct layers namely the input, the signal-processing and the output layer. The Input layer comprising 13 growth factors that directly bind to three receptor ERBB1, ERBB3 and ERBB4. The signal processing layer composed by ERBB receptors (EGFR, ERBB3 and ERBB4) the core process and transcription factors. The output layer that gives rise to cellular responses (proliferation, migration, differentiation and apoptosis) through multiple transcription factors. Depending on the exact combination of transcription factors and the cellular context, the output of the network regulates cell behavior. Positive (ERBB2, HB-EGFR, neuregulins (NRG) and TGFa) and negative feedbacks (Cbl, MIG6, LRIG1 and SPRY) act for system control, while HSP90 functioning as chaperone enabling damaged component to maintain proper function (buffering), act as molecular switch that regulates heterodimer formation and catalytic function as well as protein stability. A. Citri and Y. Yarden. Nature review 2006.

1.3. EGFR pathway

The autonomous receptor ERBB1 binds to multiple ligands and forms homodimers, as well as three functional heterodimers.

Ligand binding to the leucine-rich repeats in domain I and III (due to the bivalent nature of the ligand) of the EGFR extracellular domain, triggers a conformational change in the receptor that exposes the dimerization loop (domain II) to other receptors on the cell surface. Exposure of domain II allows for homo or heterodimerization with other HERs family members activating EGFR kinase function (Fig. 3A).

Several tyrosine-based motifs recruit a number of signal transducers to the phosphorylated form of ERBB1, such as the adaptor proteins GRB2 and Shc, which are responsible for the

recruitment of Ras and activation of the mitogen-activated protein kinase (MAPK) cascades. The three primary signalling pathways activated by EGFR include, the RAS/RAF/MEK/ERK (ERK pathway), PI3K/AKT and JNK axes culminating in cell fate decisions. (Fig. 3B)

ERK pathway regulate entry into the cell cycle, thus cell proliferation accounted as a central element in many human tumours. After ligand binding and autophosphorylation, C-terminal phospho-tyrosine residues on EGFR act as binding site for the SH2-domain-containing protein GRB2. GRB2 recruits the guanine nucleotide exchange factor SOS via its SH3 domain, and promotes binding of GTP to Ras, a small G-protein responsible for activation of the MAPK cascade. Ras-GTP initiates this cascade by binding to and activating the RAF kinase (MAPKKK). Activated RAF in turn binds to and phosphorylates MEK (MAPKK), which then phosphorylates ERK1/2 (MAPK). Upon activation, ERK kinases can translocate to the nucleus and activate several other kinases including MNK1 and MNK2, MSK1 and MSK2, and RSK. MAPK can also phosphorylate several transcription factors including Elk-1, peroxisome-proliferator-activated receptor γ (PPARγ), signal transducer and activator of transcription 1 and 3 (STAT1 and STAT3), C-myc and AP-1. Activation of transcription factors leads to an increased transcription of genes involved in cellular proliferation, most notably cyclin D1[26].

PI3K/AKT pathway regulate cell survival. Activated RTKs can recruit PI3K to the cell membrane. PI3K phosphorylation of phosphatidylinositol-4,5-bisphosphate (PIP2) yields the second messenger phosphatidylinositol (3,4,5)-trisphosphate (PIP3). PIP3 serves as a membrane-docking site for the serine/threonine protein kinase AKT, which binds to PIP3 with high affinity through its pleckstrin homology (PH) domain. Once positioned on the plasma membrane, AKT is phosphorylated by two kinases, phosphoinositide dependent kinase 1 (PDK1) and the mammalian target of rapamycin complex 2 (mTORC2), leading to its full activation. Phosphorylated AKT regulates a variety of different substrates, influencing cell survival, proliferation and cellular metabolism[16].
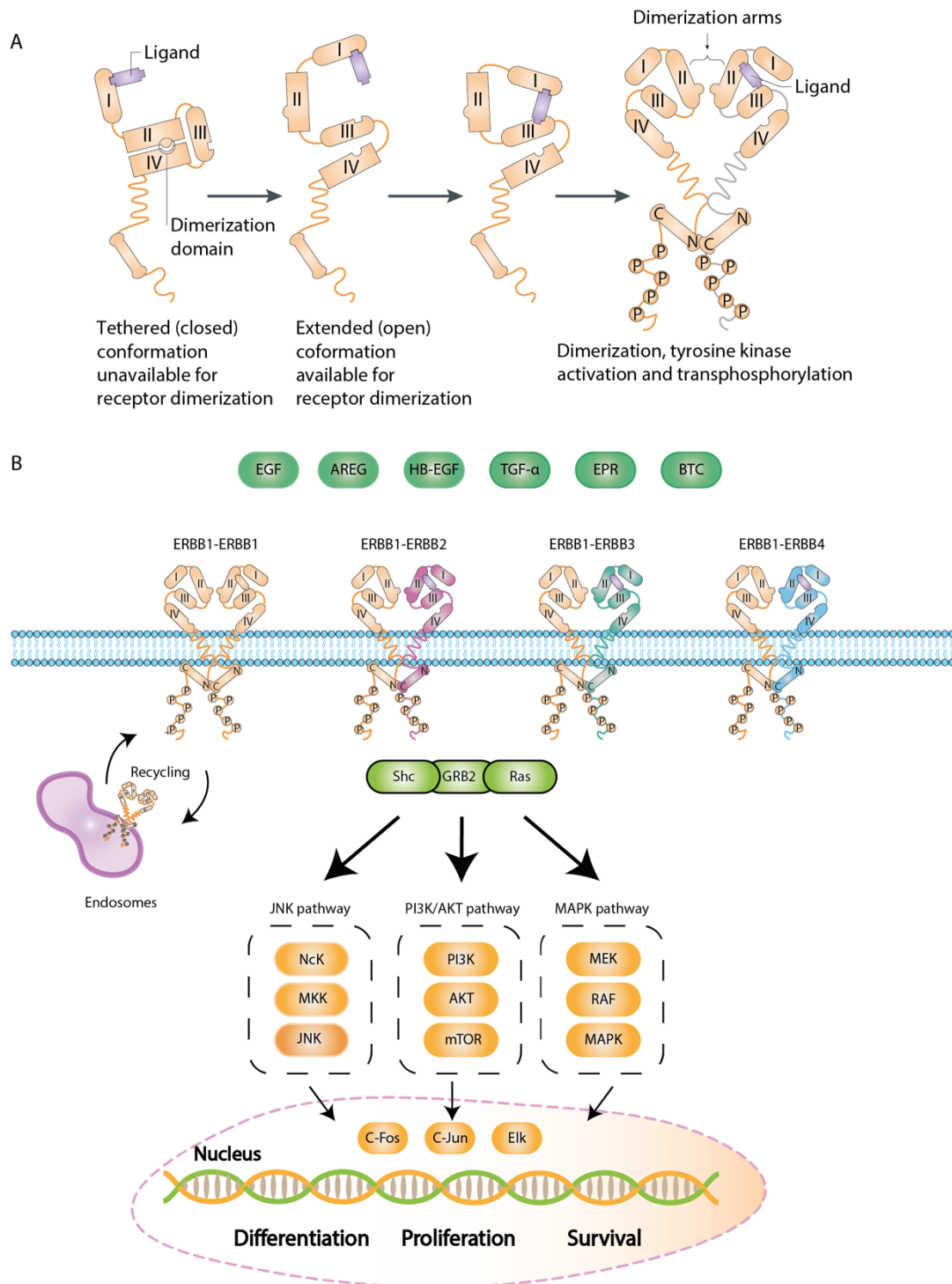
Figure 3: EGFR conformational change on ligand binding and signal pathway. (**A**) Ligand is able to contact domain I and III within the same receptor promoting substantial conformational changes in the extracellular region of EGFR which unmask the dimerization arm in domain II. Before ligand binding domain II is not exposed and EGFR is in a "tethered" state in which both ligand binding and dimerization domain are auto-inhibited. Ligand binding break the tethered conformation allowing domain II to interact with a second ligand bound receptor molecule. (**B**) Schematic representation of EGFR signal pathways. Six EGFR ligands namely EGF, AREG, HB-EGF, TGF-a, epiregulin (EPR) and betacellulin (BTC) bind the receptor and induce the formation of homo- (ERBB1-ERBB1) or ethero-(ERBB1-ERBB2, ERBB1-ERBB3 and ERBB1-ERBB4) dimers. Three main signal axes are activated (JNK, PI3K/AKT and MAPK pathway) leading to different cell fate: differentiation, proliferation and survival.

To dynamically control the amplitude, kinetics and frequency of output signals, the ERBB network evolved positive- and negative-feedback circuits contributing to maintain robustness.

Positive feedback loops enhance the amplitude and prolong the active state of signalling pathways to convey robustness in the face of variable inputs[27]. In the case of EGFR, the output following binding of the ligand to the receptor, is the identity of the secondary receptor and in this context ERBB2 can be considered as an important positive regulator functioning as the preferred secondary receptor and ERBB2-containing heterodimers evade negative regulation[28].

Another important mechanism of positive feedback is based on autocrine and paracrine loops in which EGF-like ligands, as well as angiogenic factors, are produced following receptor activation. For example ERBB-mediated activation of Ras-MAPK pathway strongly induces the transcription of multiple ERBB ligand, including TGFα and HB-EGF[29]. Similarly. Transactivation of ERBB1 by G-protein-coupled receptors occurs through the stimulation of surface proteinases, generating mature active HB-EGF[16].

On the other hand, negative feedback regulation plays a major role in restricting the activity of the EGFR, thus ensuring the generation of stable and reproducible signal output as, an excessive EGFR signalling might pose a serious oncogenic threat. Negative feedbacks can exert their function immediately (early loops) relying on pre-existing molecules comprising both protein translocations and post-translational modification. In addition, negative feedbacks can be driven by the synthesis of RNA and proteins (late loops).

One major early negative feedback loop is ligand-induced receptor endocytosis where ligand binding to ERBB1 receptors and their subsequent dimerization induces receptor internalization into endosomes. They reach a tubulovesicular sorting or early endosomes from where they can either recycle back to the plasma membrane, following the route of transferrin receptor, or progress toward the lysosome for degradation[30]. In the endosomes, auto-phosphorylation of EGFR enables it to recruit GRB2 and E3 ubiquitin ligase Cbl and undergo ubiquitylation followed by proteasome degradation. Although receptor endocytosis is a major negative feedback loop, the internalized receptors remain active

while *en route* for recycling or degradation[31] (Fig. 4A). Because activation-dependent internalization and degradation of EGFR crucially determine signalling duration this process is strictly regulated primarily by intercepting the stability and activity of Cbl or by reversing two essentials covalent modifications, ubiquitylation and phosphorylation. In contrast late loops, relying on newly induced RNAs and proteins, can be divided into three temporal phases: primary response, with immediate and delayed early genes (IEGs and DEGs) and secondary response genes (SRGs) (Fig. 4B). The IEGs have an initial wave of transcription up to 45 minutes from stimulation comprising a limited set of genes which have primarily positive activities. The group of DEGs are transcribed within 45-120 minutes from stimulus comprising both positively and negatively acting components. The SRGs >120 minutes confer stable phenotypes in a cell context-specific manner.

Figure 4: EGFR negative feedbacks. (**A**) detailed description of EGFR ligand-induced endocytosis and early regulatory negative feedback. Ligand-EGFR complex internalization can be either recycled or degraded in lysosomes (or muti-vescicular body). (**B**) Pink line shows immediately downregulated microRNA (ID-miRs) which allows the onset of immediate early genes (IEGs). Green line shows the time-frame of activation IEGs with a peak of transcription after 45 minutes. Blue line shows the wave of activation of delayed early gene (DEGs) with a peak of activation after 45-120 minutes while secondary response genes (SRGs) are depicted in yellow activated after 120 from stimulus.

1.4. Colorectal cancer

Aberrant expression or activity of the EGFR has been identified as an important biological factor in many human epithelial cancers including head and neck squamous cell carcinoma (HNSCC), non-small cell lung cancer (NSCLC), colorectal cancer (CRC), breast, pancreatic and brain cancer.

CRC represents the main oncologic disease of gastrointestinal tract with an incidence of 1.2 million cases per year. Nowadays, CRC is the second most common cancer among women, with 614,000 annual cases (9.2% of all female cancers) and the third most frequent male cancer, accounting 746,000 annual cases (10% of all male cancers) [32,33]. Despite mortality has declined progressively in the past decades [34], CRC is the second most frequent cause of cancer-related death, both in Europe and in the USA, with an overall 600,000 deceases worldwide [35]. At the time of diagnosis, 20-25% of patients have already developed metastases, while another 20-25% will evolve a metastatic disease afterwards [36].

The etiological factors and pathogenetic mechanisms underlying CRC development is complex and heterogeneous. Contributory agents and mechanisms in CRC include dietary and lifestyle factors along with inherited and somatic mutations. Indeed, among the most significant risk factors for CRC aside from elder age and male sex, factors such as family history of colorectal cancer, smoking, alcohol abuse, reduced physical activity and an enriched diet in unsaturated fats and red meat have been correlated to an increased risk of CRC occurrence [37].

CRC is traditionally divided in two types: the majority of 70-80% of cases are sporadic while around 20-30% of CRC are familial due to either uncommon or rare, high-risk syndromes such as lynch syndrome (LS), familial adenomatous polyposis (FAP) and a small subset caused by inflammatory bowel disease (IBD)[38]. Sporadic CRC that account for the most cases, is mainly characterized by genetic instability. Now, the main consensus is that two main molecular features are responsible for CRC development: chromosomal instability (CIN) and microsatellite instability (MSI). CIN, the canonical pathway, which account 80% of sporadic CRC follows the Fearon and Vogelstein model which correlates specific genetic events with evolving tissue morphology. According to this model defined multi-step path

starting from adenomas formation and ending with transition to malignancy and tumour progression occur, along with specific genetic alterations in tumour suppressors genes or oncogenes [39]. On the other hand MSI is characterized by a huge accumulation of mutations in microsatellite sequences, short sequences repeated in tandem throughout the genome and arise in a defective DNA mismatch repair (MMR) genes context[40].

CRC is a frequently lethal disease with heterogeneous outcomes, in terms of its clinical manifestations, molecular characteristics, sensitivity to treatments and prognosis. Nowadays, clinopathological characteristics of CRCs along with MSI status, RAS and BRAF mutations are used in the clinical setting as prognostic and therapeutic markers. However, patients groups defined by these molecular markers still differ remarkably in outcome and therapy response. Different approaches have been able to delineate certain CRC subtypes, based on combination of clinical and histopathological parameters, gene expression, epigenetic and single gene characterization.

Several molecular classifications based on the gene expression profile of the tumour exist. However, there are some differences between them, especially in terms of the number of proposed subtypes. The main molecular classifications that have been proposed for CRC are: colon cancer subtype (CCS) system[41], the colorectal assigner (CRCA) system[42], Colon cancer molecular subtype (CCMS) system[43], CRC intrinsic subtypes[44].

To resolve inconsistencies among the reported gene expression-based CRC classifications and facilitate clinical translation, it has been established a general framework that integrates and compare multiple strategies for disease stratification in gene expression-based sub-typing of CRC. Guinney et al.[45] showed marked interconnectivity between six independent classification systems coalescing into four Consensus Molecular Subtypes (CMS) with distinguishing features. These molecular subtypes differ in their genetic and epigenetic characteristics, expression of signal pathways, and clinical features (Table 1).

CSM1 represent 14% of CRC tumours characterized by MSI and strong immune infiltrate. Hypermutation is due to defective DNA mismatch repair with MSI (microsatellite instability) and MLH1 silencing and accordingly CpG island methylator phenotype (CIMP)-high with frequent BRAF mutations, while having a low number of somatic copy-number

alterations (SCNAs). Also, gene expression profiling furthermore revealed evidence of strong immune activation (immune response, PD-1 activation, NK cells, Th1 cell and cytotoxic T cell infiltration signatures) in CSM1, consistent with pathological descriptions of prominent tumour-infiltrating CD8+ cytotoxic T lymphocytes. Patients with the CSM1 subtypes had a very poor survival rate after relapse[46].

CSM2 (canonical, 37%) epithelial, with marked WNT and MYC signalling activation. CSM3: (metabolic 13%) epithelial and evident metabolic dysregulation. The CMS4 subtype (mesenchymal, 23 %) CRC showed increased expression of epithelial-mesenchymal transition (EMT genes and evidence of prominent transforming growth factor-β activation, with expression of genes implicated in complement-associated inflammation, matrix remodelling, stromal invasion and angiogenesis. Patients with the CMS4 subtype had a worse overall survival and worse relapse-free survival than patients of the other groups [45].

Table 1: Taxonomy of Colorectal cancer

CMS1 MSI immune	CMS2 Canonical	CMS3 Metabolic	CMS4 Mesenchimal
14%	37%	13%	23%
MSI, CIMP high, hypermutation	SCNA high	Mixed MSI status , SCNA low, CIMP low	SCNA high
BRAF mutations		KRAS mutations	
Immune infiltration and activation	WNT and MYC activation	Metabolic deregulation	Stromal infiltration, TGF- β activation, angiogenesis
Worse survival after relaps e			Worse relapse-free and overall survival

1.5. Colorectal cancer treatments

In spite of large-scale screening efforts CRC patients present advanced, metastatic disease. Metastatic CRC (mCRC) is considered incurable, remaining a significant cause of morbidity and mortality worldwide with an overall survival (OS) of 18 to 21 months[47]. Systemic chemotherapy in this setting has traditionally been based on fluorouracil, with the more recent introduction of other cytotoxic agents, irinotecan, oxaliplatin, and capecitabine[48].

As knowledge about cancer biology and genetics expands, new treatment targets have been discovered and drugs developed to affect tumours in more rational fashion than impacting all cells actively in the cell cycle.

What is emerged from molecular studies is that CRC is a tumour highly dependent on EGFR playing a critical role in CRC carcinogenesis. For this reason, over the last three decades EGFR targeting has been intensively pursued as treatment strategy for mCRC. In 2004 FDA approved cetuximab (CTX) for patients with EGFR-expressing mCRC refractory to irinotecan-based chemotherapy. CTX exhibited promising antitumor activity in clinical trials as either monotherapy on in combination with chemotherapy and/or radiation, particularly in the setting of mCRC[49]. CTX is a chimeric mouse/human IgG1 mAbs that binds to the extracellular domain III of EGFR. Several CTX mechanism of action have been described so far (Fig. 5).

In 2006 FDA approved panitumumab a fully humanized IgG2 antibody that binds with high affinity to the extracellular domain of EGFR. Panitumumab is used in combination with chemotherapy regimens for use in mCRC expressing EGFR, for patients who had progressed on or after initial therapy with similar mode of action to CTX[50].
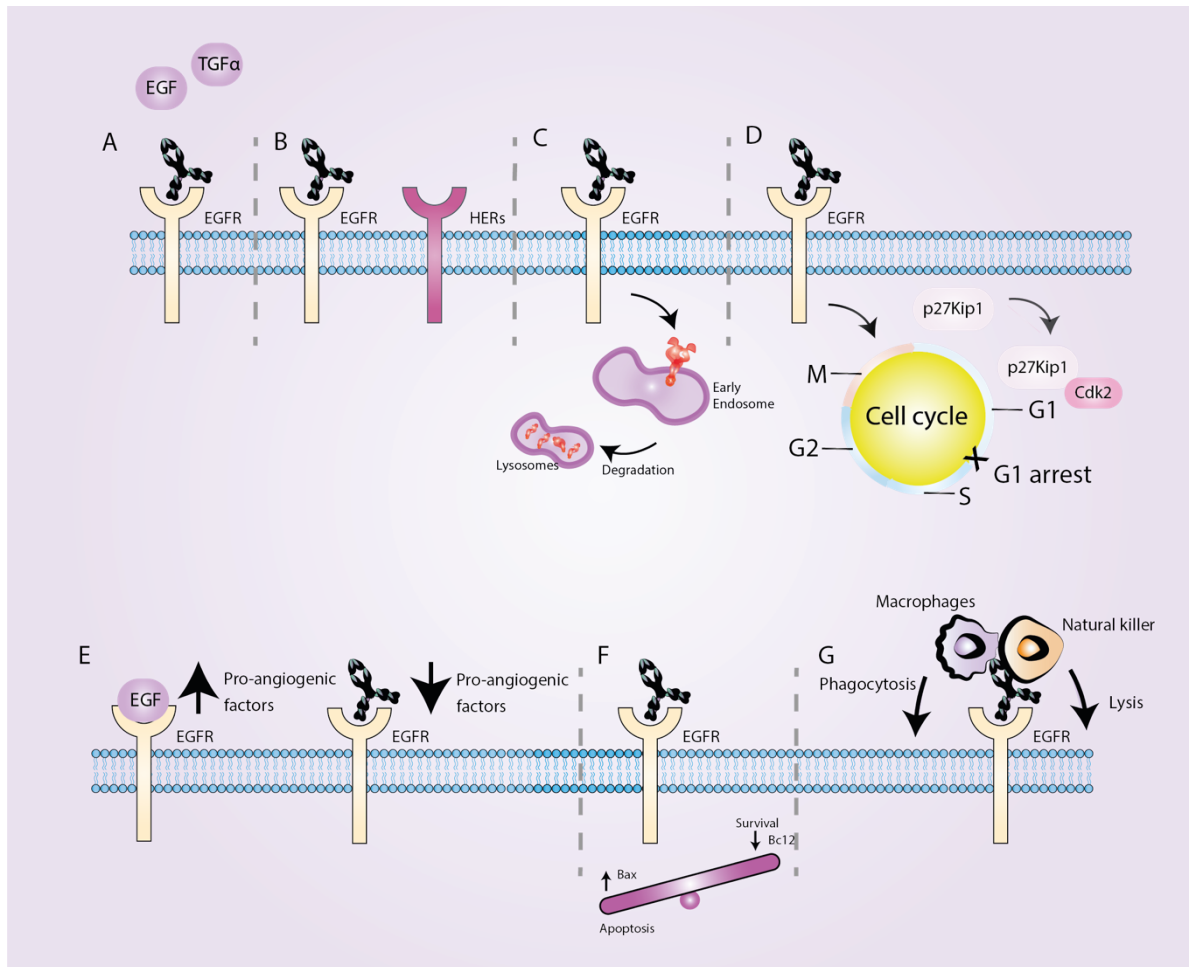
Figure 5: mechanisms of action of cetuximab. (**A, B**) CTX interaction with the extracellular domain of EGFR partially blocks the ligand-binding domain and sterically hinders the correct extended conformation of the dimerization arm on domain II. Thus, cetuximab prevents both ligand binding and the proper exposure of the EGFR dimerization domain, preventing dimerization with other HER family members. (**C**) Cetuximab promotes the internalization and degradation of EGFR, abrogating its downstream signalling cascades. (**D**) Cetuximab induces arrest in the G1 phase of the cell cycle by increasing levels of p27kip1. This in turn results in increase in the dimerization of p27Kip1Cdk2 complexes, which ultimately prevents exit from G1[125]. (**E**) Activation of other proapoptotic molecules has also been reported. Inhibition of angiogenesis, blockade of EGFR activation by cetuximab and by low-MW tyrosine kinase inhibitors results in a significant decrease in tumour-cell production of angiogenic growth factors such as basic fibroblast growth factor, vascular endothelial growth factor, and interleukin-8. The decrease in angiogenic growth factors, in turn, correlates with a significant decrease in micro vessel density and an increase in apoptotic endothelial cells in human tumour xenografts. (**F**) Potentiation of apoptosis, in some cases, G1 arrest is followed by apoptosis, this can be attributed to the induction of Bax and activation of caspase 8. (**G**) Antibody-dependent cellular cytotoxicity (ADCC) mediated by CTX. Recruitment of macrophages and natural-killer cells (NKs) have cytotoxic effect in tumour cells. The activation of these cells takes place following binding CD16aa (FcyRIIIa).

The role of angiogenesis and lymphangiogenesis in tumour growth is well established. Over-expression of vascular endothelial growth factor (VEGF) gene and high level of circulating VEGF protein are both associated with worse prognosis in CRC[51]. For this reason,

several agents to inhibit VEGF and the cognate receptors (VEGFR-1 and VEGFR-2) have been developed.

The first VEGF/VEGFR targeted drug was bevacizumab, a recombinant humanized IgG1 antibody against all isoforms of VEGF-A (Fig 6B), approved in 2004 by FDA, for use in combination with chemotherapy in the first-line treatment of mCRC. The VEGF is an integral component of the angiogenic switch. When secreted by tumour cells, VEGF binds to the extracellular domain of its receptor, VEGFR, stimulating a signalling cascade that results in activation of the angiogenic responses. When used alone, the efficacy of bevacizumab is limited; however, in combination with chemotherapy, it was originally shown to improve response rates (RRs), progression free survival (PFS) and overall survival (OS) in patients with mCRC[52].

In 2012 FDA approved aflibercept, a recombinant decoy VEGFR1 and VEGFR2 fusion protein, linked via the Fc segment of IgG1, with anti-angiogenic and vascular permeability activity targeting multiple members of the VEGF family, including VEGF-A, VEGF-B and placental growth factor 2 (PlGF-2) (Fig. 6C). Binding these growth factors prevents their activity at the VEGFR-1 and VEGFR-2 receptors, which are found on the surface of endothelial cells and leukocytes. Its activity results in regression of tumour vasculature, inhibition of new vascular growth and remodelling of surviving vasculature.

The first mAb against VEGFR was approved by FDA in 2015 namely ramucirumab, a recombinant, fully humanized IgG1 monoclonal antibody directed against the extracellular domain of the VEFGR2 (Fig. 6D). It binds to this receptor with high affinity, and thereby blocks ligand binding, primarily VEGF-A but others as well. It was approved in April 2015 for use in combination with FOLFIRI for the treatment of patients with mCRC who have progressed on or after prior therapy with bevacizumab, oxaliplatin, and a FP.
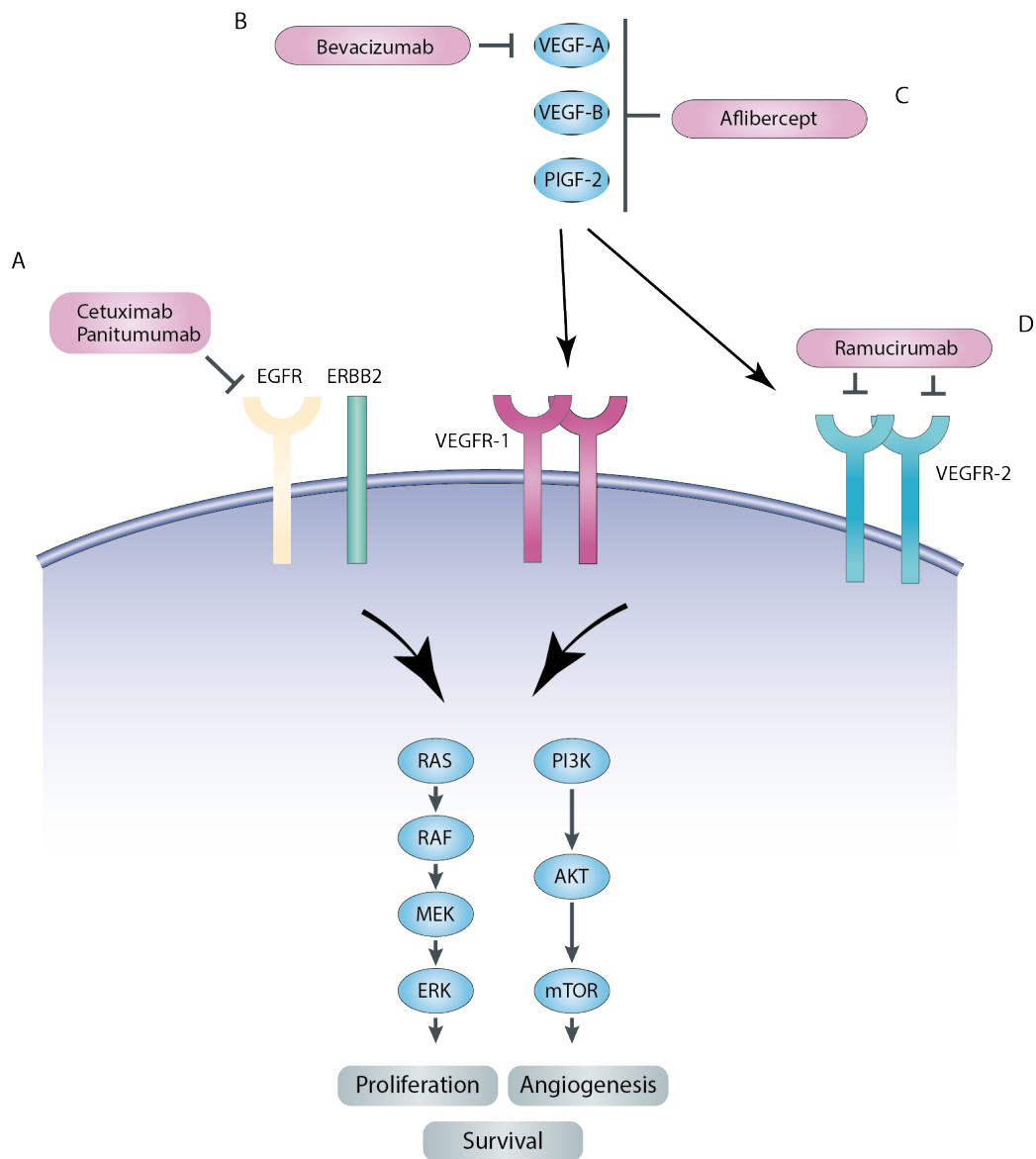
Figure 6: monoclonal antibodies treatment for mCRC. Epidermal growth factor receptor (EGFR) and vascular endothelial growth factor receptor (VEGFR) represent the main two targets intercepted in mCRC impairing proliferation, survival and angiogenesis. (**A**) Cetuximab (a chimeric mouse/human IgG1 antibody) and panitumumab (a fully humanized IgG2 antibody) were approved by FDA in 2005 and 2006 respectively for the treatment of mCRC. They both bind epidermal growth factor receptor (EGFR) blocking its function with different mechanism of action (see Fig. 5 for details). (**B**) Bevacizumab (a recombinant humanized IgG1 antibody) is able to intercept all isoforms of VEGF-A. (**C**) Aflibercept is a recombinant decoy (approved by FDA in 2012) comprising the extracellular domain of VEGFR1 and VEGFR2 and Fc (IgG1) segment able to sequester VEGFA/B and PIGF-2 from the microenvironment preventing the binding of the ligands to the cognate receptor. (**D**) Ramucirumab is the first mAb against VEGFR2 approved by FDA in 2015.

1.6. CTX resistance

In 1983 Sato et al. isolated four mouse hybridomas secreting immunoglobulin G (IgG) against EGFR on A431 cells. Three of the antibodies M225 IgG, M528 IgG and M579 IgG blocked 95% of EGF binding to human A431 cells as well as competing with each other in binding assay. Further, each antibody could immunoprecipitated EGFR from A431 cells, but not from three rodent cell lines tested, demonstrating their specificity. Finally, each antibody effectively blocked EGF-induced phosphorylation of the receptor resulting in reduced proliferative potential of the cell lines examined[53].

M225 resulted with higher anti-EGFR efficacy compared to M528 and M579. The clinical trial for M225 was successful but all patients developed human-anti-mouse antibodies. For this reason M225 was converted to a human:murine chimera C225 with an IgG1 Fc isotype. The Fc isotype was chosen for its potential to enhance the immune contribution to C225 antitumor effects. Subsequently C225 IgG1 was developed for clinical use namely cetuximab (Figure 7).
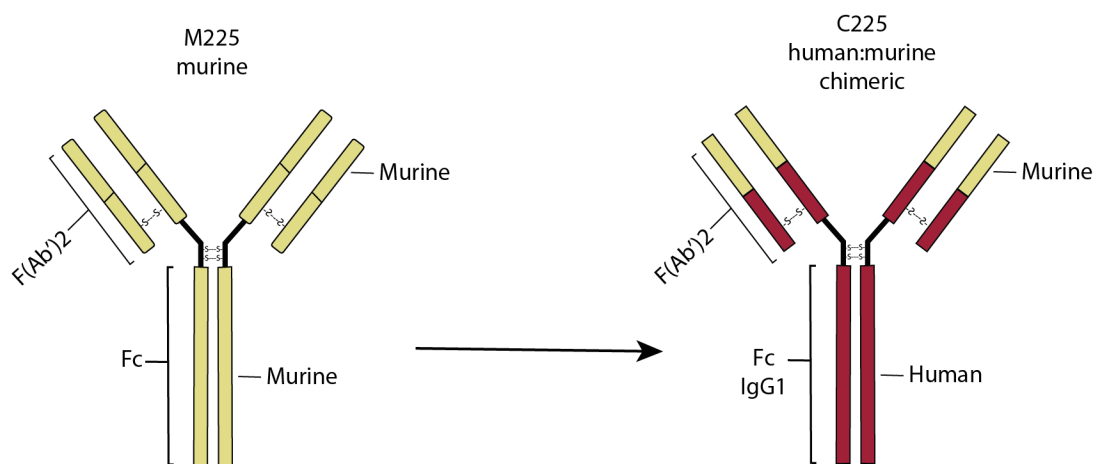

Figure 7: Schematic representation of Cetuximab development and subunits. On the left murine 225 (M225) hybridoma comprising the Fc subunit and the EGFR binding domain (F(Ab')2). Clinical trial on M225 mAb proved the development of human-anti-bouse antibodies. For this reason M225 was engineered to a human:murine chimera C225 (cetuximab) with an IgG1 Fc isotype (on the right in red) enhancing the antitumor efficacy by stimulating the host immune response against tumor. Cetuximab is currently utilized in the clinic as monotherapy or in combination with chemotherapy for the treatment of mCRC patients.

From early studies conducted in heavily pretreated chemotherapy-refractory patients and also in chemotherapy-naïve patients with mCRC, became clear that only 10% to 20% of

patients clinically benefited from anti-EGFR mAbs. These evidences triggered a flourish of studies on the molecular mechanisms of resistance to cetuximab. Resistance to CTX was associated to alteration of the target itself, bypass mechanisms, upregulation and activation of downstream effectors, or cross-talk between associated pathways which activate complementary cell survival and growth pathways[54]. Firstly, what emerged is that the expression level of EGFR was not correlated with clinical response to cetuximab and panitumumab[55]. These finding lead to subsequent investigations to the mutational status of EGFR immediate intracellular molecules, as molecular event associated with resistance to CTX[56] namely KRAS, NRAS BRAF and PIKCA. Since then, a rapidly accumulating body of knowledge has indicated that resistance to EGFR blockade in mCRC is related to constitutive activation of signaling pathways downstream EGFR. Initial retrospective analyses led to the breakthrough finding that, patients with CRC carrying activating KRAS mutation do not benefit from cetuximab therapy[57]. KRAS mutation have since emerged as the major negative predictor of efficacy in patients receiving CTX, unequivocally confirmed by three large, randomized, phase III cetuximab clinical trials, OPUS, CRYSTAL and NCIC-CTG, monotherapy study conducted in relapsed/refractory patients or those with contraindications to chemotherapy[58]. Given these results, European health authorities and FDA has restricted the use of CTX to patients with wild-type KRAS mCRC only. Mutation in KRAS led to continuous activation of the downstream ERK signaling, regardless of whether the EGFR is pharmacologically inactivated.

Although the presence of RAS mutations accounts around 50% to 60% of patients with mCRC refractory to EGFR blockade, molecular alteration in additional nodes of the EGFR signaling network also seem to be clinically relevant. For example, mutations in BRAF have been recently shown to impair responsiveness to cetuximab in patients with mCRC. In a cohort of 132 patients none of the patients responsive to CTX displayed BRAF mutation while 11 of 79 non-responder carried BRAF V600E allele[59]. Of note KRAS and BRAF are known to be mutually exclusive in CRC.

In addition to KRAS and BRAF, EGFR activate PI3K signaling pathway. From the overall analysis of the published works, it seems that PIK3CA mutations along with the loss of

PTEN are in fact associated with the resistance[60]. Importantly, although KRAS and BRAF seem to be mutually exclusive, PI3KCA mutation and loss of PTEN can coexist with KRAS/BRAF mutations. Furthermore, it has shown that PI3KCA mutations located in the exon 9 and 20 hotspots exert different biochemical and oncogenic properties and are differently activated by KRAS. Thus, considering the relative low frequencies, that can co-occur with KRAS and BRAF, and the different oncogenic properties of the different PI3KCA mutations it will be necessary to analyze large cohorts of patients for definitive conclusion. It is likely that PI3KCA and PTEN status will be useful to further optimize the criteria for eligible patients however these two marker are not yet ready to be used in the clinic[61].

Recently data indicate that when expression of PTEN and mutations of KRAS, BRAF and PI3KCA are concomitantly assessed up to 70% of mCRC unlikely to respond to anti-EGFR therapies can be identified[62] namely all-RAS wild-type.

Clinical data indicate that even the best response obtained in KRAS/BRAF wild-type tumors are transient, and even in the best cases, they do not last for longer that 12 to 18 months[63]. Little is known why the response is temporary and, tumors after a massive initial reduction rapidly begin to regrow and concomitantly became refractory to further anti-EGFR treatment.

Genetic alterations in the tyrosine kinase receptors other than EGFR can be accounted as mechanism of resistance, providing an alternate pathway of survival and/or proliferation. Genetic aberration of the tyrosine kinases ERBB2 and MET have been shown to bypass EGFR signaling and activate the MEK-ERK cascade. ERBB2 gene amplification was found in a small fraction of RAS and BRAF wild-type mCRC patient-derived xenograft unresponsive to CTX also, activation of ERBB2 signaling, dependent of either gene amplification or overproduction of the ERBB3 ligand heregulin was present in a subset of patients with mCRC exhibiting *de novo* resistance to CTX[28,64]. Another tyrosine kinase receptor, MET is amplified in a small fraction of RAS and BRAF wild-type mCRC patient-derived xenografts unresponsive to CTX[65]. Therefore, these pathways may offer primary escape mechanisms allowing tumors to circumvent one pathway that has been pharmacologically blocked.

Non-genetic mechanisms could also play a role in resistance to EGFR blockade. Notably, in biopsies from patients who relapsed upon CTX therapy only a fraction of cells carry RAS mutations, suggesting that wild-type cells can also survive the treatments[66]. This finding suggests that non-genetic mechanisms could also play a role in driving acquired resistance to EGFR blockade. For example, recent data reported that wild-type cells can survive in the presence of CTX when in company with their resistance derivatives. Notably, it was found that cells bearing acquired RAS mutations over-secrete the EGFR ligands TGFα and amphiregulin which protect the surrounding wild type-cells[67].

Autocrine/paracrine loops and dependency on alternative pathways, that confer survival and/or proliferation advantages is an emerging field that could potentially explain the subsets of patients with *de novo* unknown resistance. For example, a study conducted with a cohort of 150 colorectal cancer xenopatients, associated poor response to CTX with increased abundance of a set of inflammatory cytokines, including IL-1α, IL-1β and IL-8 [68]. Moreover, has been reported that IL-1 receptor 1 (IL-1R1) expression predicts disease relapse free survival in a cohort of 1700 colorectal cancer patients, and it appears intriguingly associated to the CMS1, thus suggesting the employment of immunotherapy to this subtype of patients [69].

1.7. IL-1 in solid tumours

During the last two decades inflammation has been accounted as a crucial feature of the malignant phenotype associated with 25% of all human cancers[70]. A causal relation between inflammation and cancer has been proposed by Virchow in 1863, who hypothesized that malignant neoplasms arise within a region of chronic inflammation causing tissue injuries and increased cell growth[71].

Interleukin-1 (IL-1), in this context has been proved to play a pivotal role in cancer development, showing to be up-regulated in several type of tumours of epithelial origin, including breast, colon, head and neck, lung, pancreas and melanomas[72].

In addition, patients with high levels of IL-1 have generally bad prognosis [73,74]. IL-1 can be directly produced by cancer cells or it can "educate" cells, within the tumour microenvironment, to do so [75].

For example, Hong et al. shown that intercepting IL-1α employing a MABp1a true human mAb, a cohort of 54 patients refractory to treatment displayed a disease control in 18 different tumour types and, its efficacy was further confirmed in 2017, in a randomized, double-blinded, placebo-controlled, phase 3 clinical trial in a cohort of 333 advanced colorectal cancer patients[76]. In support to these findings, employing Canakinumab (an anti-IL-1β mAb) significantly reduce the incident of lung cancer in a cohort of 10.061 patients[77].

More recently, Kaplanov et al. (2019) proved that a combined neutralization of IL-1β and PD-1 was responsible for an astonishing abrogation of tumour development in mammary carcinoma murine model[78] and tumour-derived IL-1β is critical for shaping tumor microenvironment (TME) of pancreatic ductal adenocarcinoma (PDA) promoting immunosuppression cell populations in pancreatic cancer[79]. As a consequence, a number of clinical trials testing the efficacy of anti-IL1 therapy in cancer are currently ongoing (Table 2).

Table 2: ongoing (August 2020) clinical trial testing anti-IL-1 drugs, alone or in combination with chemotherapy, in cancer therapy. Gelfo et al. Int. J. Mol. Sci., 2020.

Therapy	Target	Tumor Type	Recruitment Status	Development status	ClinicalTrial.gov Identifier	Sponsor	Start Date	Estimated Completion Date
Anakinra + Everolimus	IL-1 Ra + anti mTOR	Neoplasm	Active, not Recruiting	Phase 1	NCT01624766	M.D. Anderson Cancer Center	June, 2012	June, 2020
Anakinra + Chemo	IL-1 Ra + anti mTOR	Pancreatic Adenocarcinoma	Active, not Recruiting	Early phase 1	NCT02550327	Baylor Research Institute	January, 2016	August, 2023
Anakinra + JCARH125	IL-1 Ra + CAR T-cells	Multiple Myeloma	Recruiting	Phase 2	NCT03430011	Juno Therapeutics	March, 2023	March, 2023
Anakinra	IL-1 Ra	Multiple Myeloma	Active, not Recruiting	Phase 2	NCT03233776	Radboud University	May, 2019	June, 2020
Anakinra	IL-1 Ra	Multiple Myeloma	Recruiting	Phase 2	NCT04099901	Radboud University	October, 2020	October, 2022
Anakinra + Axicabtagene Ciloleucel	IL-1 Ra + CAR T-cells	Neoplasm, Large B-Cell Lymphoma	Not yet recuiting	Phase 1,2	NCT04432506	M.D. Anderson Cancer Center	July, 2020	January, 2025
Anakinra + Axicabtagene Ciloleucel	IL-1 Ra + CAR T-cells	B-Cell Non-Hodgkin Lymphoma	Not yet recuiting	Phase 2	NCT04359784	Fred Hutchinson Cancer Research Center	August, 2020	December, 2021
Anakinra + Axicabtagene Ciloleucel	IL-1 Ra + CAR T-cells	Non-Hodgkin Lymphoma	Not yet recuiting	Phase 2	NCT04150913	Marcela V. Maus, M.D.;Ph.D.	July, 2020	November, 2024
Anakinra	IL-1 Ra	B-Cell Lymphoma and Non-Hodgkin Lymphoma	Recruiting	Phase 2	NCT04148430	Memorial Sloan Kettering Cancer Center	October, 2019	October, 2022
Anakinra + Axicabtagene Ciloleucel	IL-1 Ra + CAR T-cells	Large B-Cell Lymphoma	Recruiting	Phase 2	NCT04205838	Jonsson Comprehensive Cancer Center	March, 2020	December, 2022
Canakinumab	mAb anti IL-1 β	Non-small Cell Lung Cancer	Recruiting	Phase 3	NCT03447769	Novartis Pharmaceuticals	March, 2018	January, 2027
Canakinumab + Spartalizumab + LAG525	mAb anti IL-1 β + mAb anti PD-1 + mAb anti LAG-3	Triple Negative Breast Cancer	Recruiting	Phase 1	NCT03742349	Novartis Pharmaceuticals	January, 2019	January, 2022
Anakinra +/− Pembrolizumab	mAb anti IL-1 β +/− mAb anti PDL-1	Non-small Cell Lung Cancer	Recruiting	Phase 2	NCT03968419	Novartis Pharmaceuticals	November, 2019	January, 2022
Anakinra + Pembrolizumab + Chemo	mAb anti IL-1 β +/− mAb anti PDL-1	Non-small Cell Lung Cancer	Active, not Recruiting	Phase 3	NCT03631199	Novartis Pharmaceuticals	December, 2018	September, 2022
Canakinumab + PDR001	mAb anti IL-1 β + mAb anti PD-1	Triple Negative Breast Cancer and NSCLC	Active, not Recruiting	Phase 1	NCT02900664	Novartis Pharmaceuticals	August, 2016	August, 2020
Canakinumab + Spartalizumab	mAb anti IL-1 β + mAb anti PD-1	Renal Cell Carcinoma	Recruiting	Early Phase 1	NCT04028245	Charles G. Drake	August, 2019	December, 2021
Canakinumab	mAb anti IL-1 β	Myelodysplastic Syndrome or Chronic Myelomonocytic Leukemia	Not yet recuiting	Phase 2	NCT04239157	M.D. Anderson Cancer Center	June, 2020	December, 2021
Canakinumab + PDR001 + Chemo	mAb anti IL-1 β + mAb anti PD-1	Non-small Cell Lung Cancer	Active, not Recruiting	Phase 1	NCT03064854	Novartis Pharmaceuticals	May, 2017	December, 2021
Canakinumab + Spartalizumab	mAb anti IL-1 β + mAb anti PD-1	Melanoma	Recruiting	Phase 2	NCT03484923	Novartis Pharmaceuticals	September, 2018	June, 2022
Canakinumab + Chemo	mAb anti IL-1 β	Non-small Cell Lung Cancer	Active, not Recruiting	Phase 3	NCT03626545	Novartis Pharmaceuticals	January, 2019	March, 2022
Xilonix + Chemo	mAb anti IL-1 α	Pancreatic cancer	Active, not Recruiting	Phase 1	NCT03207724	Andrew Hendifar, MD	October, 2017	December, 2020
CAN04 + Pembrolizumab	mAb anti IL1RAP + mAb anti PD-1	Non-Small-Cell Lung, Urothelial Carcinoma Malignant Melanoma, Head and Neck Squamous Cell Carcinoma	Not yet recuiting	Phase 1	NCT04452214	Cantargia AB	September, 2020	January, 2022
CAN04 + Chemo	mAb anti IL1RAP	Non Small Cell Lung Cancer, Pancreatic Ductal Adenocarcinoma, Triple Negative Breast Cancer, Colorectal Cancer	Recruiting	Phase 1/2	NCT03267316	Cantargia AB	September, 2017	June, 2021

1.8. IL-1 receptor family

IL-1 receptors (IL-1Rs) belong to the Ig-like receptor superfamily characterized by the presence of Toll/interleukin-1 receptor (TIR) domain, which is essential for IL-1 activities. In 1996, the link between TIR domain and innate immunity was identified for the first time. These receptors are now called Toll-like receptors (TLRs) and known to be involved in the innate immune response[80]. During the last ten years, IL-1R family has been expanded to coreceptors, decoy receptors, binding proteins, and inhibitor receptors. Particularly, IL-1 family ligands include seven molecules with pro-inflammatory activity: IL-1α, IL-1β, IL-18, IL-33, IL-36α, β and γ. These seven agonists bind 4 different receptors belonging to the IL-1R family; IL-1α, and IL-1β bind IL-1RI (IL-1R1), IL-18 binds IL-18Ra (IL-1R5), IL-33 binds ST2 (IL-1R4) and IL-36α, β and γ bind IL-1Rp2 (IL-1R6). Apart from IL-18 that uses an accessory protein, all the other IL-1 family ligands, through their binding, induce the cognate receptor to form a heterodimer with IL-1R accessory protein (IL-1RAcP, IL-1R3).

The receptors are characterized by an extracellular domain consisting of three immunoglobulin (Ig)-like domains, a trans-membrane and an intracellular domain characterized by a TIR domain, shared by all TLR, essential for signalling via the MyD88 adaptor protein. Once the complex is made (i.e., IL-1R1/IL-1RAcP/IL-1), the recruitment of the signalling adaptor, myeloid differentiation primary response 88 (MyD88), to the TIR domain initiates the signal cascade by phosphorylation of several kinases. This activation leads to the expression of a large number of inflammatory genes[81,82] (Fig. 8) and, IL-1 remains the model for mediating inflammation.
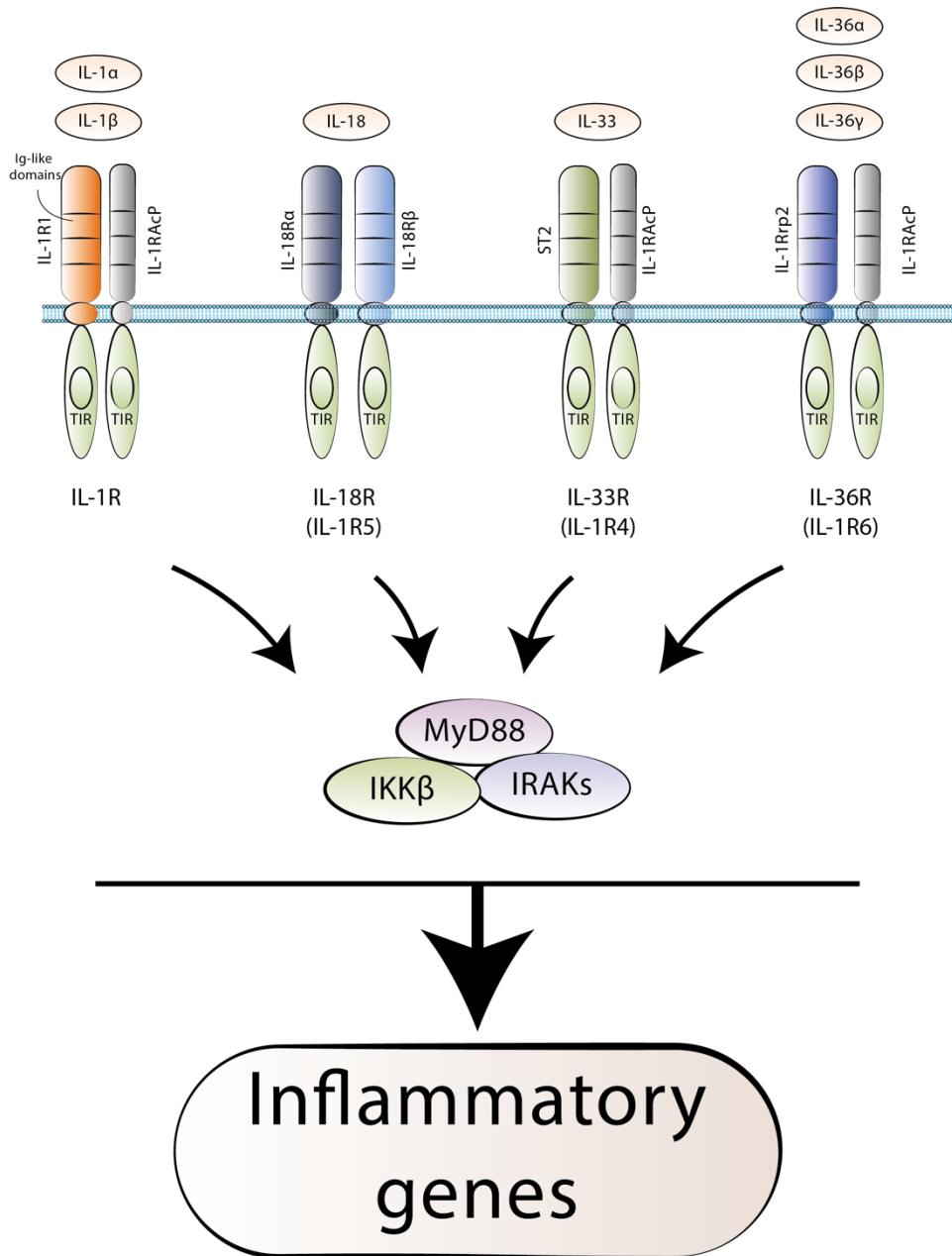
Figure 8: Schematic representation of IL-1 receptors family. Seven pro-inflammatory ligands (IL-1α and β, IL-18, IL-33, IL-36α, β and γ) bind to four different heterodimeric receptors (IL-1R, IL-18R, IL-33R and IL-36R). IL1RAcP represent the co-receptor to which IL-1R1, ST2 and IL-1Rrp2 form heterodimers. IL-18Rα utilize IL-18Rβ for heterodimerization. After a ternary complex is formed namely receptor, co-receptor and ligand, TIR domain of each receptor chain approximate and can recruit MyD88, followed by phosphorylation of receptor-associated kinases (IRAKs) and inhibitor of NF-kB kinase β (IKKβ) resulting in a signal to the nucleus that lead to transcription of inflammatory genes.

As regulator of immunological and inflammatory responses, IL-1 exerts a crucial role in mediating autoinflammatory, autoimmune, infectious and degenerative diseases. In the central nervous system, IL-1 induces fever and the activation of hypothalamus-pituitary-

adrenal (HPA) axis. Like the other ligands, IL-1α and IL-1β are encoded by distinct genes. Although they bind the same receptor and show similar biological properties, the impact on inflammation and cancer differs[83]. IL-1α (like IL-33) is active both in its precursor and cleaved forms and it is usually found as a cell-associated cytokine or secreted in the extracellular milieu, exerting a dual-function. The intracellular precursor (pro-IL1α) is constitutively expressed in epithelial layers of the gastrointestinal tract, lung, liver, kidney, endothelial cells, monocyte and astrocytes. It contains a nuclear localization sequence (NLS), responsible for a nuclear localization, where it modulates gene transcription [80–82,84]. Upon apoptosis, cytosolic pro-IL-1α translocate into the nucleus and remains tightly bound to the chromatin, failing to induce inflammation. In contrast, in presence of necrotic signals, cytosolic pro-IL-1α, is released and fully active; it functions as alarmin by rapidly initiating a cascade of cytokines and chemokines which account for sterile inflammation[85]. Furthermore, the pro-IL-1α might behave as an oncoprotein since its expression induces neoplastic changes in cells. For example, it has been demonstrated that upon IL-1R1 signalling blockade, pro-IL-1a stimulates IL-8 production in different cells and promotes inflammation[86].

Unlike IL-1α, the IL-1β precursor (pro-IL-1β) is not functionally active. It needs to be cleaved by intracellular caspase-1 or extracellular neutrophilic proteases in order to be active in the extracellular space[82]. Moreover, IL-1β is not expressed in homeostatic conditions, but it is induced upon inflammation and its secretion is tightly controlled at transcription, translation and post translational levels[83]. IL-1β is mainly produced in response to TLR stimuli by hematopoietic cells such as blood monocytes, tissue macrophages, skin dendritic cells and brain microglia[82].

1.9. IL-1 Pathways

The initial step in IL-1 signal transduction is a conformational change induced by ligand binding in the first extracellular domain of the IL-1RI that facilitates recruitment of IL-1RacP. Through conserved cytosolic regions TIR domains, the trimeric complex quickly assembles two intracellular signalling proteins, MyD88 and IRAK (interleukin-1 receptor–activated protein kinase) 4. IL-1, IL-1RI, IL-RAcP, MyD88, and IRAK4 form a stable IL-1–induced first signalling module.

This is paralleled by the (auto)phosphorylation of IRAK4, which subsequently phosphorylates IRAK1 and IRAK2, followed by the recruitment and oligomerization of tumour necrosis factor–associated factor (TRAF) 6. Both IRAK1 and 2 function as adaptors and protein kinases to transmit downstream signals.

IRAK1/2 and TRAF6 dissociate from the initial receptor complex and TRAF6 serves as ubiquitin E3 ligase that together with UBC12-UEC1A (ubiquitin E2 ligase complex) form the second module, able to attach different polyubiquitin chains to several IL-1-signalling intermediates including IRAK1, TAB2/3 (transforming growth factor -β (TGF-β)-activated protein kinase binding protein 2 and 3) and TAK1 (TGF-β-activated protein kinase). This second module can be considered a node of signal diversification. Oligomerization of TAF6 and subsequent formation of two TAK1 and MEKK3 signalling complexes activate three main pathways namely, NF-kB, JNK and p38 MAPK axes. IKK1, IKK2 and NEMO for the IKK complex. Activated IKK complex phosphorylates IkBα which promotes polyubiquitination and its proteasomal degradation, p50/p65 are released and translocate to the nucleus. p50/p65 bind the DNA in conserved sequences activating IL-1-responsive genes like IkBα, IL-6, IL-8, MCP1 and COX-2[87–89]. Activation of TAK1 and MEKK3 also trigger activation of MKK3, 4. 6 and 7 activate JNK axis. JNK and c-Jun play a key role in IL-1 induced expression genes encoding for IL-6 and IL-8. On the other hand MKK3, 4 and 6 activate p38 MAPK axes that play an important role to stabilize the mRNA and translation of newly made transcripts by inhibiting mRNA-destabilizing factors controlling the abundance of many IL-1-regulated transcripts[90].

IL-1 signalling pathway is transient and different mechanisms and proteins are involved in the attenuation of the signal. The IL-1R binds the adaptor toll-interacting protein (TOLLIP), which inhibits IRAK1, targets internalized IL-1RI to endosomes, and is required for efficient degradation of IL-1R. IL-1 also activates several negative-feedback inhibitors that shut-off IL-1R signalling. p38 MAPK-mediated phosphorylation of TAB1 inactivates TAK1; p65 NF-κB-mediated mRNA and protein synthesis of IκBα shuts-off the NF-κB response; and inducible expression of the gene encoding MAPK phosphatase 1 (MKP1) dephosphorylates active MAPKs[91] (Fig. 9).
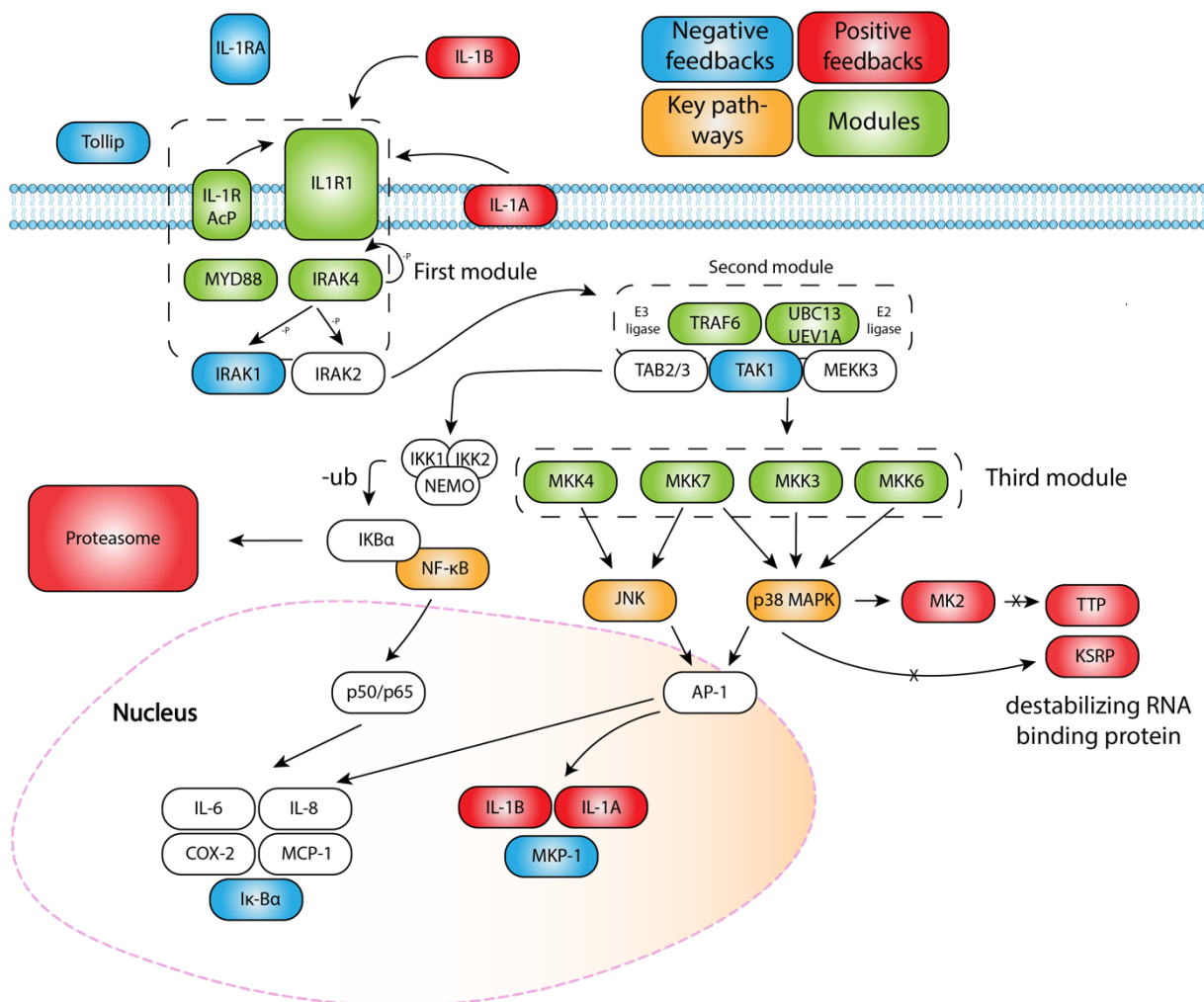
Figure 9: schematic representation of IL-1 signaling pathway. IL-1 pathway is activated up ligand (IL-1) binding assembling the first module protein complex (composed by IL-1R1, IL-1RAcP and IL-1) this, in turn lead to the activation of the second module of proteins complex comprising E2 and E3 ligase able to activate a kinase cascade followed by a diversification of IL-1 signal. Three main axes are activated: NF-kB, JNK and p38 MAPK. Through these three axes genes associated with inflammation response are transcribed. Blue and red depict negative and positive feedbacks respectively. In orange are depicted the three main pathways IL-1-activated and in green proteins belonging to the three modules.

2. Aim of the thesis

Epidermal Growth Factor Receptor (EGFR) activates a robust signaling network to which tumors often become addicted [92]. Over the last three decades, EGFR targeting has been intensely pursued as a treatment strategy for metastatic colorectal cancer (mCRC). One approach uses monoclonal antibodies (mAbs) to inhibit the extracellular domain of EGFR, thus blocking natural ligands binding. Unfortunately, patients often develop resistance, with consequent tumor growth and relapse. Tumors heterogeneity has been addressed as the main culprit for multiple escaping mechanisms, reflecting the high level of molecular heterogeneity in each metastatic site. Mechanisms of cancer cell resistance include either acquisition of new mutations or non-genomic activation of alternative signaling routes and, in this context, a role of IL-1 is emerging. For example IL-1 expression proved to be elevated in human breast, colon, lung and head and neck cancers [93], and patients with IL-1 producing tumors have generally bad prognosis [72]. Our studies, performed with a cohort of 150 colorectal cancer xenopatients, associate poor response to CTX with increased abundance of a set of inflammatory cytokines, including IL-1α, IL-1β and IL-8 [68].

Stemming from these observations, our working hypothesis assumes that resistance to CTX is acquired, in a subset of CRC patients, through cell plasticity and consequent rewiring of signalling networks, which confer dependency on the IL1 pathway. This hypothesis foresees an auto-stimulatory feedback loop dependent on the IL-1 produced by the tumors, with consequent immunosuppression and tumor progression. Thus, combining IL-1 and EGFR neutralization may synergistically impair CRC response to CTX *in vivo*.

3. Material and Methods

3.1. Cells and reagents

MCF10A cells were cultured with DMEM/F12 medium (GE Healthcare) as previously described [97] supplemented with 10 µg/ml Insulin (I6634, Sigma), 0.5 µg/ml Cholera Toxin (C8052, Sigma), 0.5 µg/ml hydrocortisone (H0888, Sigma), 5% heat inactivated horse serum and 10ng/ml EGF (E9644, SIGMA) and maintained in a 37 °C atmosphere containing 5% CO_2 incubator. MCF10A were kindly provided by Yosef Yarden Laboratories.

Caco-2 (human coloncancer adenocarcinoma) and MC38 (murine colorectal adenocarcinoma) cell lines were cultured with Dulbecco's minimal essential medium (DMEM), supplemented with 10% of fetal bovine serum (FBS) and antibiotics (1% penicillin-streptomycin) in a 37 °C atmosphere containing 5% CO_2. Cells were routinely tested for mycoplasma contamination.

3.2. Western blot

Naïve and mEGFR MC38 cells were lysed with Novagen PhosphoSafe Extraction Reagent (EMD Millipore) plus Protease Inhibitors Cocktail (Sigma-Aldrich) and incubated for 10 minutes on ice. Protein concentration in the supernatants was determined by DC Protein Assay (Bio-Rad) using bovine serum albumin as the standard. Proteins (30 µg of total lysate) were separated on 8% or 10% polyacrylamide gel and then transferred to polyvinylidene difluoride membranes (Bio-Rad). After blocking with PBS containing 0.1% tween 20 plus 5% BSA (Bio-Rad) for one hour at room temperature, membranes were incubated overnight at 4°C with primary antibodies diluted in blocking buffer. The following primary antibodies were used: anti-AKT rabbit polyclonal antibody (100 ng/mL, #9272), anti-phospho-AKT (Ser473) (D9E) XP rabbit monoclonal antibody (100 ng/mL, #4060), anti-EGFR (D38B1) (29 ng/mL, #4267), anti-EGFR phospho tyr1068 (D7A5) (423 ng/mL, #3777) (Cell Signaling Technology, Danvers, MA, USA); anti-ERK2 (D-2) mouse monoclonal antibody (200 ng/mL, sc-1647) and anti-p44/42 MAPK (Erk1/2) mouse monoclonal antibody (10 ng/mL, M1859, Sigma Aldrich, St. Louis, MO, USA). Anti-GAPDH was used as loading control. Peroxidase-conjugated AffiniPure Goat Anti-Human IgG, Fc Fragment Specific (800 ng/mL, 109-035-

098, Jackson ImmunoResearch, Ely, Cambridgeshire, UK). Protein was detected by incubation with anti-rabbit or -mouse horseradish peroxidase-labeled secondary antibody (Dako EnVision+ System- HRP Labelled Polymer) followed by chemiluminescent reaction (Clarity Western ECL Substrate, Bio-Rad). Chemiluminescence was detected with the ChemiDoc XRS+ system (Bio-Rad).

3.3. Alamar

Cells were seeded in 96-well plates, 2.000 cells for each well, in 100 l of 5% FBS medium. Quantification of initial time (time 0) was performed the following day using Alamar Blue (20 M) in medium 0% FBS, measuring the fluorescence after 5 hours of incubation. Fluorescence was quantified using VICTOR^{2}TM 1420 multilabel counter (Perkin Elmer, Massachusetts, USA), at a wavelength of 595 nm. Cells were then treated according to the experiment and, after 72-96h proliferation was measured using Alamar Blue, following the same procedure. Data were analysed subtracting background values, normalizing the endpoint values on the initial time ones, calculating for each treatment the median value and transforming it as percentage of the untreated control. Data points represent the median +/- SD.

3.4. Colony forming assay

2.000 cells were seeded in 12-well plates in 1 ml of medium. Treatments were added immediately or the following day, according to the information included in the figure legends. After one weeks following treatments a picture of each well was taken and the covered area was measured using IncuCyte S3® Live-Cell Analysis system (Essen Bioscience). The mean value from covered area values returned by the software was calculated for each treatment and recorded as a percentage of control.

3.5. Soft-agar

To inhibit cellular adhesion to the plastic surface, 6-well plates were covered with a layer of agar 0.6% (bottom agar). Agar 1.8% was autoclaved and diluted to 0.6% with full medium; 2 ml of 0.6% agar was used to cover each well and the agar layer was left to dry before seeding cells. 5.000 cells for each well and treatments were added (in 2 ml of medium). After 21 days of treatment, pictures of randomly non-overlapping spheroids for each well were collected using the microscope at 4X magnification. Spheroids of each picture were counted, and the length of the major and minor axis of each spheroid was measured using ImageJ Software. Axis values below 60 A.I. were excluded as not corresponding to mature spheroids and volume was calculated applying the sphere adapted formula (major axis x minor axis)2/2.

3.6. Scratch assay

40.000 MC38 or MC38 hEGFR cell per well were seeded in a 96-well ImageLock (Essen Bioscience Cat. No. #4379) and left settled over night in the incubator with standard condition (37°C, 5% CO_2). The day after a wound has been created with a 96-pin IncuCyte WoundMaker Tool (Essen BioScience Cat. No. #4563) to simultaneously create a wound in all wells. Then the media was aspirated and well was washed twice with PBS, then 100 uL of FM 10% FBS supplemented with appropriate treatments was added as specified in the figure legend. Cell invasion was followed in time-laps for 12 hours. Statistical analysis and images were obtained using IncuCyte S3® Live-Cell Analysis system (Essen Bioscience)

3.7. Invadopodia detection and Gelatin degradation assay

Dehydrated gelatin was reconstitute 1 mg/mL by adding 5mL of ddH2O to the vial. The stock (100uL) was stored at -20°C protected from light. The working solution was prepared heating the stock aliquot to 60°C (in a water bath) and dilute to the final concentration of 0.2 mg/mL in PBS with 2% sucrose (keep the working solution protected from light). For the preparation of gelatine-coated coverslips gelatine working solution was heated to 60°C (in a water bath), then added 100uL over the first coverslip. Once the gelatine was evenly distributed and the excess removed the coverslip was placed in a 12-well plate protected

from light. Allow the coverslip to dry. 1mL of 0.5% glutaraldehyde was added in cold PBS and incubated 15' on ice. Then, the glutaraldehyde was aspirated and washed 3 times with PBS. 1mL of Sodium Borohydride (NaBH4) 5mg/mL in freshly prepared PBS was added and incubated at room temperature 3'. It was aspirated and washed 3 times with PBS. Under biosafety hood transfer the coverslips into a sterile 12-well. After coverslips sterilization with 70% ethanol for 15 min, 40,000 cells were seeded in 1mL complete medium/well and incubated for 24h. Cells were fixed in 4% PFA in PBS for 10'-15' at RT and without light. Then blocking with BSA (3% in PBS containing 0.1% Triton X-100) at same condition. Cells were stained with Phalloidin (1:250) in PBS containing 0.3% BSA and 0.1% Triton X-100) for 30'-1h. Coverslips were mounted on a slide containing one drop of mount + DAPI. The results were observed with fluorescence microscope (Olympus BH-2 CCD). Quantification should be done on at least 15 fields per coverslip, generally at 40X, using all three channels. Quantification invadopodia activity: The black and white images related to the green channel were analysed with ImageJ. Then, the threshold was manually adjusted in order to detect only the areas actually corresponding to the degradation. The area fraction was measured and normalized over the number of DAPI cores in the same field to obtain the 'normalized' area fraction.

3.8. Construction of murine TRAP IL-1 plasmid

For mIL1R1 mRNA from ID8 cell line was extracted using RNeasy kit (Qiagen Cat. No. 74104) following manufacturer's instructions and quantified. 1 ug of mRNA from ID8 cells was retrotranscribed using qScript cDNA synthesis kit (Cat. No. 95047-025) following manufacturer's instructions. Amplicon of extracellular domain of mIL1R1 was obtained amplifying by PCR ID8 cells cDNA. The following primers were used for PCR amplification of mIL1R1: mIL1R1 FW CCGCTCGAGATGGAATGGAGCTGGGTCTTTCTCTTCTTCCTGTCAGTAACTACAGGT GTCCACTCCCTGGAGATTGACGTATGTACAG and mIL1R1 RV: CTTACAACCACAATCCCTGGGCACGCTGCCGCCGCCACCACCAGAACCGCCACCG CCCTTGAAGTCAGGGACTGGGT. After PCR amplification mIL1R1 amplicon was

isolated from gel using QIAquick Gel extraction kit (Cat. No. 28704) following manufacturer's instruction and quantified.

Amplicon for mFc was obtained amplifying by PCR using as template pIRES mTRAP (ERBB4-EGFR)-Fc[98] kindly provided from Prof. Y. Yarden (Weizmann Institute of Science). The following primers were used for PCR amplification: mFc FW ACCCAGTCCCTGACTTCAAGGGCGGTGGCGGTTCTGGTGGTGGCGGCGGCAGCGT GCCCAGGGATTGTGGTTGTAAG and mFc RV: GGGAGTTTGTGGAAAATTCTGAATGCATAGCGGCCGCTCATTTACCCGGAGTCCGG GAGAAGC. Primers were specifically designed for the target sequences containing, XhoI and NotI-HF restriction sites, the leader sequence and a linker for mIL1R1 and mFc domain. mIL1R1 and mFc amplicons were first isolated using the QIAquick gel extraction kit (Qiagen, Cat. No.28704) and then fused by PCR obtaining the full-length mIL1R1-Fc

3.9. Cloning and sequencing of mTRAP IL-1 insert

mTRAP IL-1 insert was ligated into pIRES expression vector, amplified in bacteria, extracted and sequence analyzed by Sanger methodology. mTRAP IL-1 and pIRES mTRAP (ERBB2-EGFR) plasmid vector were both double-digested with XhoI (New England Biolabs, R0146S) and NotI-HF (New England Biolabs, R3189S) restriction enzymes following the manufacturer's instructions and isolated from the gels.

Subsequently, mTRAP IL-1 insert was ligated pIRES expression vector (pIRES mIL1R1-Fc) employing a T4 DNA ligase enzyme (New England Biolabs, M0202S) following the manufacturer's instructions. In order to amplifying the number of copies of pIRES mTRAP IL-1 plasmid DH5α competent cells (Invitrogen, Cat. No. 18265-017) were used and five different bacteria colonies (colonies 1-5) were randomly selected after over-night incubation. pIRES mTRAP IL-1 plasmid vector was isolated from bacteria using a mini-prep kit (Qiagen, Cat. No. 27104). pIRES mTRAP IL-1 plasmid vector isolated was used as template for PCR amplification. Primers specifically designed covering mTRAP IL-1 insert sequence (1751 bps size) were used: mTRAP IL-1 (Forward) ATAGGCTAGCCTCGAGATGG and mTRAP IL-1 (Reverse): CGGCCGCTCATTTACCAGGA. pIRES mTRAP IL-1 was double-digested with XhoI (New

England Biolabs, R0146S) and NotI-HF (New England Biolabs, R3189S) restriction enzymes following the manufacturer's instructions. mTRAP IL-1 plasmid vector was analyzed with Sanger technique for gap/mismatch detection.

3.10. Expression and purification of TRAP IL-1

A total of 1.000.000 HEK293T TRAP IL-1 cells has been seeded in T75 flask in DMEM 10% FBS. After reaching 80% confluence, cells have been splitted (1:10) and seeded in DMEM with 10% FBS concentration decreasing by 2% at every split (10%, 8%, 6%, 4% and 2%). DMEM 2% FBS has been replaced with a serum-free, protein-free, chemically-defined medium (CD293 medium for Suspension Cultures by Gibco Cat. No. 11913-019)) specifically formulated for HEK293T cultivation and recombinant protein expression, supplemented with 2% FBS. At this stage, cells detached and start growing in suspension, thus increasing the TRAP secretion. CD293 2% FBS has been replaced with CD293 0% FBS and cells grown at 37°C until reaching a high confluence, to burst TRAP production. After seven days soup has been collected for TRAP isolation. For TRAP isolation Protein G Sepharose™ 4 Fast Flow kit (from GE Healthcare, Lifescience) was used following manufacturer's instructions. Briefly, soup has been collected and centrifuged (10.000g x 10 minutes) and filtered through a 0.45 um filter in order to eliminate gross contaminants (i.e. dead cells and debris). A poly-prep column (Bio-RAD) has been packed with a resin of Protein G Sepharose™ containing beads specifically designed to strongly bind the Fc region of human IgG and extensively washed with 20 mM sodium phosphate buffer (pH 7). Soup containing TRAP IL-1 (sample) has been filtered throw the Protein G Sepharose matrix and the adsorbed TRAP IL-1 has been eluted with 0.1 M glycine solution (pH 2.7) and stored at -20°C for further analysis. Total amount and purity of proteins has been assessed by Lowry assay and Western Blot respectively.

3.11. In vivo experiment and Hematoxylin-Eosin staining

A total of $1x10^6$ MC38 and MC38 mEGFR cells suspended in 0.1 mL of calcium- and magnesium free PBS per mouse has been injected subcutaneously (s.c.) in the left flank of 6-

to 7-week-old male wild-type C57BL/6 mice. Tumor growth has been evaluated by measuring two perpendicular diameters, length and width of tumor nodule with Vernier caliper, and calculated according to the following equation V=3.14x(LxW2)/6. After reaching the limiting volume (1500 mm^3) mice were sacrificed and tumor were processed for Hematoxylin-Eosin staining.

4. Results

4.1. Long-term exposure to antibody-mediated EGFR inhibition leads to the emergence of resistant cell clones

We established cetuximab-resistant cells from the human colorectal cell line Caco-2, which is wild-type for *KRAS*, *BRAF* and *NRAF*, and dependent on EGFR as a mitogenic stimulus, as previously characterized[99]. Caco-2 cells were made resistant to CTX by continuous exposure over six months to increasing concentrations of the drug, ranging from 10 ng/ml to 20 µg/ml. We first confirmed resistance, by measuring cell growth using the Alamar assay. Caco-2 parental cells and CTX, hereinafter referred as parental (Caco-2 P), and cetuximab resistant (Caco-2 CXR) respectively, were treated with increasing concentrations of CTX for 72-96 hours and their proliferation was compared to cells treated with vehicle only (Fig. 10A). While parental cells displayed growth inhibition under CTX treatment, with maximal inhibition achieved at 1 to 5 µg/ml of the antibody, the resistant sub-line Caco-2 CXR displayed undisturbed viability under CTX treatment, confirming acquired resistance (Fig. 10A). We next performed a long-term clonogenic assay, by seeding a very low number of cells in twelve well plates with the indicated treatments. After 10 days, the cells were fixed and stained with crystal violet, and clonogenic cell growth was evaluated by measuring the portion of covered area of the plate. In this assay, parental cells displayed a ~50% and ~70% growth inhibition upon CTX treatment (Fig. 10B). In contrast, no change in clonogenic cell growth was detected in Caco-2 CXR clones. Finally, we performed the sequence analyses of KRAS exon, in order to test whether acquisition of KRAS mutation could explain the observed resistant phenotype. Interestingly, none of the CXR cells displayed acquired mutation (Fig. 11C).
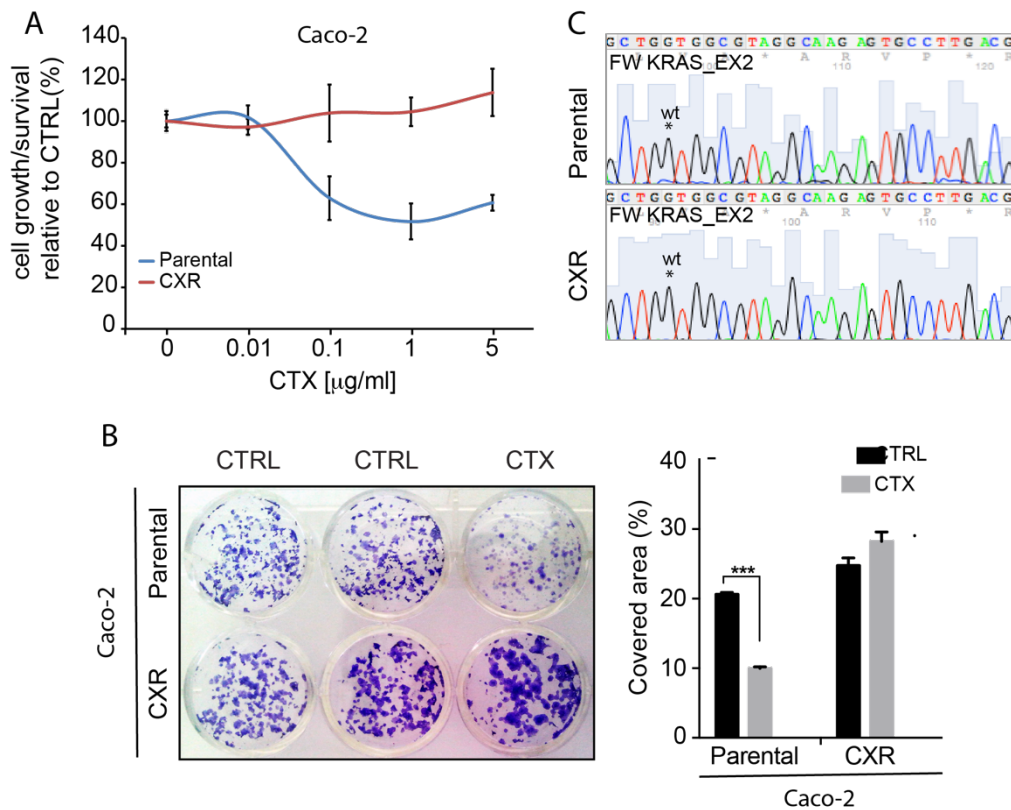
Figure 10: Establishment of colorectal cells resistant to cetuximab. Human colorectal cancer Caco-2 cells were made resistant to cetuximab (CTX) by continuous exposure to increasing doses of drug and maintained with 1 µg/ml of CTX. (**A**) Cell proliferation analysis by Alamar assay of Parental (Caco-2 P) and cetuximab-resistant (Caco-2 CXR) cells following treatments with increasing concentration of cetuximab in medium containing 1% serum for 72h. The graphic represents the relative proliferation/viability of the cells following 72 hours of treatment related to control; (**B**) Colony formation assay of Caco-2 P and Caco-2 CXR cells. Cells were grown in the absence or presence of CTX (1 µg/ml) for 10 days in medium containing 1% of serum, then fixed, stained with Crystal Violet and photographed. Representative figures (left) and quantification (right) of the covered areas by ImageJ is provided in B. The statistic was calculated by 2-way ANOVA, *** P<0.0001, ** P<0.01. These experiments were repeated at least three times. (**C**) Sequence analyses of KRAS Exon 2, showing the wild type sequence detected in Caco-2 Parental and Caco-2 CXR cells.

4.2. Resistant clones display anchorage-independent growth as spheroids

The ability to grow in suspension is a hallmark of the neoplastic phenotype. Notably, only a small percentage, about 0.5% of Caco-2 from parental cells displayed the ability to grow in suspension and form spheroid-like structures. In contrast, more than 1.2% of CXR clones displayed the ability to form spheroids (Fig.11A). Statistically, parental cell spheroids were fewer and larger in size, when compared to CXR cells as depicted in the representative image (left) and quantification (right) of figure 11A. CTX treatments decreased sphere volumes in parental cells while CXR clones displayed no effects in terms of either spheroid size or number, supporting the lack of sensitivity of these cells to EGFR-targeting drugs (Fig. 11A).

Next, we investigated the morphology of the spheroids by embedding them into paraffin blocks, preparing 8-10 μm slides and staining them with haematoxylin-eosin (H&E). Parental cells displayed a well-organized architecture, with multiple layers of nuclei polarized on the external region and a hollow lumen filled with cell debris and matrix, as shown in Fig. 11 B-C and illustrated by Fig. 11D. On the other hand, CXR cells displayed poorly organized structures, with sparse nuclei in the entire volume and smaller and filled lumen (Fig. 11B and 11C). Furthermore, 3D rendering elaboration of the actin and nuclei signals, obtained by rotating the y axes and cutting the lower part of the spheroids helped to visualize the spheroid lumen, which appeared filled in the resistant cells (Fig. 11C).

Summarizing, the CXR cells acquired a robust ability to grow in suspension. Parental spheroids are well organized and display a hollow lumen, whereas CXR spheroids are smaller, poorly organized and their lumen is filled or partially filled with cells. These findings support the notion that the adaptation to cetuximab lead to resistant clones characterized by a more malignant phenotype, which enable the cells to grow in suspension.
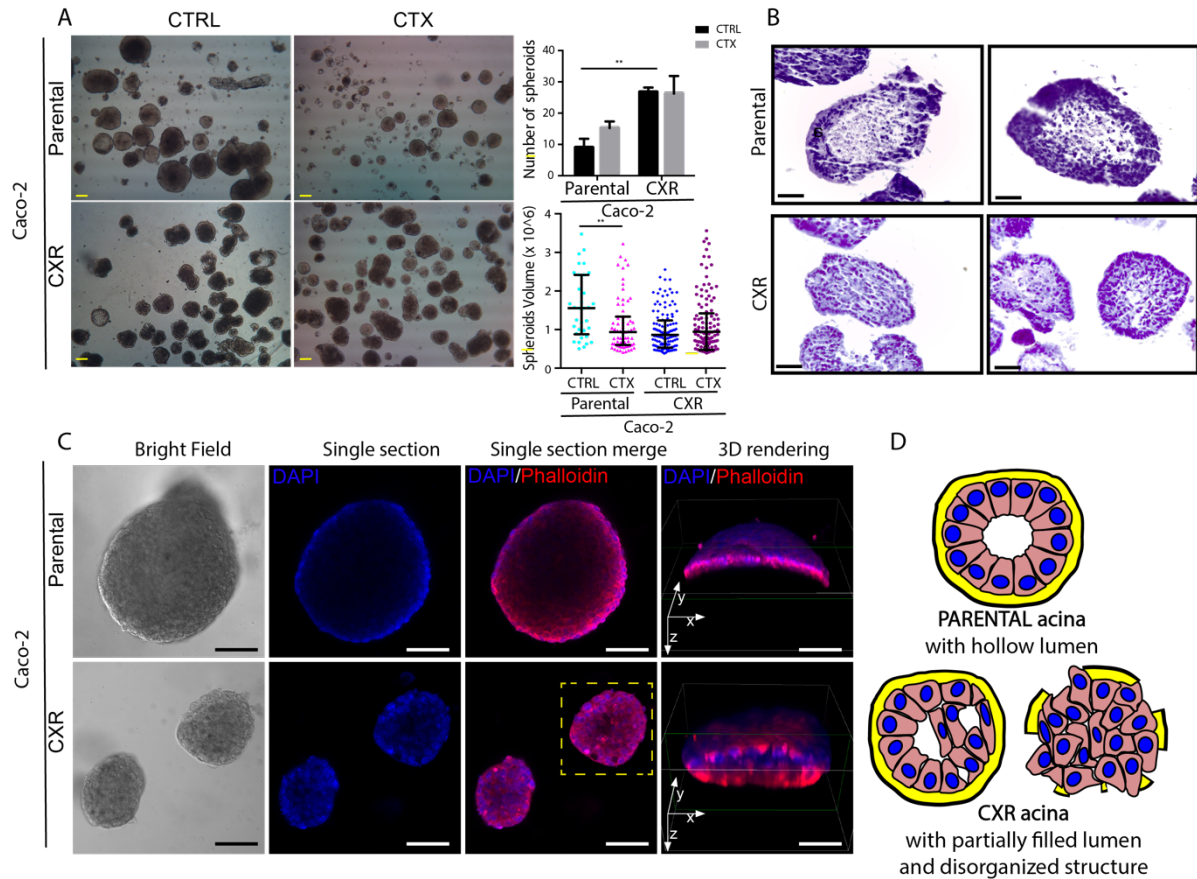
Figure 11: Cetuximab resistant cells displayed increased ability to growth in suspension as colonspheres. We investigated the morphology of Caco-2 Parental and CXR cells when forced to grow in suspension. (**A**) On the left 4X magnification of Caco-2 producing "spheroid-like" structures, under the indicated treatments. Scale bar 100µm; on the right, number of filled spheroids presented as average ± S.E.M. 2-way ANOVA with Bonferroni Test, ** $p<0.01$; ****$p<0.0001$; Quantification of spheroids sizes measurements under the indicated treatments in 5% FBS (EGF 10 ng/ml, CTX 1 µg/mL) is presented as dots plot. Each dot represents the quantification of a single spheroid (n= 117 for Parental cells, n=332 for CXR). Bar represents volume averages ± S.E.M, 1-way ANOVA, ** $p<0.01$; ****$p<0.0001$; (**B**) Analysis of Caco-2 Parental and CXR paraffin-embedded spheroid morphology by H&E staining. Scale bar 50 µm; (**C**) Single section passing through the maximum diameter of spheroids and 3D confocal morphology of parental and CXR spheroids. Left panel: bright field imaging; central panels: DAPI and Phalloidin confocal microscopy; right panel: three-dimensional reconstructions of both signals, obtained by rotating the y axes and cutting the lower part of the spheroids (green lines) to observe the inner structures; scale bar 100 µm; (**D**) Illustration depicting a schematic representation of the parental and CXR spheroid morphology.

4.3. A module of inflammatory cytokines is induced in cetuximab resistant cells

Secreted growth factors and cytokines have been shown to contribute to drug resistance by imparting compensatory survival cues [100–102]. We sought to analyse the secretome of parental and resistant Caco-2 cells, in the presence or absence of cetuximab. The analysis included inflammatory cytokines (*IL1A, IL1B, IL8*), as well as critical components of positive ERBB feedback regulatory loops (such as the EGFR ligands *TGF*A, *HBEGF*), which were recently found to be involved in cetuximab resistance [103,104]. To provide further functional annotation, we extended our analysis to specific negative feedback loops of the EGFR pathway, namely inhibitors of EGFR/ERBB signaling, such as *LRIG1, LRIG3* and *ERRFI1* [105,106]. Finally, the differentiation status of these cells was also tested by interrogating markers of the Epithelial to Mesenchymal Transition (EMT), such as E-cadherin, vimentin, *SNAIL*, *LEF1* and *SOX2* (a transcription factor associated with stemness) [107].

The results are displayed in Fig. 12 as heat-maps, with red boxes corresponding to relatively high expression of the respective transcript and green boxes correspond to low expression. Under monolayer conditions, EGFR inhibition by cetuximab in parental cells led to a slight expression of *IL1A, IL1B, IL8*; while, these cytokines were markedly overexpressed in cetuximab-resistant clones (Fig. 12A). Similarly, the autocrine ligands *HB-EGF* and *TGFα* were upregulated in cetuximab-resistant clones (Fig. 12A). Resistant cells also featured increased levels of markers of epithelial-mesenchymal transition and stem-like features, with reduced expression of *CDH1* (E-cadherin) and increased expression of vimentin, the EMT inducer *SNAIL*, and the stem-cell transcription factors *LEF1* and *SOX2* (Fig. 12A). Finally, resistant cells had increased levels of negative feedback regulators, most probably as a consequence of increased EGFR pathway deregulation (Fig. 12A).

Most of the transcriptional modulations that occurred in 2D resistant cells could be also observed in resistant spheroids (Fig. 12B), indicating maintenance of these traits irrespective of culture conditions. Acquired production of the positive feedback components, such as *HB-EGF* and simultaneous inhibition of EGFR by negative feedback might reflect a shift toward HER2 heterodimer activation, as previously reported [108,109].

Of note, spheroids from parental cells did not experience any obvious transcriptional reprogramming following exposure to cetuximab, apart from increased expression of some EGFR negative regulators. The weak transcriptional consequences of EGFR blockade in parental spheroids could be related to initial selection of cells growing in suspension, which might have enriched for clones that are resistant to any kind of pro-apoptotic insult, including anchorage-independent growth and EGFR blockade. Analyses of the signalling pathways downstream to EGFR helped us to characterize signalling differences between Parental and CXR cells. Indeed, while parental cells responded to CTX treatment, by decreasing both phosphorylation of AKT and ERK (Fig. 12C), resistant cells appeared not sensitive to CTX inhibition on AKT phosphorylation. Interestingly, the basal level of pERK was in general higher in resistant cells, and CTX displayed his inhibitory capability on pERK, although less effective (Fig. 12C). Collectively, this analysis shows that the resistant phenotype is accompanied by increased expression of inflammatory cytokines and EGF-like growth factors, feedback activation of EGFR negative regulators, and EMT/stem-like features.

These data are further supported by the evidence that EGFR activation in epithelial cells, such as MCF10A human mammary cells, immediately produce a module of inflammatory cytokines, namely *IL1B, IL8* and *CXCL1*, by active transcriptional production (Fig. 13A). Furthermore, co-treatment with Dexamethasone (DEX), a powerful anti-inflammatory agent, dampened this production, pointing to a direct involvement of the EGFR pathway in the induction of an inflammatory-like response (Fig. 13A). Because EGF simultaneously up-regulated several inflammatory cytokines, we assumed that the inflammation-regulating transcription factor, NF-κB, is stimulated by EGF in the mammary epithelial cells we employed. In line with this model, we observed concentration-dependent activation of NF-κB (p65) by EGF (Fig. 13B). To extend these observations to the protein level and also to assay additional cytokines, we utilized a cytokine array (Fig 13C-D). This analysis detected high basal levels of IL-1α in untreated cells, which was increased following EGF stimulation and dampened by the DEX co-treatment. Interestingly, IL-1β, IL-8 and CXCL1 displayed very low basal levels with strong induction upon the growth factor stimulus, and once again

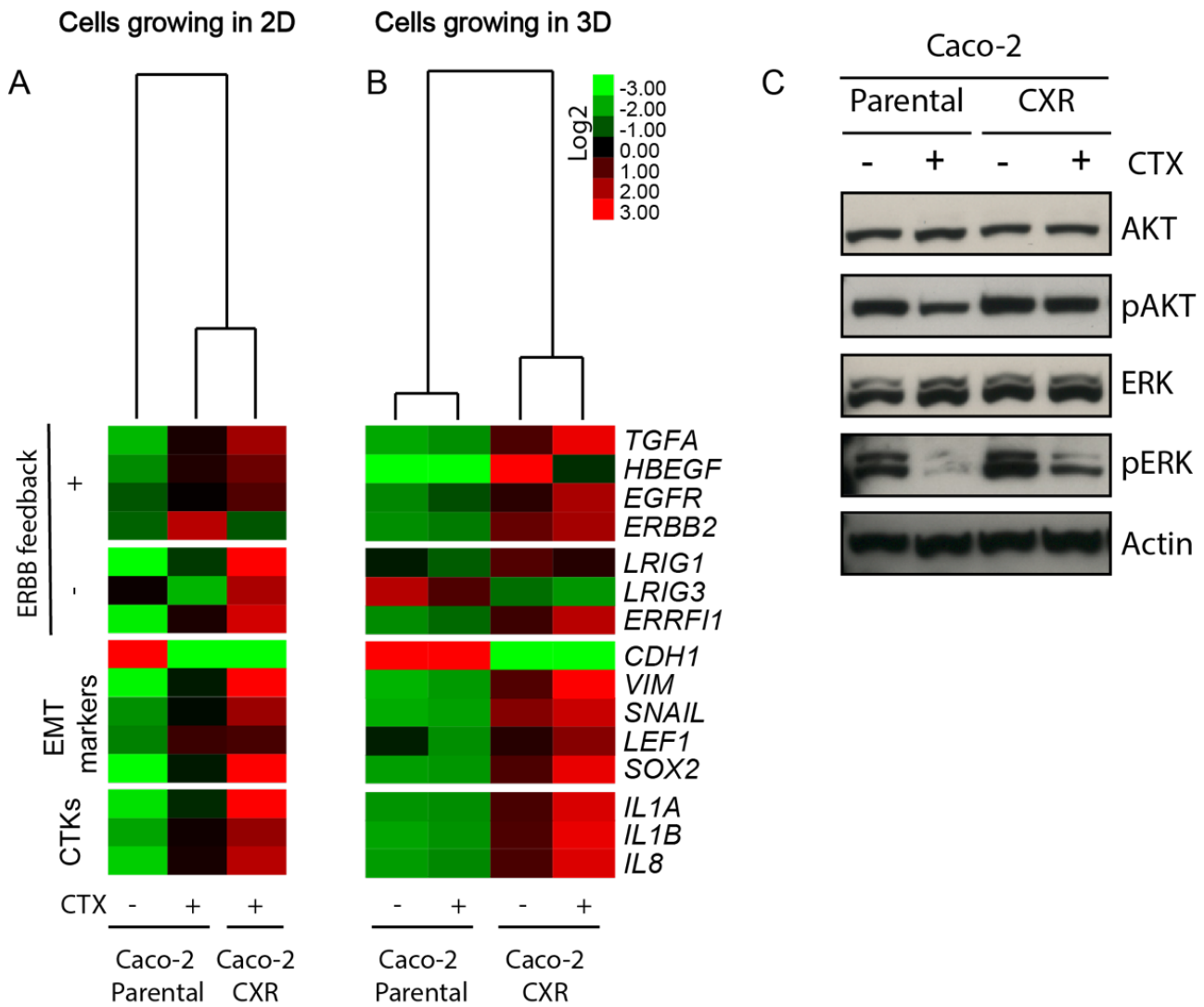the anti-inflammatory action of DEX was able to block production of these cytokines.

Figure 12: Gene expression analysis of parental and CXR cells. (A-B) PCR analysis of parental or cetuximab resistant (CXR) cells growing as monolayer (**A**) or as spheroids (**B**) were collected, both under CTX (2µg/ml) treatment or regular medium conditions. A set of genes probing EGFR positive/negative feedback loop, EMT phenotype and inflammatory cytokines were analysed and displayed as heatmap. (**C**) Western blot analysis of phospho-AKT (pAKT), AKT, phospho-ERK (pERK) and ERK levels in Caco-2 Parental and CXR cells treated over-night with and without cetuximab. Actin served as a loading control.
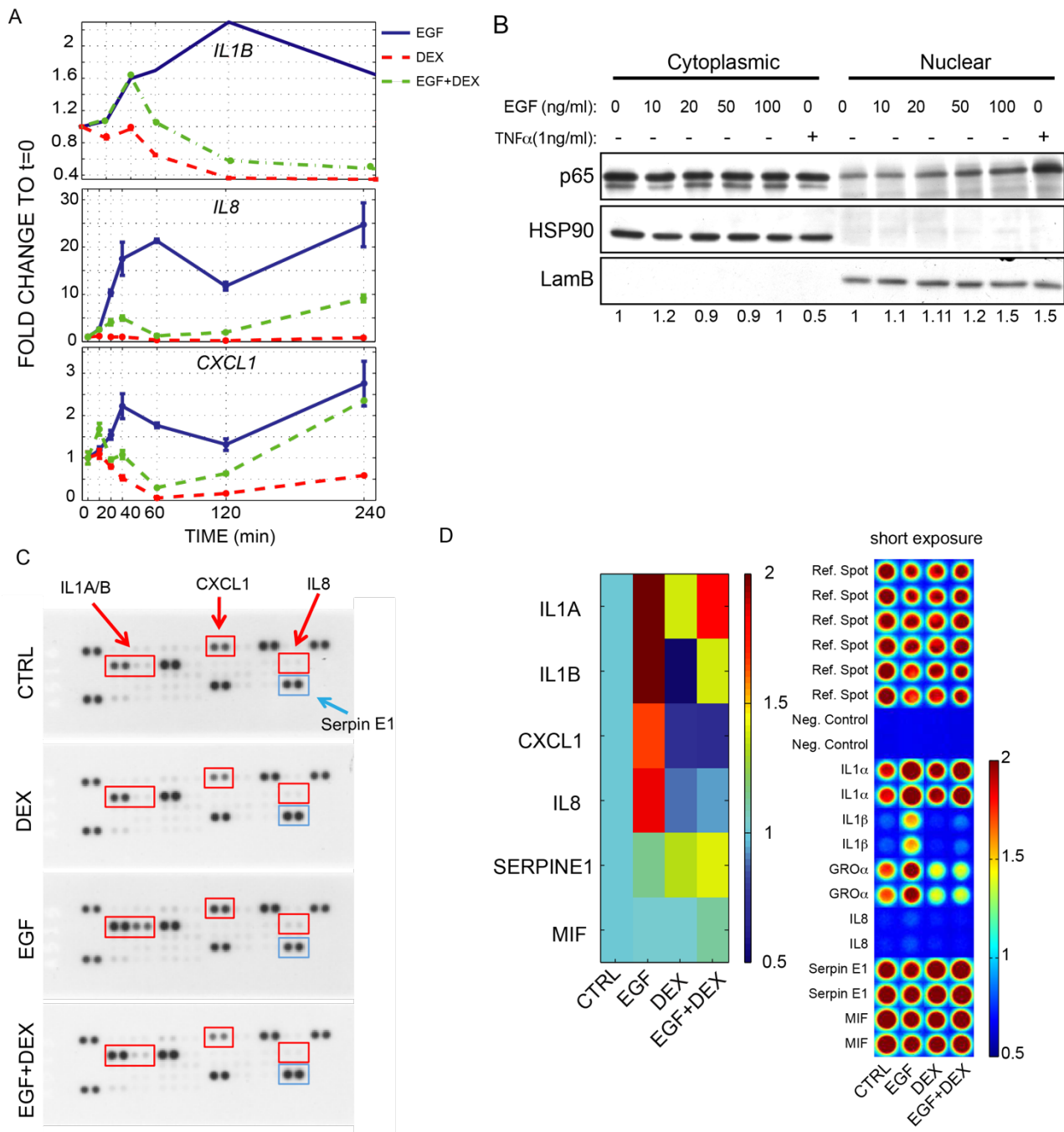
Figure 13: EGFR activation controls the production of a module of inflammatory cytokines in MCF10A. (A) Expression levels of the module of inflammatory cytokines (*IL1B* and *IL8* and *CXCL1)* analysed by Real-Time PCR in MCF10A following EGF (10 ng/mL) or DEX (100 nM) administration, alone or in combination, over a time course of 4h; (**B**) Western blot of NF-kB in cytoplasmic and nuclear fraction of MCF10A cells following administration of increasing doses of EGF (from 1 to 100 ng/ml). TNF-α (1 ng/ml) treatment was used as positive control for NF-kB (p65) activation and nuclear translocation. Laminin B and HSP90 were used as loading control for the nuclear and cytosolic fraction, respectively; C and D) Cytokine array of MCF10A cells following administration of EGF (10 ng/mL), DEX (100 nM), alone or in combination. Representative pictures are provided in (**C**). Quantification of chemioluminescence along with images of normalized spots are provided in (**D**).

4.4. Analysis of patients' specimens

Our data *in vitro* pointed out the increased expression of a panel of inflammatory cytokines in cells resistant to cetuximab. We therefore decided to analyse the panel of selected cytokines in patients colorectal xenograft. Gene expression information was analysed in colorectal tumorgrafts from 98 patients with wild type *KRAS*, *BRAF*, *NRAS*, and *PIK3CA* genotypes ("quadruple negative" tumours) and from 61 individuals with KRAS (G12) mutations. *KRAS* G12 mutations lead to a constitutively activated K-Ras protein, which confers an intrinsic resistance to EGFR blockade. WT quadruple negative tumorgrafts were tested for cetuximab response, as described by Bertotti (Bertotti et al. 2011b). In this condition, the human stroma is supposed to be substituted by murine components; therefore, this analysis covers only receptors and autocrine ligands expressed by cancer cells[110]. Interestingly, we observed an inverse association between elevation of inflammatory cytokines *IL1A*, *IL1B* and *IL8* and the overall response to cetuximab (Fig. 14). In accordance with our *in vitro* data, *IL1A*, *IL1B* and *IL8* were overexpressed in tumorgrafts that proved to be resistant to EGFR blockade (tumor volume increase of at least 35% compared to the initial, pre-treatment volume). Furthermore, *IL8* expression appeared over represented also in a group with limited sensitivity to cetuximab, with tumour volume changes between 35% increase and 50% reduction, which is considered as stable disease (SD). Interestingly, the pattern of increased expression of this module of inflammatory cytokines was maintained in the group of *KRAS* mutant tumours, which by definition are resistant to treatment. These results suggest that gradual tumour adaptation to EGFR blockade might be associated with up-regulation of the module of inflammatory cytokines, which might activate a compensatory pathway overcoming EGFR inhibition.
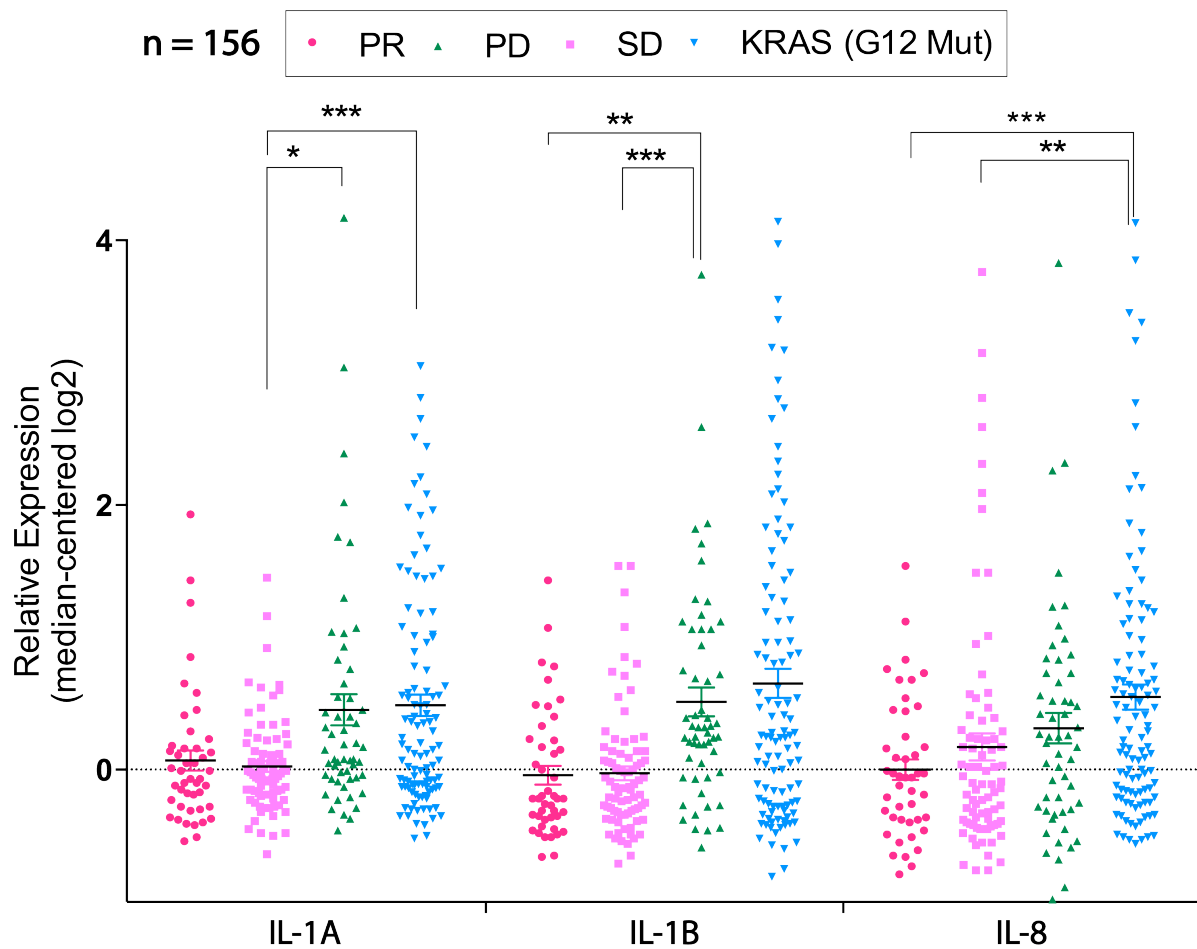
Figure 14: A panel of inflammatory cytokines correlates with cetuximab response in colorectal patients. Expression analysis of *IL1A, IL1B* and *IL8* in colorectal quadruple wild type (wild type for *KRAS*, *BRAF*, *NRAS* and *PIK3CA*) tumors, subdivided by response to Cetuximab therapy: disease regression (PR), disease stabilization (SD), disease progression (PD). The KRAS (G12 Mut) group was included as control for lack of response to CTX;

4.5. Overexpression of IL-1R1 correlates with reduced patient sensitivity to cetuximab

Several clinical studies indicate that overexpression of inflammatory cytokines, such as IL-1, IL-8, IL-6 or CXCL1, correlates with cancer progression and decreased response to EGFR targeting therapy [111,112]. We previously reported that the abundance of IL-1 cytokines predicts sensitivity to EGFR blockage [68]. To further assess the clinical relevance of our results, we explored whether the receptor for IL-1, namely IL-1R1, was enriched in tumors from patients exhibiting attenuated response to anti-EGFR antibodies. We started by mining the gene expression profile from a publicly available microarray data set, comprising KRAS wild-type CRC patients, treated with cetuximab monotherapy, as described by Khambata-Ford et al. [113] (GSE5851). Only one sample was excluded, because of its uncertain rectal origin. We observed that IL-1R1 is overexpressed in a distinct subpopulation of patients categorized as progressive disease (PD), defined as an increase in tumor burden upon CTX treatment. Consistently, patients with stable disease (SD) or an overall response (OR) to CTX therapy displayed lower IL-1R1 expression than the non-responding patients (Fig. 15). In line with our previous work [68], we conclude that increased expression of both IL-1 ligands (IL-1α and IL-1β) and receptor (IL-1R1) is associated with resistance to EGFR targeted therapy.

Next, we evaluated the association of IL-1R1 with AREG and EREG, two EGFR ligands whose expression was previously reported to determine CTX efficacy. Indeed, high levels of AREG and EREG are predictive of response to CTX [113], whereas high levels of IL-1R1 are predictive of poor response. Pearson analysis reported a moderate negative correlation between IL-1R1, AREG and EREG (-0.50, p=0.00057 and -0.44 p=0.003308 respectively): Table 1. These data support the notion that IL-1R1 is a marker of decreased patient sensitivity to CTX blockage, pointing to a role of this pathway in the progression and aggressiveness of colon cancer.

Table 1. Pearson correlation of IL-1R1 to AREG and EREG.

	AREG vs. IL-1R1, *p*-Value	EREG vs. IL-1R1, *p*-Value
PD	−0.50 (0.00057)	−0.44 (0.003308)
SD	−0.55 (0.01881)	−0.47 (−0.04905)
OR	−0.05	−0.08

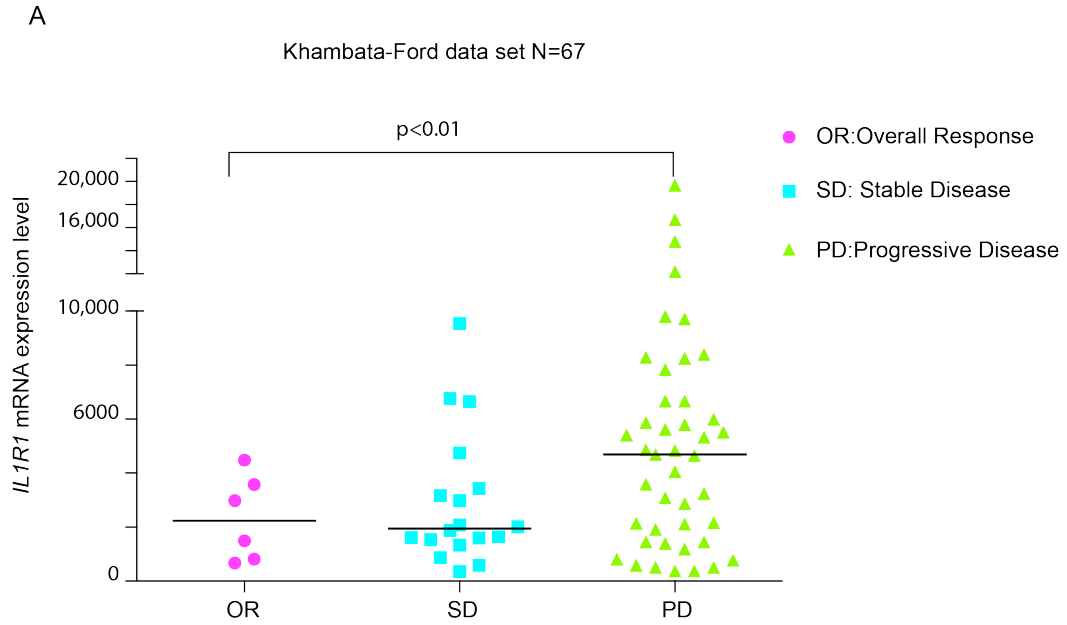PD: Progressive disease, SD: stable disease, OR: Overall Response.

A

Khambata-Ford data set N=67

Figure 15: IL-1R1 abundance predicts response to CTX in patients. Expression analysis of IL-1 receptor in 67 CRC patients treated with CTX. Responsive patients (OR) as well as stable disease (SD) display low amounts of IL-1R1 compared to the non-responsive patients (PD). The differences in IL-1R1 expression between individual groups (OR/SD/PD) were determined by one-way analysis of variance (ANOVA), followed by Fisher LSD test.

4.6. A recombinant decoy containing IL-1R1 inhibits growth *in vitro*

To address the question whether intercepting "IL-1" cytokines (which refers both to alpha and beta isoforms in the following text), would improve response to EGFR-targeted therapies, we developed an engineered cell system producing a soluble receptor, named hTRAP IL-1, comprising the extracellular domain of human IL-1R1 linked to a soluble human Fc domain of immunoglobulin G as previously described [98].

This IL-1 inhibition strategy assumes that the ligand-binding specificity of IL-1R1 would be able to sequester the majority of IL-1 ligands, thereby intercepting essential autocrine/paracrine loops. As an initial step, we designed a construct of the IL-1R1 binding domain fused to a six-histidine tag (Fig. 16A). Then, we stably transduced this construct in CRC Caco-2 cells (TRAP IL-1 cells). By Elisa assay, we confirmed that TRAP IL-1 was able
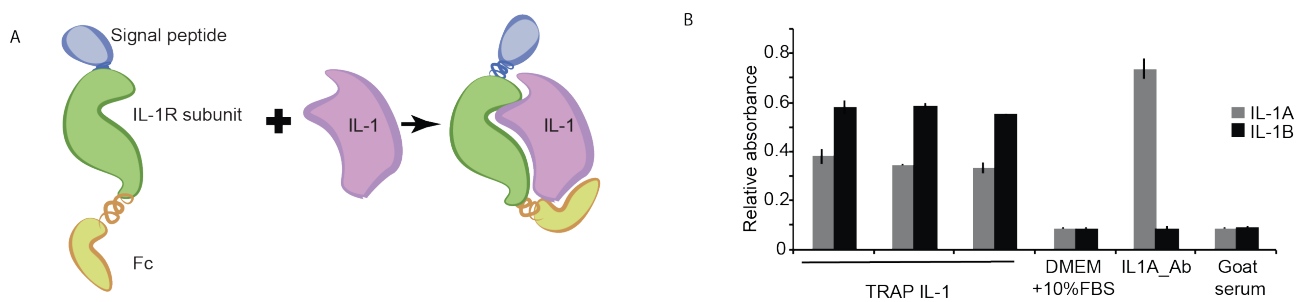

Figure 16: TRAP IL-1 recombinant decoy is able to bind IL-1A/B. (**A**) Design of the recombinant decoy hTRAP IL-1 depicting Fc, IL-1R and signal peptide subunits. Fc domain is a human immunoglobulin G. IL-1R subunit is the IL-1 binding site of human IL-1 receptor and signal peptide for the extracellular localization. Once TRAP IL-1 is secret from the cells, intercept IL-1 (both IL-1α and IL-1β) from the tumor environment preventing his agonist action. (**B**) Elisa assay testing the ability of three TRAP IL-1 clones, here referred to as TRAP 1/2/3, to specifically bind purified IL-1α/β. Briefly, 96 wells plates were coated with IL-1α and IL-1β and hTRAP IL-1 medium was added. After incubation, medium was washed out, and absorbance was detected. DMEM with 10% FBS and Goat serum served as negative control, a commercial anti IL-1α antibody was used as positive control.

to bind specifically the cognate ligands IL-1α and IL-1β (Fig. 16B).

Analyses of total cell lysate showed the successful stable integration of hTRAP IL-1 (Fig. 17A), which was secreted in the growing medium of TRAP IL-1 stable clones, whereas the Caco-2 control cells (Fc) displayed no product (Fig. 17B). Importantly, Fc cells displayed undisturbed proliferation and partially responded to CTX treatment, while TRAP IL-1 cells displayed impaired proliferation and enhanced ability to respond to CTX treatment (Fig.

17C). Next, we tested several colonies for the amount of secreted TRAP IL-1 in the medium. In detail, medium was collected after five days in culture and analyzed by western blot. Purified TRAP IL-1 (diluted at 10 ug) was used as a positive control (Fig. 17D). The proliferation capability and cell death in TRAP IL-1 clones was then evaluated and reported (Fig 17E). Interestingly, TRAP IL-1 positive clones displayed decreased proliferation (Fig. 17E), without significant changes in cell death (Fig. 17E), thereby excluding a toxic effect of the secreted TRAP IL-1. We then employed one of the clones characterized by high TRAP IL-1 production, for further phenotypical evaluations, confirming that cells stably overexpressing the TRAP IL-1 display impaired growth compared to the Fc control (Fig. 17F). These *in vitro* data support TRAP IL-1 adjuvant role in inferring with cell proliferation and CTX response.
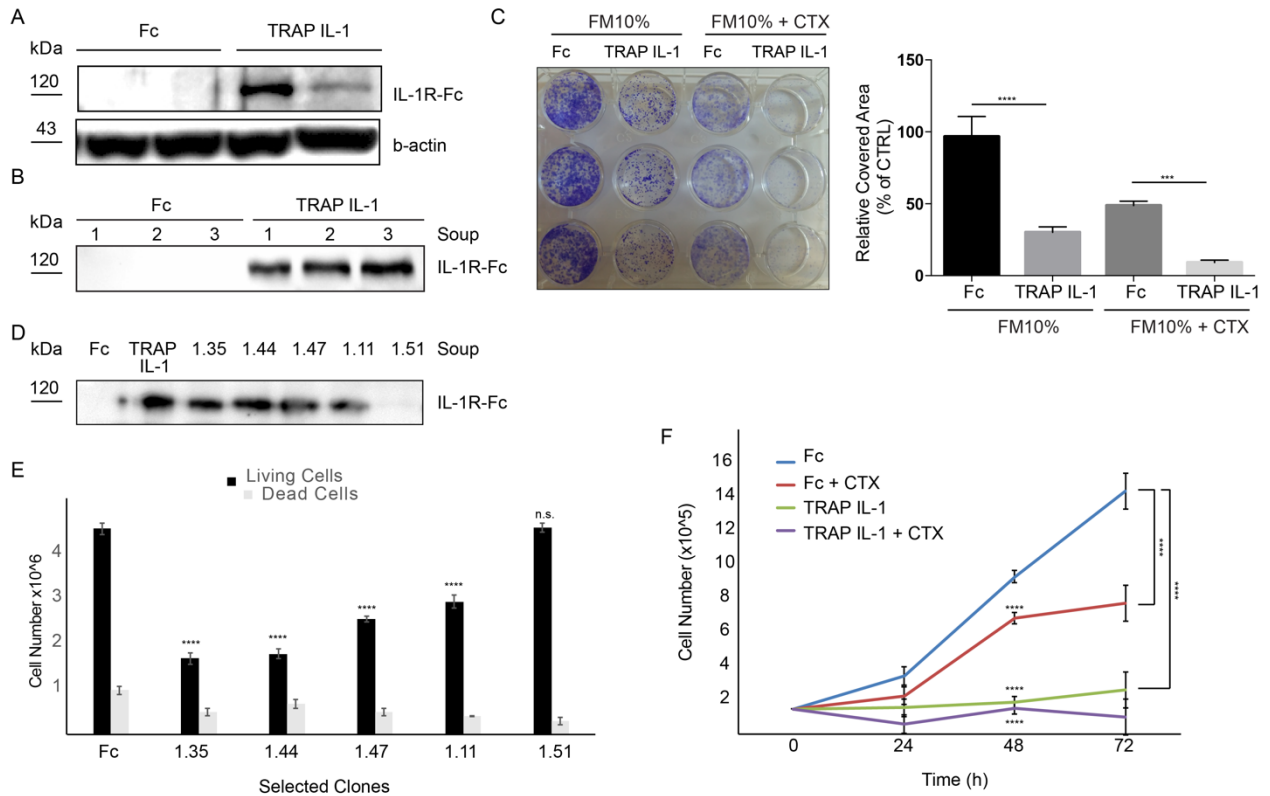
Figure 17: A recombinant decoy containing IL-1R1 inhibits Caco-2 growth. (**A**) Western Blot analysis of Caco-2 TRAP IL-1 and Fc. Actin served as loading control. 500k cells were plated in medium with 10% FBS, then cells were starved overnight (DMEM 0% FBS). The day after cells were harvested, total proteins extracted and quantified. Anti- IgG, Fc$_\gamma$ Fragment Specific human receptor monoclonal antibody was used for TRAP IL-1 detection. (**B**) Western blot analysis of three replicates of Caco-2 Fc and Caco- TRAP IL-1 soup. 500k cells were plated in DMEM supplemented with 10% FBS and after 5 days the soup was harvested and 20 μL used for Western Blot analysis. (**C**) Colony-forming assay of Caco-2 Fc and Caco-2 TRAP IL-1. 4000/well were plated and grown in the absence or presence of CTX (5 μg/mL) for 10 days in medium containing 10% of serum. Then fixed, stained with crystal violet and photographed. Representative figures (left) and quantification (right) of the covered areas by ImageJ are provided. The statistic was calculated by 2-way ANOVA, *** P<0.0005. These experiments were repeated at least three times. (**D**) Western Blot analysis of Caco-2 TRAP IL-1 clones soup. 1.35 - 1.44 - 1.47 – 1.11 and 1.51 are clones derived from a single cell. Each clone soup was collected 4 days after seeding. TRAP (purified protein) and Fc are intended as positive and negative controls respectively. (**E**) Clones from D were seeded and both living and death cells were counted. Statistical analysis was performed by one-way Anova, comparing the mean of proliferation of each clone to the control cells. Dunnet correction for multiple comparisons was applied. **** P<0.0001. (**F**) Cell count of Caco-2 Fc and Caco-2 TRAP IL-1 (clone 1.35). 100k/petri were seeded with 10% of serum. After 24h medium was changed with 10% of serum in the presence or absence of CTX (5 μg/mL) and cells were counted after 24, 48 and 72 hours. A 2-way Anova was performed, by comparing the matched values for each time point (24, 48 and 72 h) to the Fc control cells. **** P<0.0001.

4.7. TRAP IL-1 clones display decreased cancer cell spheroidogenesis in 3D

We sought to identify the phenotype of TRAP IL-1 in a defined 3D microenvironment, based on the lack of attachment to the plastic tray and forcing the cells to grow as spheroids. Fifteen days after suspending single cells in EGF supplemented medium, Fc cells formed hollow lumen cysts (Figure 18A). Similarly, TRAP IL-1 expressing cells were also able to form spheroids cyst-like structures, but these appeared rounded and smoother than the Fc counterpart (Fig. 18A). Next, we evaluated the Fc derivative both for colonsphere size and number. Fc appeared smaller than TRAP IL-1, which on the counterpart retained a decreased ability to form spheres (Fig. 18B). Indeed, by measuring more than 200 spheroids per condition, we found that the average size of TRAP IL-1 was larger than Fc, but the number of spheres was significantly lower (Fig. 18C).

By confocal microscopy, we analyzed the inner organization of Fc and TRAP IL-1 spheres. Fc spheres appeared loose and with low nuclear density on the outermost layer, while TRAP IL-1 displayed a pronounced nuclear density and an overall organization, suggesting an increased cell polarity. Fc displayed enhanced actin accumulation at the internal surfaces lining the central cavity, with a clear lumen, which was present in the majority of the cells.

These results are in line with previous reports by time-lapse microscopy suggesting that the hollow lumen occurs through a process of internal expansion without cell proliferation or cell death [114,115]. On the other hand, TRAP IL-1 still retained a wide and hollow lumen, but the cyst-like formation was much more emphasized in comparison to the control, while the ability of forming spheres was dramatically decreased in these cells (Fig. 18B-D). These data suggest a role for the TRAP IL-1 decoy in impacting on CRC growth both in monolayers and in 3D.
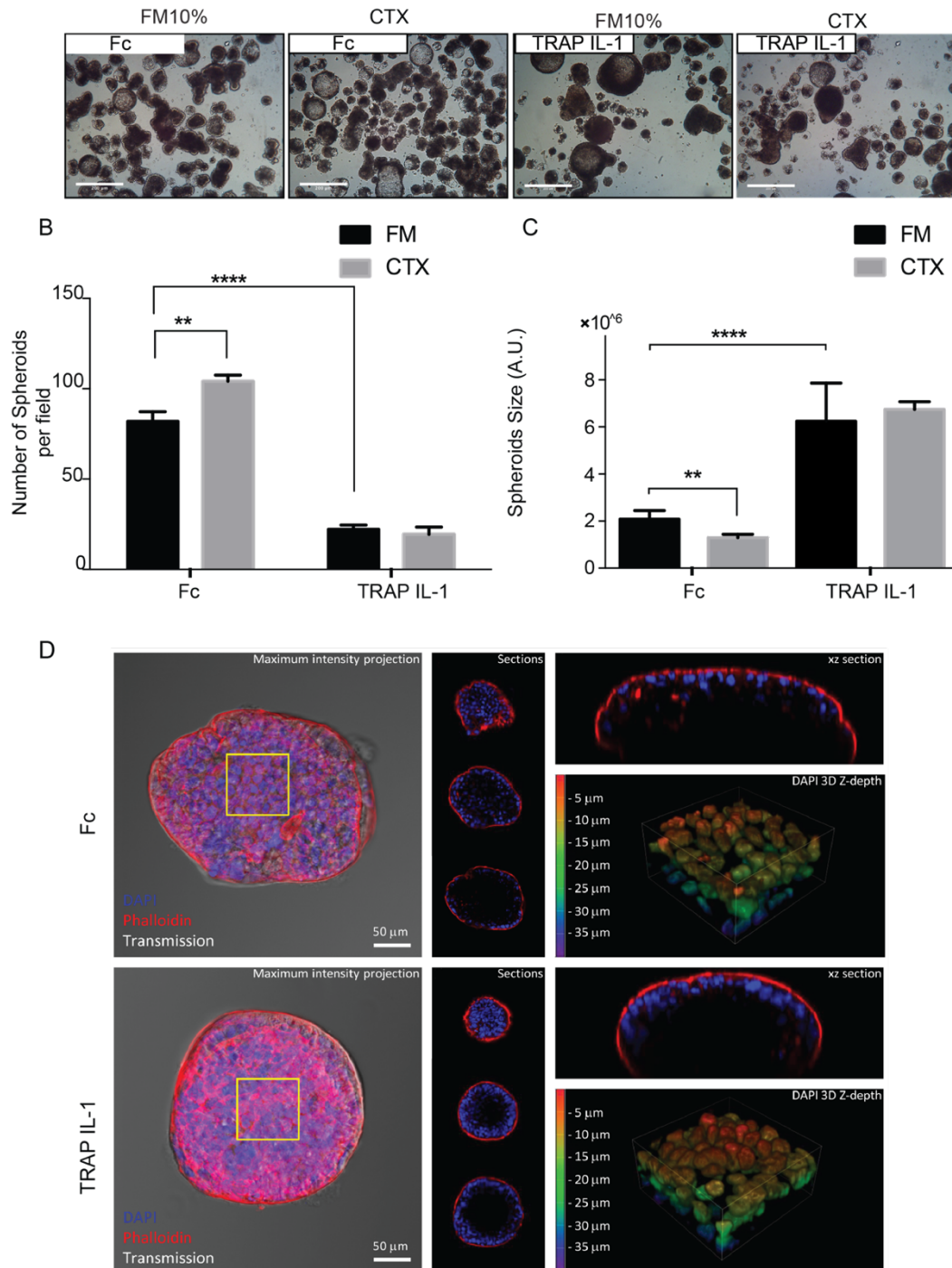
Figure 18: Caco-2 TRAP IL-1 displays decreased growth in suspension as colonspheres. (**A**) 4X magnification of Caco-2 Fc and Caco-2 TRAP IL-1 producing "spheroid-like" structures, under the indicated treatments. Scale bar 100 μm. (**B**) Number of filled spheroids presented as average ± S.E.M. 2-way ANOVA with Bonferroni Test, ** p<0.01; ****p<0.0001; (**C**): Quantification of spheroid size measurements under the indicated treatments in 10% FBS supplemented with EGF 10 ng/mL and CTX 5 μg/mL. Columns represent volume averages ± S.E.M, 1-way ANOVA, ** p<0.01; ****p<0.0001; (**D**) 3D confocal microscopy of colonspheres Fc and TRAP IL-1. In the left panel is reported the DAPI and phalloidin staining. In the middle panel are featured single optical sections collected at 15 μm intervals. In the panel on the right, the xz optical section passing through the maximum diameter of the spheroids (upper part) and 3D rendering focused on the nuclear density and z-depth of the spheroids (yellow square), reported as a scale of colors, red indicates a 5 μm depth and blue 35 μm depth (bottom part).

4.8. IL-1 pathway inhibition impairs MAPK signaling

In order to verify if the functional secreted and soluble TRAP IL-1 was able to neutralize IL-1 ligands, we treated Fc and TRAP IL-1 cells with IL-1α (10 ng/mL) over a long-time course, up to 24 hours. We analyzed both the mitogen activated protein kinase (MAPK) and the AKT axes. IL-1α treatment displayed an immediate mild activation of both ERK and AKT signals, followed by a secondary enhanced and delayed activation, as reported in the quantification in figure. 19B. According to these results, TRAP IL-1 was able to nullify the action of IL-1 on MAPK signaling activation, thus proving an effective neutralization of IL-1 stimulus *in vitro*. Furthermore, TRAP IL-1 production spared the basally active ERK and AKT. Interestingly, both ERK and AKT displayed a bimodal activation (Fig. 19B), which was also blunted by TRAP IL-1. Next, we tested the abundance and the activation of EGFR under IL-1α stimulus, by measuring the phosphorylation of tyr1068. We detected an increase in EGFR abundance and phosphorylated EGFR upon 3 hours of IL-1α treatment. This effect could be related to an impaired degradation followed by a fast recycling of the receptor to the cell surface, a phenomena well described under TNFα or UV stress [116]. Secondarily, we detected a new hit of phospho-EGFR at 12 hours of treatment, which was not followed by an enhanced EGFR protein, and it was consistent with the bimodal activation of MAPK and AKT. These data suggest that IL-1 boosts EGFR levels and that a positive feedback loop engaged by IL-1R1 stimulation may be responsible for sustaining the MAPK and AKT signals, through secondary activation of EGFR pathway. TRAP IL-1 was able to blunt EGFR production with a very low amount of pEGFR, an effect attributable to a decreased EGFR abundance, which might explain an overall lower activation of the downstream signaling pathways (Fig. 19A and C).

Moreover, TRAP IL-1 is influencing endogenous expression of IL-1R1, which is stable in control cells under IL-1 treatment, but it appears downregulated in TRAP IL-1 cells. We speculate that this is the consequence of a chronic sequestration of IL-1 that might be responsible for a loss of dependency from this receptor in this cell system (Fig. 19C).

To sum up, these results indicated that secreted TRAP IL-1 molecules successfully dampen EGFR abundance and lead to a decreased activation of ERK and AKT.
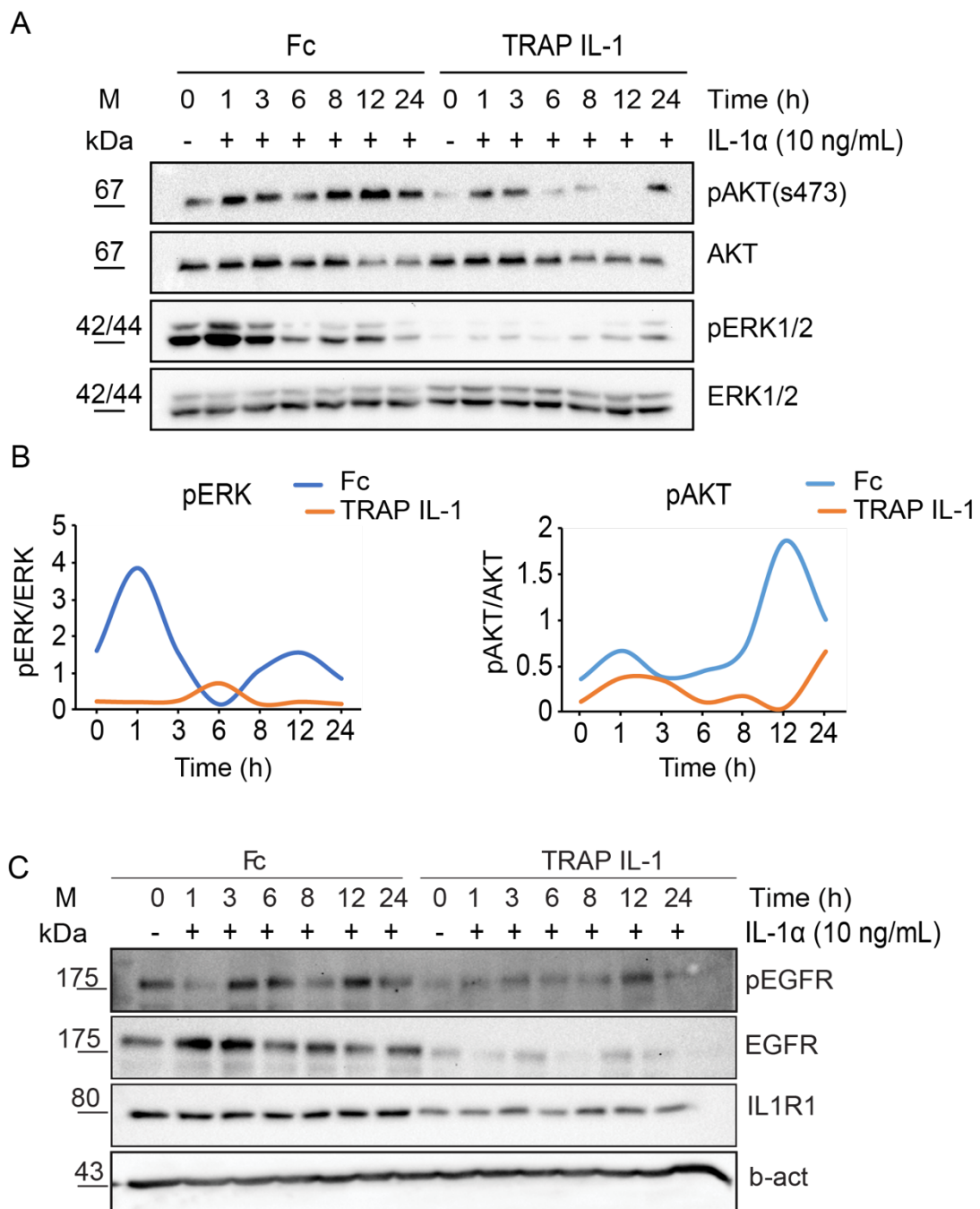

Figure 19: Bimodal activation of ERK and AKT after stimulation with IL-1A. (**A**) Western blot analysis of phospho-AKT s473 (pAKT) and phospho-ERK (pERK) levels in Caco-2 Fc and Caco-2 TRAP IL-1 (time course). At day one, 500k cells were plated for each condition in medium with 10% FBS. At day 2, cells were starved overnight (DMEM 0% FBS) and the day after IL-1A (final concentration 10 ng/mL) was added to the medium of growing cells for 1, 3, 6, 8, 12 and 24 hours. After treatment cells were harvested, total proteins extracted and quantified. Monoclonal antibody against total AKT and ERK1/2 served as loading control. (**B**) Quantification of pAKT and pERK by Image Lab is provided. (**C**) Western blot analysis of phospho-EGFR Tyr1068, EGFR and IL-1R1 in Fc and TRAP IL-1 cells treated as in A. B-actin served as loading control.

4.9. IL-1 receptor abundance predicts relapse-free survival in CRC patients

IL-1α and IL-1β signal through the same receptor complex. The response is initiated when the ligand binds to its primary receptor subunit IL-1R1 [81]. The receptor contains extracellular immunoglobulin domains and a Toll/IL-1 receptor domain in the cytoplasmic portion. Binding of the ligand allows the recruitment of a second receptor subunit the IL-1R1 accessory protein (IL-1RAP). Formation of the receptor heterodimer induces signaling because the juxtaposition of the two Toll/IL-1 receptor domains enables the recruitment of myeloid differentiation primary response protein 88 (MYD88), IL-1R1 associated kinase 4 (IRAK4), tumor necrosis factor receptor-associated factor 6 and other signaling intermediates [91]. *In vitro,* our data pointed to an involvement of IL-1 in tumor growth and the lack of response to EGFR interception. We further addressed the question of IL-1R1 expression associated with CRC progression in patients by performing a bioinformatic study in a cohort of 2166 CRC patients [117]. The Kaplan Meier estimated the fraction of CRC patients resected for colorectal cancer and having a follow-up of a period of 200 months. We compared the relapse free survival (RFS) of 1211 patients, by splitting the dataset according to each cut off level between the lower and upper quartile of the expression level of the IL-1R1 gene. We computed false discovery rate (FDR) to correct for multiple testing, and accepted only results with a FDR below 5%. The initial analysis was not restricted to specific categories, and interrogated the entire dataset. We distinguished two sets of patients with high and low IL-1R1 mRNA (probe 202948_at) expression respectively, and the association with patient survival. High levels of IL-1R1 were predictive of a worse disease-free survival and death with an HR of 1.75 and P-value of 1.6 $e^{\wedge-06}$. Median relapse-free survival was 21 months and 66 months in the low and high IL-1R1 expression cohort, respectively.

These results highlight the role of IL-1R1 in CRC patients and suggest that IL-1R1 interception could represent an effective clinical strategy to improve prognosis and survival. Next, we attempted to stratify colorectal tumors into unique features according to their genetic profiles. We employed the consensus molecular subtype (CMS) as classified by Guinney et al. [45]. They showed a marked interconnectivity among six independent classification systems coalescing into four CMSs with distinguishing features; CMS1

(microsatellite instability-immune), covering about 14% of CRC tumors, CMS2 encompassing the canonical subtype with epithelial markers, CMS3 characterized by a metabolic dysregulation, and CMS4 with TGFβ activation, stromal invasion and angiogenesis. The abundance of IL-1R1 appears higher in CMS4 and CMS1, than in CMS2 and CMS3 (Fig. 20B). IL-1R1 had a strong impact on patient survival in the CMS1 subtype (Fig. 20C), with an impressive HR of 2.74 and P-value: 0.00036. We then employed the de Sousa stratification, which associates patients with three distinguished colon cancer subtypes (CCS) CCS1, CCS2 and CCS3. CCS1 patients have the lowest risk of recurrence after tumor resection compared to patients belonging to the other subtypes [41]. Interestingly, IL-1R1 overexpression is associated with more aggressive subtypes (Fig. 20D), with a strong association in CSS2, HR of 2.9 and P-value: $8.5*e^{-05}$ and in CSS3 HR of 1.55 P-value: 0.016 but in this case FDR was over 50%, whereas no subtypes [41] association was found for CSS1. Notably, IL-1R1 overexpression is also predictive of survival in the CSS3 subtype, which has very unfavorable prognosis and is refractory to EGFR-targeted therapy.
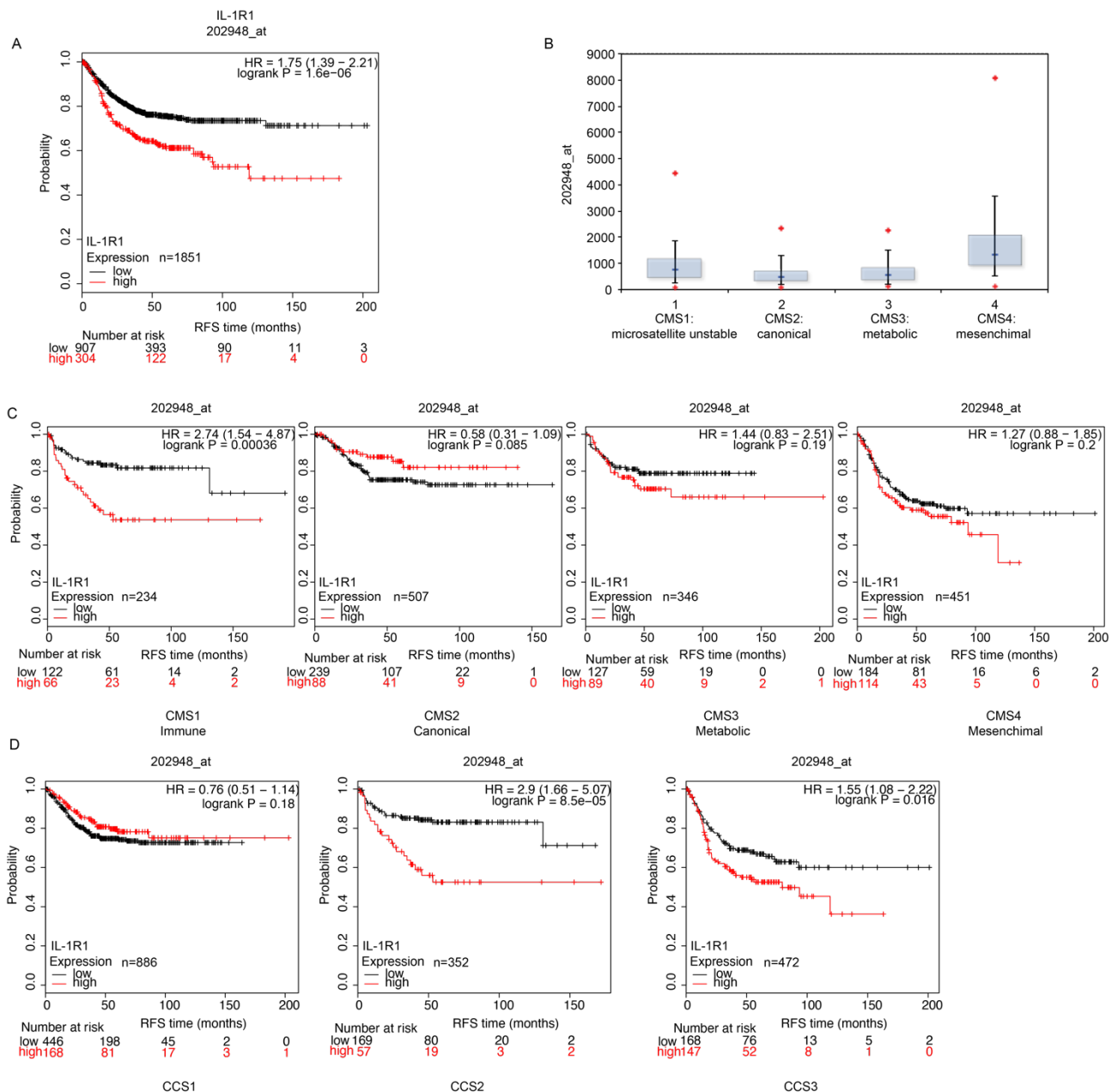
Figure 20*: **IL-1 receptor expression predicts survival in CRC patients. (A**) A cohort of 1211 patients was divided into two groups according to IL-1 receptor abundance. In the Kaplan-Meier plot, the black line represents patients with an overall low IL-1R1 expression, while the red line represents subjects with high expression of IL-1R1. For each patient, the relapse free survival (RFS) is reported over time and expressed in months. (**B**) mRNA abundance of IL-1R1 in the four consensus molecular subtypes (CMS) subtypes. (**C**) Stratification of patients using the CMS criterion. Patients are divided into four subtypes. CMS1 (Immune): hypermutated, microsatellite unstable and strong immune activation. CMS2 (Canonical): epithelial, marked WNT and MYC signaling activation. CMS3 (Metabolic): epithelial and evident metabolic dysregulation. CMS4 (Mesenchymal): prominent transforming growth factor-b activation, stromal invasion and angiogenesis. (**D**) KM plot of IL-1 receptor expression using de Sousa Classification of Colon Cancer subtypes.

4.10.   HERK293T engineering with TRAP IL-1 and clones selection

HEK293T cell line were engineered with a recombinant decoy namely Fc-IL1R1 (hereafter referred to as TRAP IL-1), which is able to sequester both IL-1α and IL-1β from the medium. Cells engineered with the recombinant protein containing only the Fc domain has been used as negative control (Figure 21A). From a heterogeneous population of engineered cells, we isolated single cell clones by serial dilution (Fig. 21A) and selected the most efficient TRAP IL-1 producing clone. As TRAP IL-1 is a soluble protein, we sought to verify the abundance of TRAP-IL1 in several clones medium. This assay was successfully applied to colon cancer cells (Caco-2) as reported in Gelfo et al., Cancers 2018[69], proving feasible obtaining cells secreting TRAP IL-1.
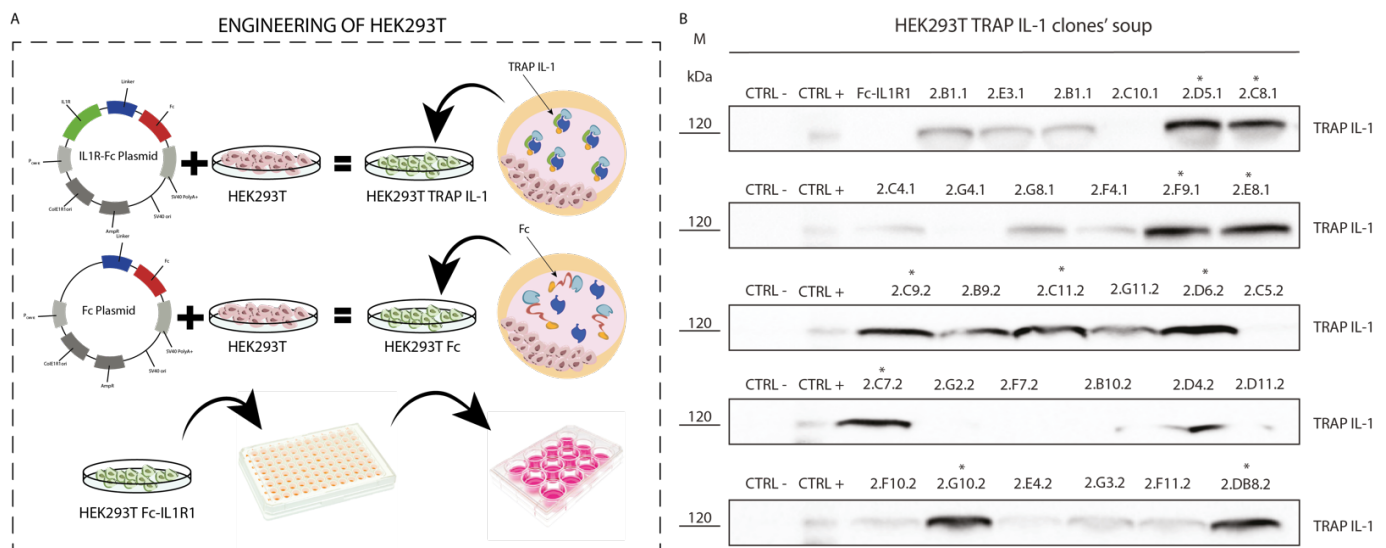

Figure 21. TRAP IL-1 recombinant decoy is released in engineering HEK293T TRAP IL-1 medium. (**A**) Engineering of HEK293T cells with TRAP IL-1 and Fc (CTRL). HEK293T TRAP IL-1 cells have been seeded at single cell dilution, in a ninety-six-well plate following puromycin selection (1 ug/mL). After colony growth, cells have been transferred and expanded in six- well plates and T25 flasks. (**B**) Western blot of clones' soup. 500.000 cells for each clone has been seeded at day 1. After 5 days soup of different clones has been collected, centrifuged and tested for the presence of TRAP IL-1 using a human anti-Fc antibody. * Clones 2.C8.1 and 2.F9.1 have been chosen for TRAP production.

Once the best TRAP IL-1 producing clones, namely HEK293T TRAP IL-1 2.C8.1 and 2F9.1 (Fig. 21B) have been identified, TRAP IL-1 has been isolated from growing medium following the protocol detailed in figure 22A and material and methods section. Total amount and purity of TRAP IL-1 has been assessed by Western Blot (Fig. 22B) and quantified (Fig. 22C)
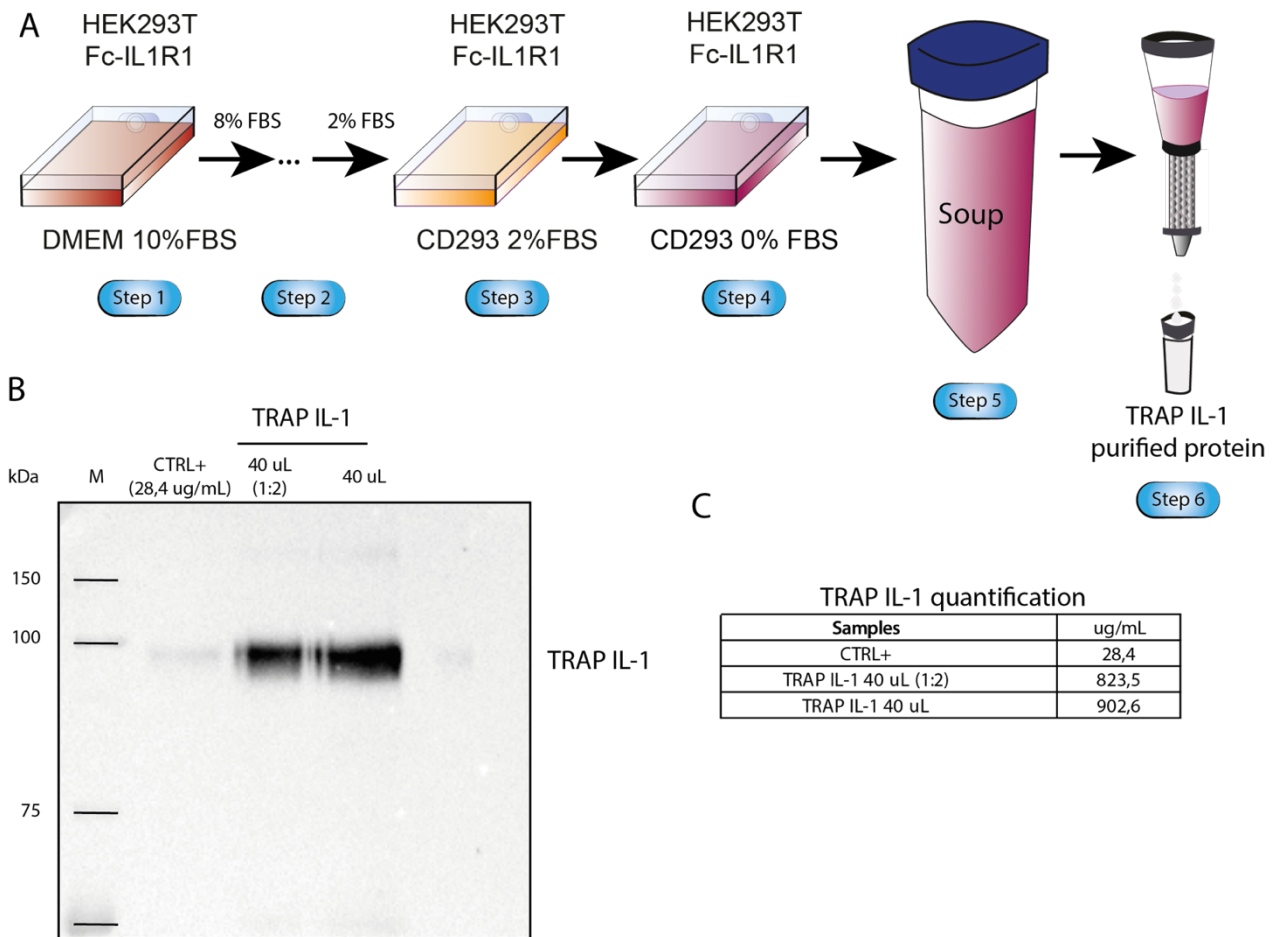

Figure 22: Purification, control quality and quantification of TRAP IL-1 recombinant decoy. (**A**) graphical scheme depicting TRAP IL-1 isolation steps. For a detailed description of TRAP IL-1 isolation steps refer to material and methods section. (**B**) Western Blot analysis of TRAP IL-1 recombinant protein following isolation as in A. in details, lane 1 is the CTRL+, with a concentration of 27 µg/mL (diluted 1:20 from a mother stock of 554 ug/mL). Lane 2 and 3, is TRAP IL-1 diluted 1:2 and not diluted respectively isolated following the protocol in A. (**C**) TRAP IL-1 quantification was performed using ImageLab software calculating the volume of the bands compared to the CTRL+.

4.11. MC38 cell line engineered with the murine EGFR (mEGFR) and GFP

To address the question whether intercepting IL-1 (which refers to both alpha and beta) would improve response to anti-EGFR therapies *in vivo*, we employed a murine colon adenocarcinoma MC38 cell line (kindly provided by Prof. M. Colombo, Istituto Nazionale Tumori). As MC38 cells line expresses EGFR at low level we transfected with murine Egfr (MC38_mEgfr). MC38_mEgfr cell line was employed for a syngeneic engraftment in C57BL/6N immunocompetent mice.

After drug selection, from a heterogeneous cell population of engineered cells we isolated MC38 mEgfr single cell clones by serial dilution. Total mEgfr protein of the cell lysate of five MC38 mEgfr different clones (1.F6, 1.C3, 1.G11, 1.B3 and 1.F2) was tested (Fig. 23A). As shown in figure 23A MC38 control cells (MC38 CTRL-) displayed no mEgfr protein level while clone 1.C3.1 resulted as the best clone expressing mEgfr and, employed for subsequent experiments.

Tumors heterogeneity has been addressed as the main culprit for multiple escaping mechanisms, reflecting the high level of molecular heterogeneity in each metastatic site. Metastasis formations include the dissemination of cancer cells from a malignant tumor and seed in distant sites inside the body and, for CRC patients lungs and livers are the major organs where metastasis disseminate. In order to evaluate whether intercepting IL-1 in combination with EGFR *in vivo* prevent metastasis formation, we obtained stable GFP-expressing MC38 and MC38 mEgfr cell lines. We infected MC38 and MC38 mEgfr with GFP viral particles and obtained respectively MC38 – GFP and MC38 mEgfr – GFP cell line as shown in figure 23B. In order to quantify the percentage of GFP expressing cells we analyzed MC38-GFP and MC38 mEgfr – GFP by cytofluorimetry. 46,14% of MC38 and 41,76% of MC38 mEgfr resulted GFP positive.
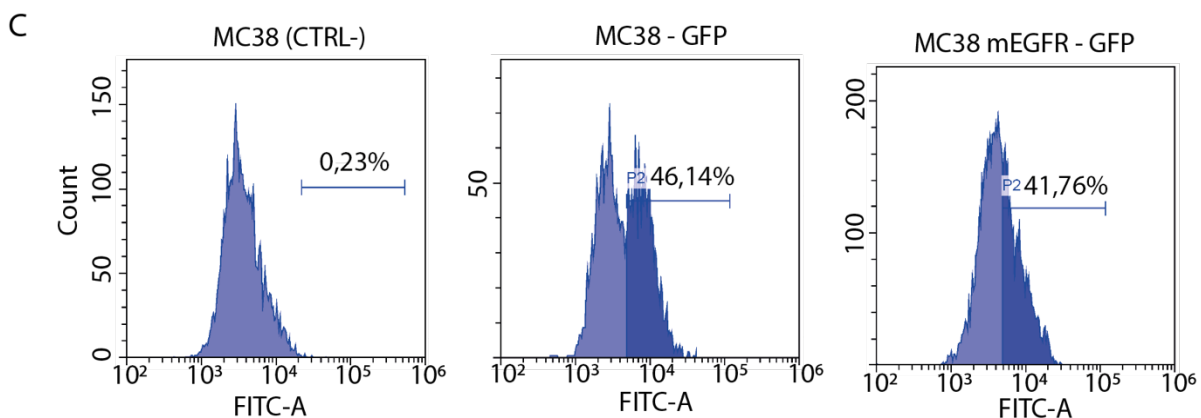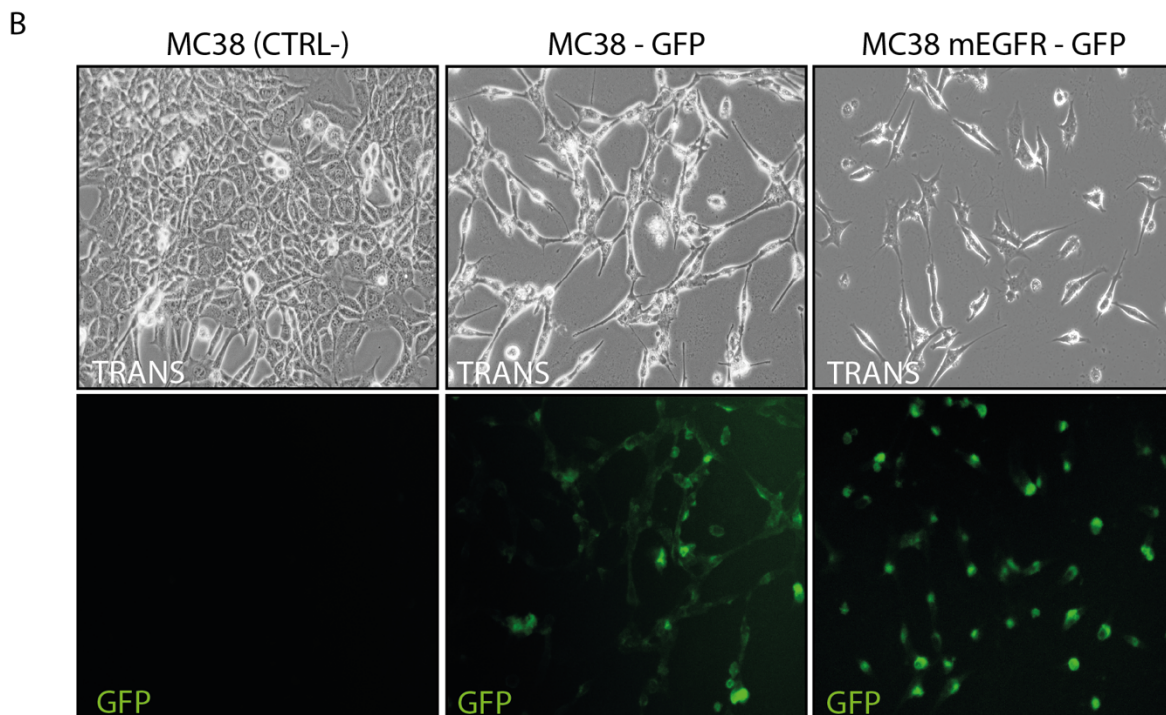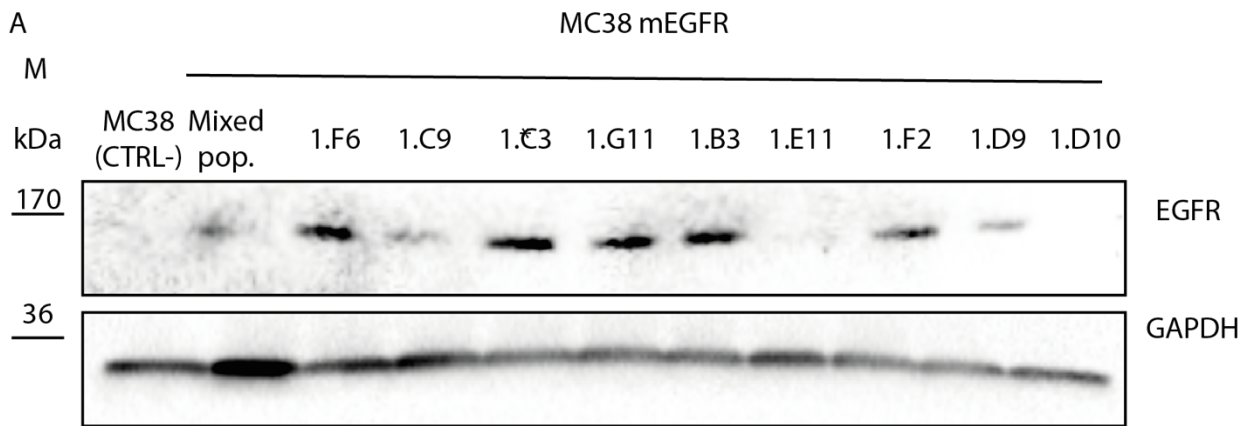
Figure 23: MC38 and MC38 mEGFR cell line were engineered with GFP. (A) Western Blot analysis of MC38 cell line engineered with murine Egfr (mEgfr). MC38 mEgfr mixed population was drug selected and plated in a 96 well plate for single cell dilution. Clones of MC38 mEgfr (1.F6, 1.C9, 1.C3, 1.G11, 1.B3, 1.E11, 1.F12, 1.D9 and 1.D10) heterogeneous population clones were tested for Egfr level. Clone 1.C3 was chosen for subsequent experiments (**B**) Photos depicting bright field (TRANS) and GFP channel of MC38 (CTRL) MC38 – GFP and MC38 mEgfr – GFP (clone 1.C3). (**C**) quantification of GFP-positive MC38 and MC38 mEgfr cells by cytofluorimetry. 50.000 events were detected for each condition.

4.12. MC38 engineered with murine EGFR displayed a more migratory and invasive phenotype

Next, we characterize the invasive phenotype of MC38 mEgfr, in vitro. For this reason, we performed a scratch-wound assay comparing MC38 naïve cell with MC38 mEgfr cells following the wound healing for 12 hours. In these settings, we observed that MC38 mEgfr displayed a more invasive phenotype when compared to MC38 control cells as shown from the quantification panel (Fig. 24B). Accordingly, the invasive phenotype was detected through a Gelatin Degradation Assay, where cellular invasion is evaluated by gelatin degradation. This assay is designed to quantify invadopodia formation and activity indicating the ability of cancer cells to invade and metastasize. MC38 and MC38 mEgfr cells were seeded in a coverslip covered by a layer of gelatin for 24 hours. After, fixation and phalloidin and DAPI staining, gelatin degradation was analyzed. In this setting MC38 mEgfr cells displayed an impressive degradation of the gelatin represented by several large black area and quantification (Fig. 24C and D respectively). These data suggested that MC38 mEgfr cell have a higher migratory phenotype and a striking invasive phenotype compared to MC38 naïve counterpart.

Next, we sought to verify in vivo, whether IL-1 interception enhances response to CTX. As CTX is a chimeric mouse:human mAbs employed in the clinic for mCRC patients, its efficacy is specific for human EGFR only. C57/BL6 mouse model will allow us to study the interplay between tumor-derived IL-1 and the host immune system. In order to verify immunological compatibility of MC38 mEgfr cells in vivo settings, we inoculated C57BL6 mice with MC38 and MC38 mEgfr cells and observed an initial slower growth of MC38 mEgfr tumor compared to MC38 CTRL tumors, followed by a sustained growth after 18 days from inoculation (Fig 24E). Next, we investigated the morphology of tumor tissue preparing 5 μm slides and staining with hematoxylin-eosin (H&E) (Fig. 24F). In H&E staining MC38 mEgfr tumor tissue displayed a very high cellular density when compared to MC38 tumor tissue as shown in the 20X magnification (Fig. 24F). This result corroborates the immunological compatibility of MC38 mEGFR cells in C57BL/6 mouse model.
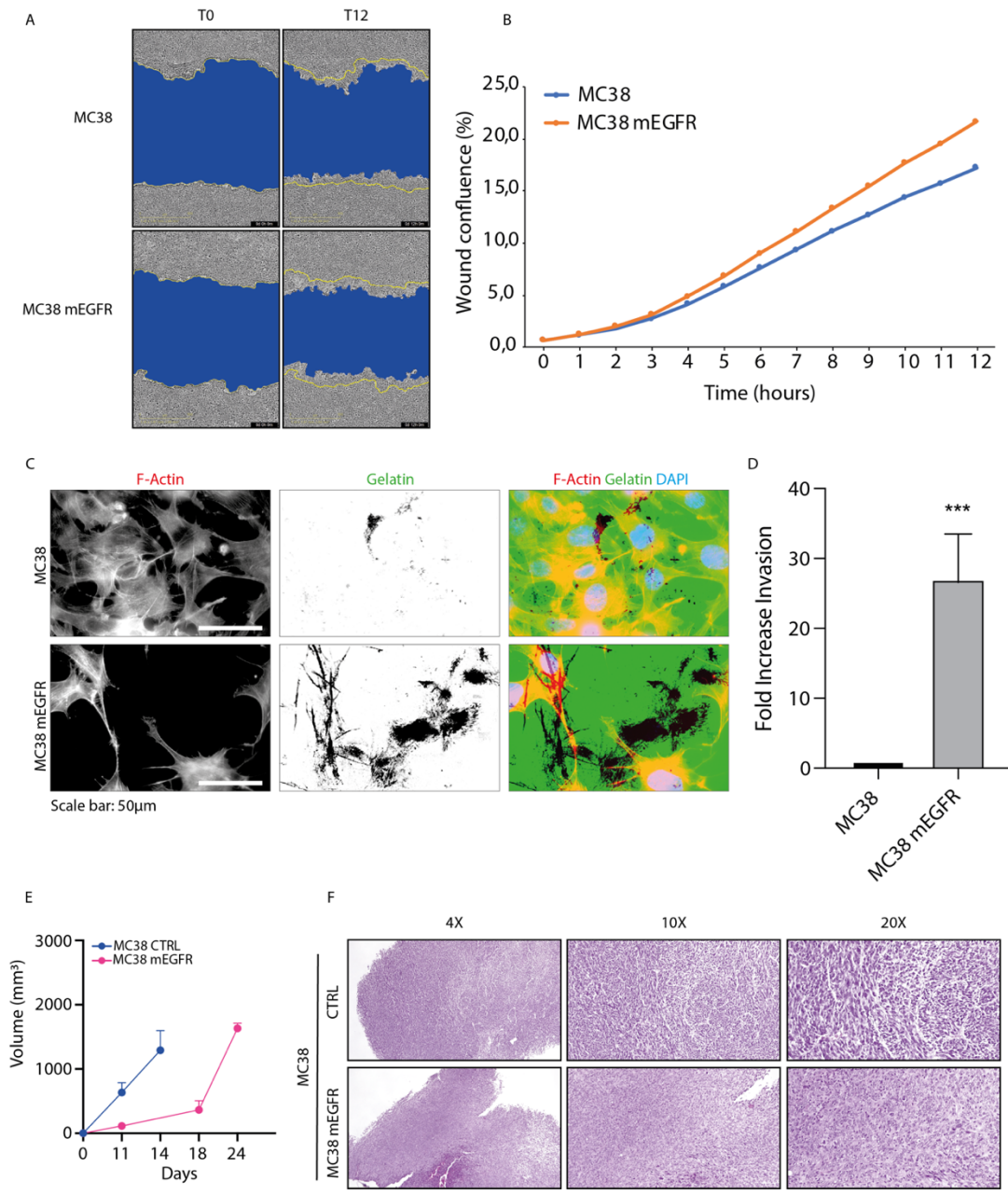
Figure 24: MC38 mEGFR cells in vitro and in vivo characterization. (**A-B**) Scratch assay was performed in murine MC38 and MC38 mEgfr cell. 75.000 cells per well were seeded in a 96-well plate. The day after a wound has been created. After washed with PBS cell invasion was followed in time-laps for 12 hours. Representative images (A) and quantification (B) are provided. (**C-D**) Gelatin Degradation Assay of MC38 and MC38 mEgfr were seeded in a coverslip covered with a layer of gelatin for 24h. Cells were fixed stained with phalloidin and DAPI and gelatin degradation was detected. The fluorescent microscope detects Alexa 488 (Oregon Green), Alexa 568 (Phalloidin), and DAPI. Gelatin degradation is detected in the green channel (Oregon Green conjugated gelatin) as dark area against the bright green background (Gelatin). The statistic was calculated by T-student Test. (**E**) 1000.000 MC38 mEgfr and MC38 (CTRL) cells were inoculated on the right flank of C57BL6 mice. Tumor volume was measured after 11, 14, 18, 24 days after cells inoculation. MC38 and MC38 mEgfr mice were sacrificed after reaching the limiting size (14 days and 24 days respectively). (**F**) MC38 and MC38 mEgfr tumors were fixed in formalin and paraffin embedded. 5 um slides were obtained for Hematoxylin-Eosin (H&E) staining. Stained slides were photographed at 4X, 10X and 20X magnification for morphology evaluation.

4.13.   Engineering of a murine recombinant decoy comprising IL-1R1

Next, we aimed to develop a recombinant decoy TRAP-Fc (namely TRAP IL-1) able to sequester IL-1 from tumour environment in immunocompetent C57BL/6 mice. TRAP-Fc is a technology already in place for several years. For example, a recombinant protein comprising ErbB-1 and ErbB-4 extracellular domain has been proved to inhibit tumorigenic growth of human cancer cells in athymic NCr-nude mice [98]. Also, our previous studies proved that a functional secreted and soluble human TRAP IL-1 is able to dampen cells growth both in monolayer and 3D environment[69]. Unfortunately, a lack of immunological compatibility and strong immune host reactivity against human TRAP IL-1 was expected. For these reasons, we developed a murine version of human TRAP IL-1 (hereafter referred mTRAP IL-1). A schematic representation and sequence comprising the subunits of mTRAP IL-1 is shown in figure 25 A and B. Thus, we cloned in-frame, into pIRES expression vector, the extracellular domain of murine IL-1R1 and Fc domain of murine immunoglobulin G (mFc). mIL1-R1 and mFc were fused and inserted into pIRES plasmid.

For the mIL-1R1 subunit, we performed a PCR employing as template ID8 cDNA library and employed specific primers designed as follows: XhoI restriction enzyme site, Kozak, leader and part of mIL-1R1 sequence for forward primer while part of mIL-1R1, liker and part of mFc sequence are present in reverse primer (Fig. 25B, lower part). We obtained mIL-1R1 PCR product of 1068 bps, then extracted and purified from gel

For the mFc subunit, we performed a PCR employing as template pIRES mTRAP (ERBB4-EGFR)-Fc (kindly provided by Y. Yarden lab) and employed specific primers designed as follows: part of mIL-1R1, linker and part of mFc sequence for forward primer while in the reverse primer part of mFc and XhoI restriction enzyme site sequence (Fig. 25D, lower part) are present. We obtained mFc PCR product of 771 bps, then extracted and purified from gel. Then, we fused mIL-1R1 and mFc (mTRAP IL-1 insert) by PCR obtaining the complete insert of 1765 bps (Fig. 25E),
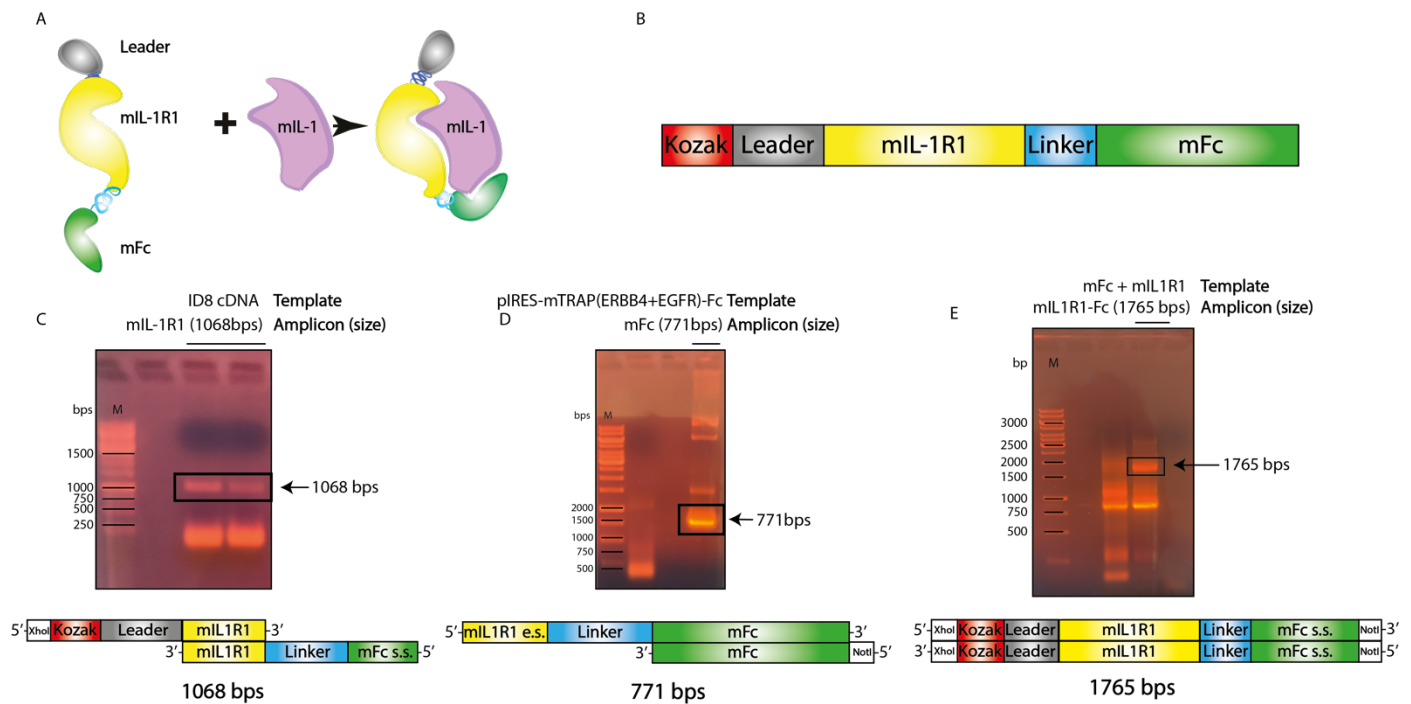
Figure 25: Engineering of pIRES mIL1R1-mFc vector. (**A**) Schematic representation of murine IL1R1 recombinant decoy (mIL1R1-Fc) depicting its ability to bind IL-1. (**B**) Linear structure depicting Kozak (red), leader (grey), Mus musculus IL1R1 extracellular domain (mIL1R1 yellow), linker (blue) and murine Fc domain of immunoglobulin G (mFc, green). (**C**) Mus musculus extracellular domain of IL1R1 (mIL1R1) obtained by PCR (upper part) using as template ID8 cDNA library. Schematic representation (lower part) of mIL1R1 depicting XhoI restriction site (white), Kozak (red), leader (grey), mIL1R1 (yellow), linker (blue) and starting sequence of mFc (mFc s.s.). (**D**) *mus musculus* Fc domain of immunoglobulin G (mFc) obtained by PCR (upper part) using as template pIRES mERBB4-EGFR-Fc plasmid[98]. Schematic representation (lower part) of mFc depicting mIL1R1 ending sequence (mIL1R1 e.s., yellow), linker (blue), mFc and NotI-HF restriction site. (**E**) mIL1R1 obtained fusing by PCR amplicon in C and D.

4.14. mTRAP IL-1 insert ligation, amplification, and sequence analysis

After we cloned mTRAP IL-1 insert into pIRES plasmid vector (Fig. 26A), as detailed in the Material and Methods section, we obtained the pIRES mTRAP IL-1 plasmid vector (Fig. 26B). PCR of pIRES mTRAP IL-1 (template) was performed utilizing primers specifically designed covering mTRAP IL-1 insert (Fig. 26C PCR – bacteria colonies). From PCR amplification we obtained a specific band of 1751 bps from colony 1, 2, 4 and 5 while from colony 3 we do not obtain a specific band (Fig. 26C PCR-bacteria colonies lane 3).). pIRES mTRAP IL-1 from colony 5 was chose for digestion with XhoI and NotI. After XhoI and NotI digestion we obtained a specific band of 1774 bps while in the CTRL a specific band was not detected (Fig. 26C Digestion). In order to exclude genetic aberration occurred during the cloning and amplification process we analyze the sequence of mTRAP IL-1 by Sanger technique. From Sanger analysis we excluded the presence of mismatch or gap in the entire sequence analyzed (Fig. 26D).

Also, we engineered and drug selected HEK293 cell line with mTRAP IL-1 (HEK293T mTRAP IL-1) as this cell line is routinely used for antibody production and has the ability to fast growth in a serum-free, protein-free, chemically defined medium optimized for the growth in suspension and burst the production of recombinant proteins. In order to prove stable integration and production of mTRAP IL-1 protein into the cell medium we detected mTRAP IL-1 protein in the cell medium of HEK293 mTRAP IL-1 cells employing an anti-mFc secondary antibody in non-denaturating condition (Fig. 26E). Purified mTRAP IL-1 protein will be employed in vivo, in combination with anti-EGFR antibody for IL-1R1 and EGFR blockade.
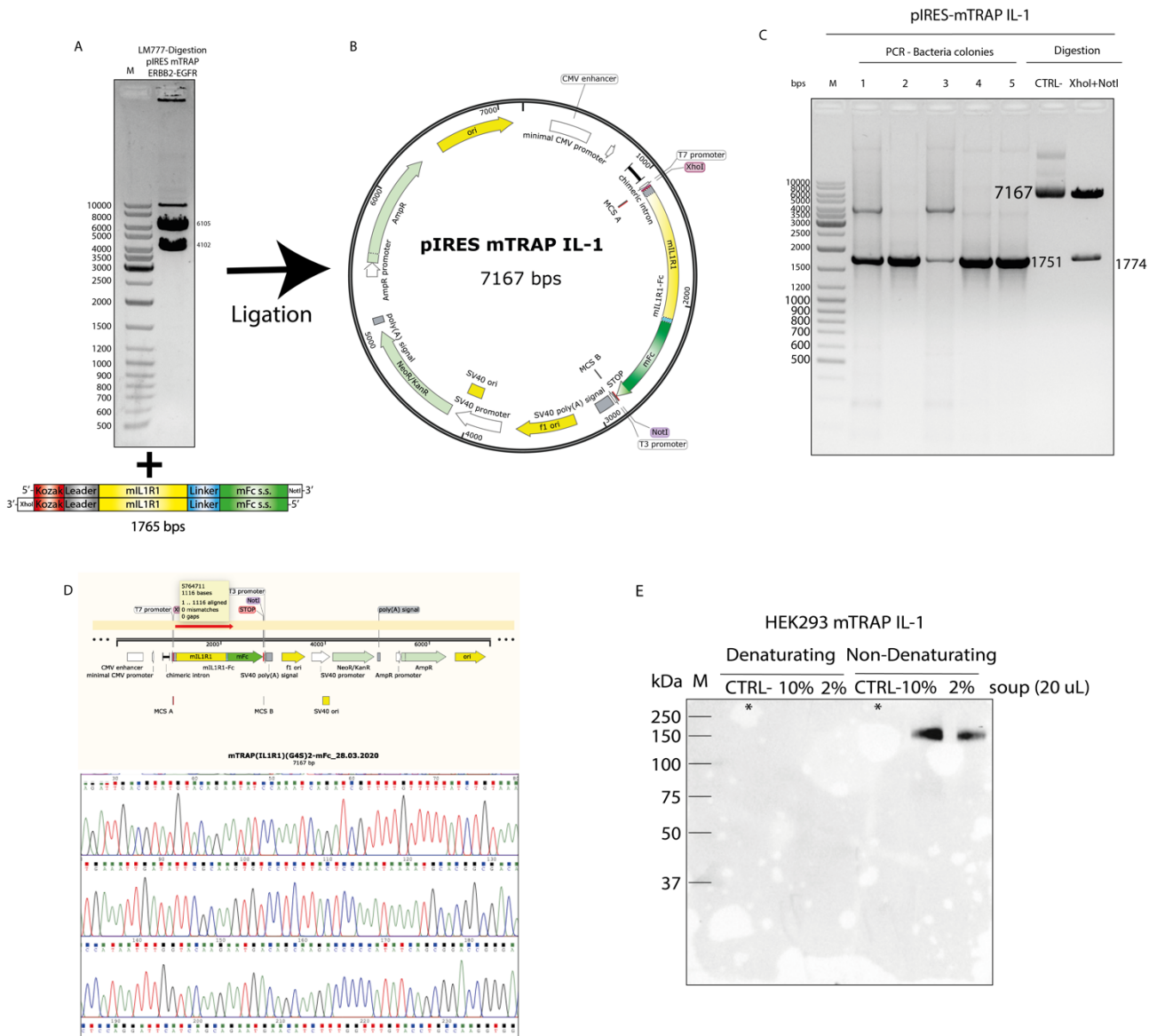
Figure 26: mTRAP IL-1 cloning. (**A**) pIRES mERBB4-EGFR-Fc plasmid was digested with XhoI and NotI restriction enzymes, (gel extracted (pIRES only) and ligated with mIL1-1R1 insert (pIRES mTRAP IL-1). (**B**) Schematic representation depicting pIRES mIL1R1-Fc obtained by ligation of mIL1R1 and pIRES vector. (**C**) pIRES mTRAP IL-1 plasmid vector was amplified in bacteria and extracted from five different bacteria colonies (1-5) and used as template for PCR amplification. Primers specifically designed covering mTRAP IL-1 insert sequence (1751 bps size) were used. pIRES mTRAP IL-1 from colony 5 was chose for digestion with XhoI and NotI. (**D**) Sanger analysis of mTRAP IL-1 sequence. (**E**) Western Blot analysis of HEK293 mTRAP IL-1 soup. 20 uL of soup were employed for each denaturating and non-denaturating setting (CTRL-, 10% and 2%). Soup has been collected, centrifuged, and tested for the presence of TRAP IL-1 using a mouse secondary antibody (Dako K4001, diluted 1:250).

4.15. IL-1 stimulus stabilizes EGFR activation in MCF10 cell line

In order to study the mechanism of IL-1 in EGFR pathway, avoiding perturbation derived from tumor transformation, we employed MCF10A, a *quasi*-normal mammary cell line highly dependent on EGFR, representing a useful tool for study EGFR signaling[68]. Thus, we assessed the effect of IL-1A and IL-1B assuming an overlapping biological activity, analyzing EGFR and the two major axes controlled by EGFR, namely mitogen activated protein kinase (MAPK) and AKT. For these reasons, we treated MCF10A cells with IL-1A (10 ng/mL) alone or in combination with EGF, over a time course, up to 2 hours. IL-1A treatment displayed a specific pattern where pEGFR, pAKT and pERK showed lack of activation while total EGFR, under the same stimulus, displayed immediate activation with an increased protein level after 10 minutes maintained up to two hours of treatment with a peak after 120 minutes from stimulus (Fig. 27A). Interestingly, when IL-1α is combined with EGF, the activated form of EGFR (pEGFR) displayed an immediate peak after 10 minutes from stimulus and a delayed decrease until 60 minutes from stimulus when compared to EGF stimulus alone. Also, the downstream activated form of AKT (pAKT) and ERK (pERK) displayed a delayed decrease when compared to EGF stimulation alone, with an immediate strong peak after 10 minutes and slowly decreasing after 30- and 60-minutes culminating with a decay of the signal after 120 minutes, as reported in the upper panel of Figure 27A and quantification (Figure 27B). In order to assess the effect of IL-1 interception from the microenvironment, we employed the recombinant decoy TRAP IL-1, produced and isolated as detailed in figure 22A, and in material and methods section. TRAP IL-1 is able to sequester IL-1α and IL-1β from the microenvironment[69]. When TRAP IL-1 is employed in combination with EGF and IL-1B we can observe a mild decrease in pEGFR activation, compared to the EGF+IL1 stimulus. Also, the activated form of AKT is lower when compared to EGF in combination with IL-1 as shown in the panel (Figure 28A) and quantification (figure 26B). Overall, these results suggest that IL-1 can increase EGFR phosphorylation and downstream AKT and ERK signals. While, TRAP IL-1 neutralization is able to impair mainly the AKT axis.
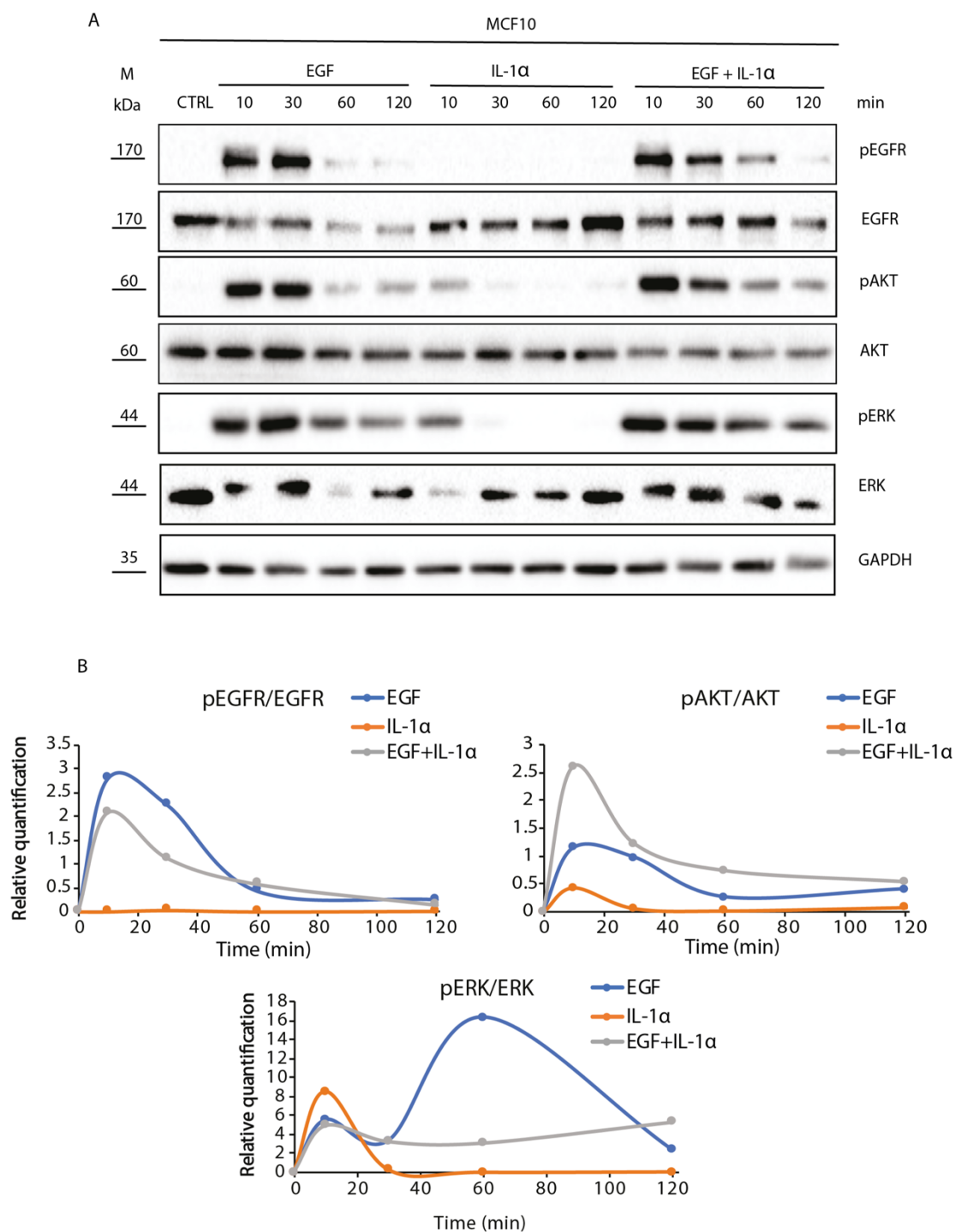
Figure 27: IL-1B stimulation enhance EGFR expression in MCF10 cell line. (**A**) Western blot analysis of pEGFR/EGFR, pAKT/AKT and pERK/ERK levels in MCF10A cell line (time course). At day one 500k cells plated for each condition in DMEM/F12 (50/50) supplemented with 5% of horse serum (HS), EGF (20 ng/m) hydrocortisone (HC, 1 μg/mL) and insulin (INS, 10 μg/mL), At day 2 cells were starved (deprived by HS, HC, and INS) over-night and the day after EGF (10 ng/mL) and IL-1α (10 ng/mL) was added alone or in combination to the medium of growing cells for 10, 30, 60 and 120 minutes. After treatments cells were harvested, total protein extracted and quantified. Monoclonal antibody against total GAPDH served as loading control. (**B**) quantification of pEGFR, EGFR, pAKT, AKT, pERK and ERK by ImageLab software is provided.
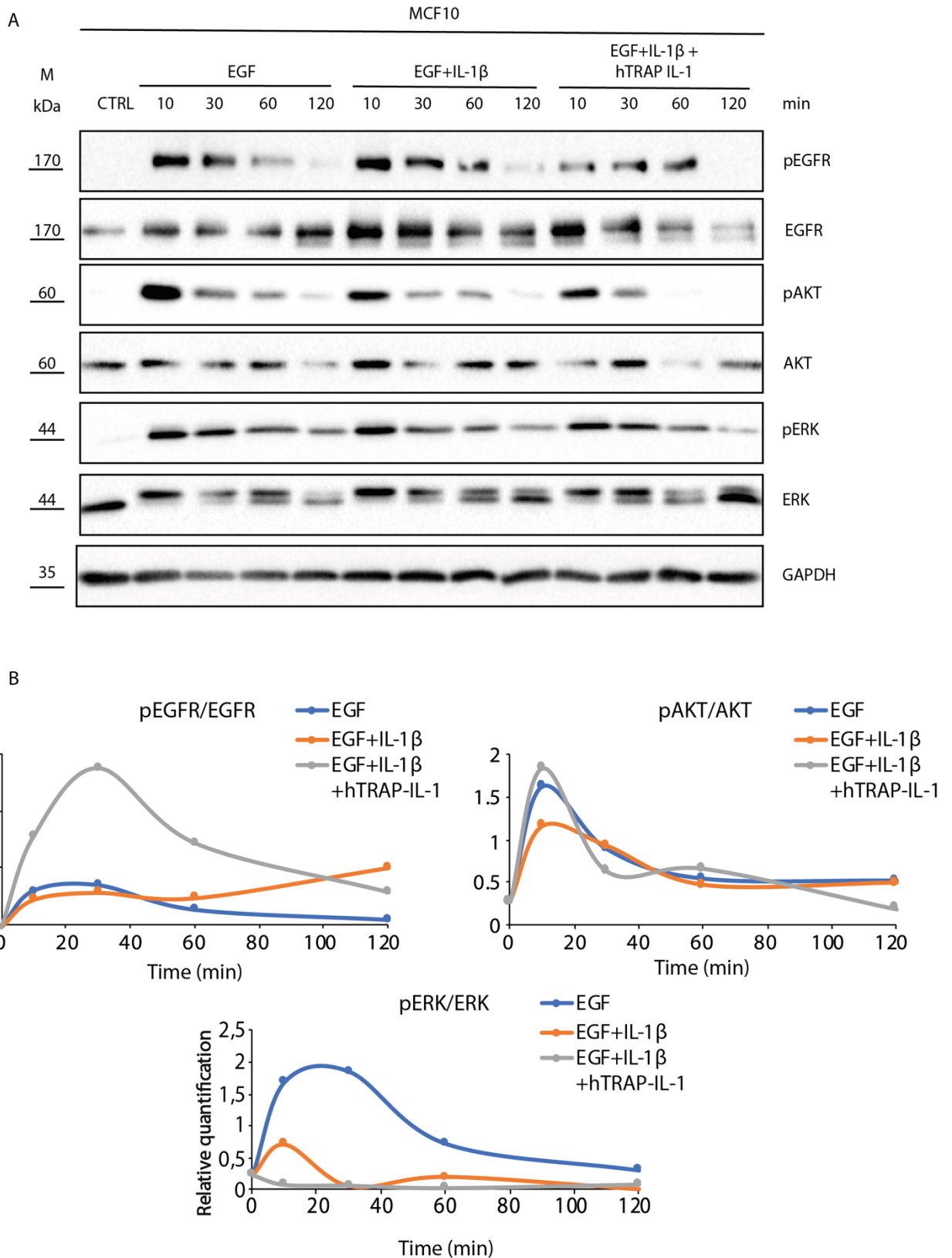
Figure 28: Interception of IL-1 axis restore EGFR level in MCF10 cells. (**A**) EGF (10 ng/mL), EGF + IL-1β (10 ng/mL) and, EGF + IL-1β + hTRAP IL-1 (50 ng/mL) was added to the medium of growing cells for 10, 30, 60 and 120 minutes. Seeding, starvation, protein extraction and quantification (**B**) were performed in the same fashion as reported in Figure 27.

4.16. IL-1 activates EGFR phosphorylation in Caco-2 CTX sensible cell line

In order to unveil the role of IL-1 in the molecular mechanism of CTX-resistance we treated Caco-2 CTX-sensitive cells over a long-time course, up to 48 hours, with CTX alone or in combination with IL-1B. We analyzed the total and activated form of EGFR (EGFR and pEGFR respectively) and IL-1R1 axes. Under CTX treatment, and compared to the control, pEGFR appeared blunted at 12 hours, but with a secondary activation at 24 hours, while both EGFR and IL-1R1 displayed a peak of production after 1 and 12 hours of treatment as displayed in the quantification panel of figure 29 B. On the other hand, Caco-2 cell line treated with CTX in combination with IL-1B displayed a specific pattern. pEGFR and IL-1R1 protein level increased after 30 minutes and 4 hours from the stimulus, by reaching the maximum level at 24 hours, while total EGFR protein remained in general lower compared to CTRL, for the entire time-course, as reported in the quantification panel of figure 29 D. Surprisingly, pEGFR/EGFR ratio under CTX and IL-1B combination, displayed a stronger activation with a peak immediately after 30 minutes and a second and third hit after 4 and 24 hours from stimulus. Overall, these results may suggest that IL-1B was able to nullify the action of CTX on pEGFR downregulation, thus suggesting an escape from the degradative faith.

This effect could be related to an impaired degradation followed by recycling of the receptor to the cell surface, a phenomena well described under TNFα or UV stress [116].
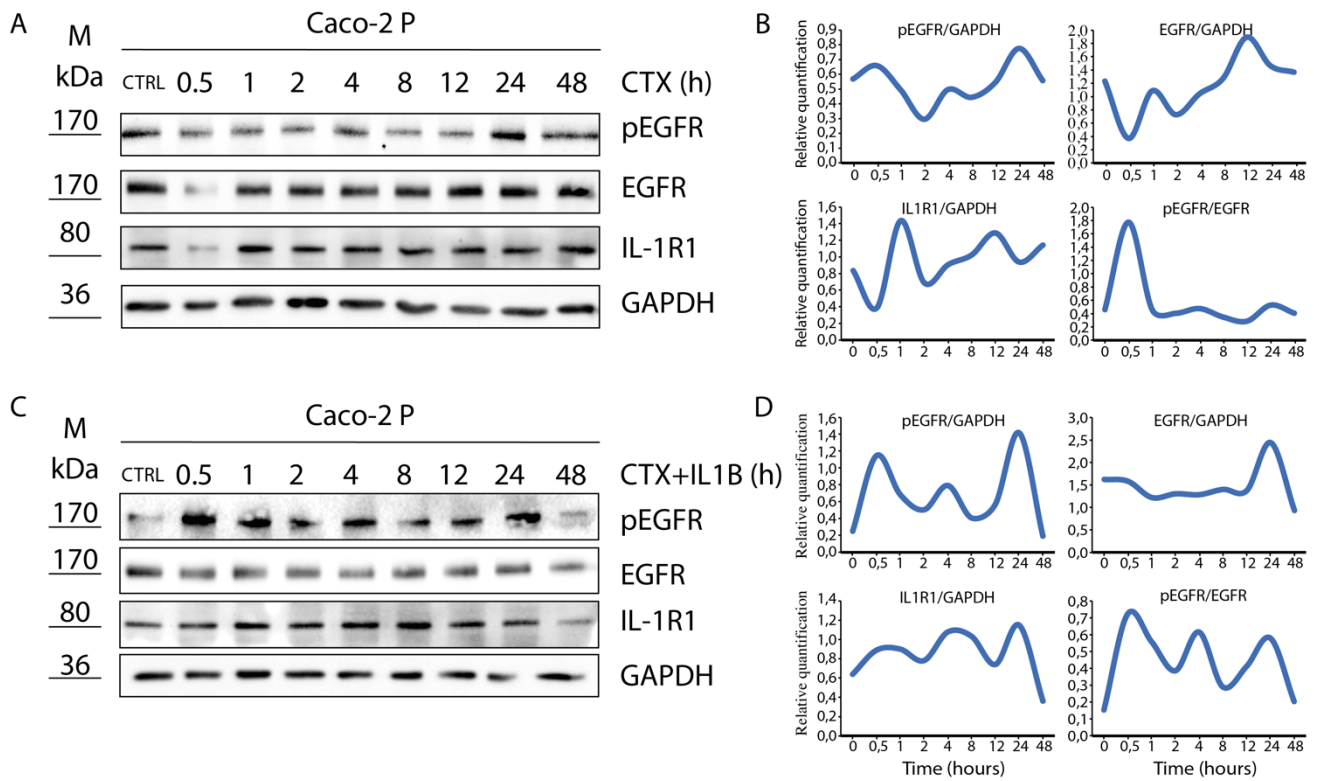
Figure 29: Western blot analysis of pEGFR, EGFR and IL-1R1 levels in Caco-2 cells (Time course). (A and C). At day one, 500k cells were plated for each condition in medium with 10% FBS. At day 2, cells were starved overnight (DMEM 0% FBS) and the day after CTX and/or IL-1B (final concentration 10 ug/mL and 10 ng/mL respectively) were added to the medium of growing cells for 0.5, 1, 2, 4, 8, 12, 24 and 48 hours. After treatment cells were harvested, total proteins extracted and quantified. Monoclonal antibody against total GAPDH served as loading control. Quantification of pEGFR, EGFR and IL-1R1 by Image Lab is provided (**B and D**). GAPDH was used for pEGFR, EGFR and IL-1R1 normalization.

5. Conclusions and discussion

The physiological role of ERBB receptors family is conserved through evolution accounting for vital cellular mechanisms such as development, survival, proliferation and differentiation. In higher eukaryotes, ERBB signal pathway has evolved from a linear pathway to a richly interactive, multi-layered network featured by modularity and redundancy that contribute to the robustness of the signal[1,118]. Monoclonal antibodies blocking EGFR, such as CTX are employed in mCRC patient. Unfortunately, patients develop resistance to the drug leading to therapy failure. Several efforts have been spent to shed light in the molecular mechanisms implicated in the emergence of CTX resistance. The evidence we provided in this thesis, suggest that resistance to EGFR blockade, may depend on activation of an alternative pathway, namely IL-1R1. Indeed, our results suggest that IL-1 derived from the microenvironment has a role in CTX responsiveness, by inducing the overexpression of IL1R1. In line with these findings, the expression level of IL-1 has been correlated with worst prognosis in many types of tumors. More recently, the employment of mAb, MABp1a against IL-1α, displayed a disease control in 18 different tumors types and its efficacy was further confirmed in a phase 3 clinical trial in a cohort of 333 advanced CRC patients[76,119]. Also the employment of Canakinumab, (an anti-IL-1β mAb) significantly reduced the incidence of lung cancer in a cohort of 10.061 patients[120].

We reported that CTX treatment is responsible for IL-1 production[68] *in vitro*. In line, the subset of patients with progressive CRC presented higher levels of IL-1R1 compared to patients responsive to the therapy. Interestingly, IL1R1 abundance was also predictive of survival specifically in CMS1, also known as the immunological subtype, mainly characterized by microsatellite instability[54]. Of note, CMS1 is characterized by increased expression of genes associated with a diffuse immune infiltrate, along with strong activation of immune evasion pathways[55]. Mechanistically, we showed that IL-1R1 stimulus by both IL-1α and IL-1β is responsible for a sustained MAPK and AKT activation, which may interfere with CTX inhibition of the pathways. Indeed, EGFR phosphorylation upon IL-1 stimulus, displayed a persistent activation suggesting a cascade of signaling events ignited by IL-1 treatment. This model suggests a trans regulatory mechanisms mediated by IL-1

pathway activation that entail EGFR receptor phosphorylation, probably as evasion from the degradative fate. These data are in line with a model of recycling of EGFR consequent to cytokine stimulus as well as UV and tumor necrosis factor [116]. Thus, we suggested a Cetuximab resistance-working model in mCRC patients (Fig 30). Furthermore, it may be closely linked to another important positive late feedback mechanism given by the autocrine loop, mediated by the MAPK pathway, that sustains growth factors signals such as tumor necrosis factor, IL-1α, and converts a transient stimulus into a sustained signal [123,124].

Stemming from these observations, we developed a working strategy combining EGFR and IL-1 neutralization *in vivo,* to overcome the emergence of CTX resistance. In order to test this hypothesis, we developed the MC38 cell line engineered with murine EGFR, assuring a complete immunological compatibility with the C57/BL6 murine model. In line, we developed a murine version of TRAP IL-1. In the next future, we plan to test our hypothesis by combining murine TRAP IL-1 with anti-EGFR antibody *in vivo.* We expect that interception of IL-1R1 axis combined with EGFR blockade will have a beneficial effect in terms of reduced tumor growth and metastasis formation.
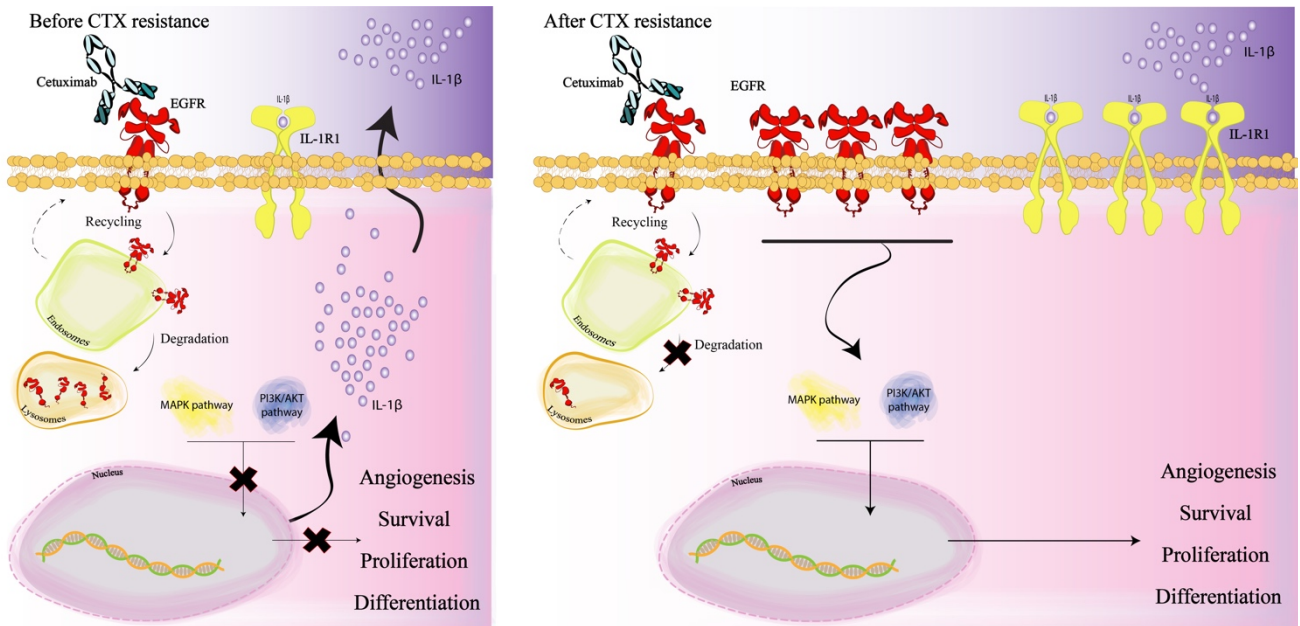
Figure 30: Cetuximab resistance-working model in mCRC patients. We proposed that upon cetuximab treatment the emergence of ressitance is sustained by activation of IL-1R1 alternative pathway. Our data suggest that in a context of CTX sensible cells, after CTX treatment (on the left) EGFR is instated to the degradative fate dampening proliferation and survival paralleled by increased expression of IL-1 from the tumor itself. The autocrine and paracrine action of IL-1 in the tumor microenviroment suggest a trans regolatory mechanisms mediated by IL-1 that entail EGFR phosphorylation and evasion from the degradative fate (on the right). This in turn feed a positive feedback loop that lead to proliferation, survival, differentiation and epithelial-mesenchimal transition (EMT).

6. Bibliography

1. Citri, A. & Yarden, Y. EGF–ERBB signalling: towards the systems level. *Nat. Rev. Mol. Cell Biol.* **7**, 505 (2006).

2. Yarden, Y. & Sliwkowski. Untangling the ErbB signaling network. *Nat. Rev. Mol. Cell Biol.* **2**, 127–137 (2001).

3. Roskoski, R. The ErbB/HER family of protein-tyrosine kinases and cancer. *Pharmacological Research* (2014) doi:10.1016/j.phrs.2013.11.002.

4. Riese, D. J. & Stern, D. F. Specificity within the EGF family/ErbB receptor family signaling network. *BioEssays* (1998) doi:10.1002/(SICI)1521-1878(199801)20:1<41::AID-BIES7>3.0.CO;2-V.

5. Klapper, L. N. *et al.* The erbB-2/HER2 oncoprotein of human carcinomas may function solely as a shared coreceptor for multiple stroma-derived growth factors. *Proc. Natl. Acad. Sci. U. S. A.* (1999) doi:10.1073/pnas.96.9.4995.

6. Guy, P. M., Platko, J. V., Cantley, L. C., Cerione, R. A. & Carraway, K. L. Insect cell-expressed p180(erbB3) possesses an impaired tyrosine kinase activity. *Proc. Natl. Acad. Sci. U. S. A.* (1994) doi:10.1073/pnas.91.17.8132.

7. Tzahar, E. *et al.* A hierarchical network of interreceptor interactions determines signal transduction by Neu differentiation factor/neuregulin and epidermal growth factor. *Mol. Cell. Biol.* (1996) doi:10.1128/mcb.16.10.5276.

8. Worthylake, R., Opresko, L. K. & Wiley, H. S. ErbB-2 amplification inhibits down-regulation and induces constitutive activation of both ErbB-2 and epidermal growth factor receptors. *J. Biol. Chem.* (1999) doi:10.1074/jbc.274.13.8865.

9. Waterman, H., Alroy, I., Strano, S., Seger, R. & Yarden, Y. The C-terminus of the kinase-defective neuregulin receptor ErbB-3 confers mitogenic superiority and dictates endocytic routing. *EMBO J.* (1999) doi:10.1093/emboj/18.12.3348.

10. Ni, C. Y., Murphy, M. P., Golde, T. E. & Carpenter, G. γ-secretase cleavage and nuclear locatization of ErbB-4 receptor tyrosine kinase. *Science (80-.).* (2001) doi:10.1126/science.1065412.

11. Riese, D. J., van Raaij, T. M., Plowman, G. D., Andrews, G. C. & Stern, D. F. The cellular response to neuregulins is governed by complex interactions of the erbB receptor family. *Mol. Cell. Biol.* (1995) doi:10.1128/mcb.15.10.5770.

12. Pinkas-Kramarski, R. *et al.* Diversification of Neu differentiation factor and epidermal growth factor signaling by combinatorial receptor interactions. *EMBO J.* (1996) doi:10.1002/j.1460-2075.1996.tb00603.x.

13. Amit, I., Wides, R. & Yarden, Y. Evolvable signaling networks of receptor tyrosine kinases: Relevance of robustness to malignancy and to cancer therapy. *Molecular Systems Biology* (2007) doi:10.1038/msb4100195.

14. Kitano, H. Biological robustness. *Nature Reviews Genetics* (2004) doi:10.1038/nrg1471.

15. Stelling, J., Sauer, U., Szallasi, Z., Doyle, F. J. & Doyle, J. Robustness of cellular functions. *Cell* (2004) doi:10.1016/j.cell.2004.09.008.

16. Schäfer, B., Gschwind, A. & Ullrich, A. Multiple G-protein-coupled receptor signals converge on the epidermal growth factor receptor to promote migration and invasion. *Oncogene* (2004) doi:10.1038/sj.onc.1207278.

17.   Haj, F. G., Verveer, P. J., Squire, A., Neel, B. G. & Bastiaens, P. I. H. Imaging sites of receptor dephosphorylation by PTP1B on the surface of the endoplasmic reticulum. *Science (80-.).* (2002) doi:10.1126/science.1067566.

18.   Berset, T. A., Hoier, E. F. & Hajnal, A. The C. elegans homolog of the mammalian tumor suppressor Dep-1/Scc1 inhibits EGFR signaling to regulate binary cell fate decisions. *Genes Dev.* (2005) doi:10.1101/gad.333505.

19.   Kario, E. *et al.* Suppressors of cytokine signaling 4 and 5 regulate epidermal growth factor receptor signaling. *J. Biol. Chem.* (2005) doi:10.1074/jbc.M408575200.

20.   Anastasi, S. *et al.* Feedback inhibition by RALT controls signal output by the ErbB network. *Oncogene* (2003) doi:10.1038/sj.onc.1206516.

21.   Laederich, M. B. *et al.* The leucine-rich repeat protein LRIG1 is a negative regulator of ErbB family receptor tyrosine kinases. *J. Biol. Chem.* (2004) doi:10.1074/jbc.M409703200.

22.   Gur, G. *et al.* LRIG1 restricts growth factor signaling by enhancing receptor ubiquitylation and degradation. *EMBO J.* (2004) doi:10.1038/sj.emboj.7600342.

23.   Batzer, A. G., Rotin, D., Ureña, J. M., Skolnik, E. Y. & Schlessinger, J. Hierarchy of binding sites for Grb2 and Shc on the epidermal growth factor receptor. *Mol. Cell. Biol.* (1994) doi:10.1128/mcb.14.8.5192.

24.   Okutani, T. *et al.* Grb2/Ash binds directly to tyrosines 1068 and 1086 and indirectly to tyrosine 1148 of activated human epidermal growth factor receptors in intact cells. *J. Biol. Chem.* (1994).

25.   Citri, A. *et al.* Hsp90 restrains ErbB-2/HER2 signalling by limiting heterodimer formation. *EMBO Rep.* (2004) doi:10.1038/sj.embor.7400300.

26.   Alao, J. P. The regulation of cyclin D1 degradation: Roles in cancer development and the potential for therapeutic invention. *Molecular Cancer* (2007) doi:10.1186/1476-4598-6-24.

27.   Freeman, M. Feedback control of intercellular signalling in development. *Nature* (2000) doi:10.1038/35042500.

28.   Yonesaka, K. *et al.* Activation of ERBB2 signaling causes resistance to the EGFR-directed therapeutic antibody cetuximab. *Sci. Transl. Med.* (2011) doi:10.1126/scitranslmed.3002442.

29.   Schulze, A., Lehmann, K., Jefferies, H. B. J., McMahon, M. & Downward, J. Analysis of the transcriptional program induced by Raf in epithelial cells. *Genes Dev.* (2001) doi:10.1101/gad.191101.

30.   Clague, M. J. & Urbé, S. Endocytosis: the DUB version. *Trends in Cell Biology* (2006) doi:10.1016/j.tcb.2006.09.002.

31.   Avraham, R. & Yarden, Y. Feedback regulation of EGFR signalling: Decision making by early and delayed loops. *Nature Reviews Molecular Cell Biology* (2011) doi:10.1038/nrm3048.

32.   Ferlay J, Soerjomataram I, Ervik M, Dikshit R, Eser S, Mathers C, Rebelo M, Parkin DM, Forman D, Bray, F. GLOBOCAN 2012 v1.0, Cancer Incidence and Mortality Worldwide: *IARC CancerBase No. 11 [Internet]. Lyon, Fr. Int. Agency Res. Cancer; 2013.* (2013) doi:https://doi.org/10.1002/ijc.29210.

33.   Sobani, Z. A., Sawant, A., Jafri, M., Correa, A. K. & Sahin, I. H. Oncogenic

fingerprint of epidermal growth factor receptor pathway and emerging epidermal growth factor receptor blockade resistance in colorectal cancer. *World Journal of Clinical Oncology* (2016) doi:10.5306/wjco.v7.i5.340.

34. Dienstmann, R. *et al.* Consensus molecular subtypes and the evolution of precision medicine in colorectal cancer. *Nature Reviews Cancer* (2017) doi:10.1038/nrc.2016.126.

35. Kolligs, F. T. Diagnostics and epidemiology of colorectal cancer. *Visceral Medicine* (2016) doi:10.1159/000446488.

36. Cremolini, C. *et al.* First-line chemotherapy for mCRC-a review and evidence-based algorithm. *Nature Reviews Clinical Oncology* (2015) doi:10.1038/nrclinonc.2015.129.

37. Haggar, F. A. & Boushey, R. P. Colorectal cancer epidemiology: Incidence, mortality, survival, and risk factors. *Clin. Colon Rectal Surg.* (2009) doi:10.1055/s-0029-1242458.

38. Müller, M. F., Ibrahim, A. E. K. & Arends, M. J. Molecular pathological classification of colorectal cancer. *Virchows Archiv* vol. 469 125–134 (2016).

39. Takayama, T., Miyanishi, K., Hayashi, T., Sato, Y. & Niitsu, Y. Colorectal cancer: genetics of development and metastasis. *Journal of gastroenterology* (2006) doi:10.1007/s00535-006-1801-6.

40. Jasperson, K. W., Tuohy, T. M., Neklason, D. W. & Burt, R. W. Hereditary and familial colon cancer. *Gastroenterology* **138**, 2044–2058 (2010).

41. De Sousa E Melo, F. *et al.* Poor-prognosis colon cancer is defined by a molecularly distinct subtype and develops from serrated precursor lesions. *Nat. Med.* **19**, 614–618 (2013).

42. Sadanandam, A. *et al.* A colorectal cancer classification system that associates cellular phenotype and responses to therapy. *Nat. Med.* (2013) doi:10.1038/nm.3175.

43. Marisa, L. *et al.* Gene Expression Classification of Colon Cancer into Molecular Subtypes: Characterization, Validation, and Prognostic Value. *PLoS Med.* (2013) doi:10.1371/journal.pmed.1001453.

44. Roepman, P. *et al.* Colorectal cancer intrinsic subtypes predict chemotherapy benefit, deficient mismatch repair and epithelial-to-mesenchymal transition. *Int. J. Cancer* (2014) doi:10.1002/ijc.28387.

45. Guinney, J. *et al.* The consensus molecular subtypes of colorectal cancer. *Nat. Med.* **21**, 1350–1356 (2015).

46. Müller, M. F., Ibrahim, A. E. K. & Arends, M. J. Molecular pathological classification of colorectal cancer. *Virchows Archiv* (2016) doi:10.1007/s00428-016-1956-3.

47. Poston, G. J. *et al.* Urgent need for a new staging system in advanced colorectal cancer. *Journal of Clinical Oncology* (2008) doi:10.1200/JCO.2008.17.6453.

48. Hammond, W. A., Swaika, A. & Mody, K. Pharmacologic resistance in colorectal cancer: A review. *Therapeutic Advances in Medical Oncology* (2016) doi:10.1177/1758834015614530.

49. Jonker, D. J. *et al.* Cetuximab for the Treatment of Colorectal Cancer. *N. Engl. J. Med.* **357**, 2040–2048 (2007).

50. Bertotti, A. & Sassi, F. Molecular pathways: Sensitivity and resistance to Anti-EGFR antibodies. *Clin. Cancer Res.* (2015) doi:10.1158/1078-0432.CCR-14-0848.

51. Jürgensmeier, J. M. *et al.* Prognostic and predictive value of VEGF, sVEGFR-2 and CEA in mCRC studies comparing cediranib, bevacizumab and chemotherapy. *Br. J.*

Cancer (2013) doi:10.1038/bjc.2013.79.

52. Tobin, N. P., Foukakis, T., De Petris, L. & Bergh, J. The importance of molecular markers for diagnosis and selection of targeted treatments in patients with cancer. *J. Intern. Med.* **278**, 545–570 (2015).

53. Sato, J. D. *et al.* Biological effects in vitro of monoclonal antibodies to human epidermal growth factor receptors. *Mol. Biol. Med.* (1983).

54. Bardelli, A. & Siena, S. Molecular mechanisms of resistance to cetuximab and panitumumab in colorectal cancer. *Journal of Clinical Oncology* (2010) doi:10.1200/JCO.2009.24.6116.

55. Chung, K. Y. *et al.* Cetuximab shows activity in colorectal cancer patients with tumors that do not express the epidermal growth factor receptor by immunohistochemistry. *J. Clin. Oncol.* (2005) doi:10.1200/JCO.2005.08.037.

56. Moroni, M. *et al.* Gene copy number for epidermal growth factor receptor (EGFR) and clinical response to antiEGFR treatment in colorectal cancer: A cohort study. *Lancet Oncol.* (2005) doi:10.1016/S1470-2045(05)70102-9.

57. Lièvre, A. *et al.* KRAS mutation status is predictive of response to cetuximab therapy in colorectal cancer. *Cancer Res.* (2006) doi:10.1158/0008-5472.CAN-06-0191.

58. Karapetis, C. S. *et al.* K-ras Mutations and Benefit from Cetuximab in Advanced Colorectal Cancer . *N. Engl. J. Med.* (2008) doi:10.1056/nejmoa0804385.

59. Di Nicolantonio, F. *et al.* Wild-type BRAF is required for response to panitumumab or cetuximab in metastatic colorectal cancer. *J. Clin. Oncol.* (2008) doi:10.1200/JCO.2008.18.0786.

60. Frattini, M. *et al.* PTEN loss of expression predicts cetuximab efficacy in metastatic colorectal cancer patients. *Br. J. Cancer* (2007) doi:10.1038/sj.bjc.6604009.

61. Bardelli, A. & Siena, S. Molecular mechanisms of resistance to cetuximab and panitumumab in colorectal cancer. *Journal of Clinical Oncology* (2010) doi:10.1200/JCO.2009.24.6116.

62. Sartore-Bianchi, A. *et al.* Multi-determinants analysis of molecular alterations for predicting clinical benefit to EGFR-targeted monoclonal antibodies in colorectal cancer. *PLoS One* (2009) doi:10.1371/journal.pone.0007287.

63. Cunningham, D. *et al.* Cetuximab monotherapy and cetuximab plus irinotecan in irinotecan- refractory metastatic colorectal cancer. *N. Engl. J. Med.* (2004) doi:10.1056/NEJMoa033025.

64. Bertotti, A. *et al.* A molecularly annotated platform of patient- derived xenografts ('xenopatients') identifies HER2 as an effective therapeutic target in cetuximab-resistant colorectal cancer. *Cancer Discov.* (2011) doi:10.1158/2159-8290.CD-11-0109.

65. Bardelli, A. *et al.* Amplification of the MET receptor drives resistance to anti-EGFR therapies in colorectal cancer. *Cancer Discov.* (2013) doi:10.1158/2159-8290.CD-12-0558.

66. Misale, S. *et al.* Emergence of KRAS mutations and acquired resistance to anti-EGFR therapy in colorectal cancer. *Nature* (2012) doi:10.1038/nature11156.

67. Hobor, S. *et al.* TGFα and amphiregulin paracrine network promotes resistance to EGFR blockade in colorectal cancer cells. *Clin. Cancer Res.* (2014) doi:10.1158/1078-0432.CCR-14-0774.

68. Gelfo, V. *et al.* A module of inflammatory cytokines defines resistance of colorectal cancer to EGFR inhibitors. *Oncotarget* (2016) doi:10.18632/oncotarget.12354.

69. Gelfo, V. *et al.* A Novel Role for the Interleukin-1 Receptor Axis in Resistance to Anti-EGFR Therapy. *Cancers (Basel).* (2018) doi:10.3390/cancers10100355.

70. Mantovani, A., Allavena, P., Sica, A. & Balkwill, F. Cancer-related inflammation. *Nature* (2008) doi:10.1038/nature07205.

71. Balkwill, F. R. & Mantovani, A. Cancer-related inflammation: Common themes and therapeutic opportunities. *Seminars in Cancer Biology* (2012) doi:10.1016/j.semcancer.2011.12.005.

72. Dinarello, C. A. Why not treat human cancer with interleukin-1 blockade? *Cancer and Metastasis Reviews* (2010) doi:10.1007/s10555-010-9229-0.

73. Apte, R. N. *et al.* The involvement of IL-1 in tumorigenesis, tumor invasiveness, metastasis and tumor-host interactions. *Cancer and Metastasis Reviews* (2006) doi:10.1007/s10555-006-9004-4.

74. Bent, R., Moll, L., Grabbe, S. & Bros, M. Interleukin-1 beta—A friend or foe in malignancies? *International Journal of Molecular Sciences* (2018) doi:10.3390/ijms19082155.

75. Malik, A. & Kanneganti, T. D. Function and regulation of IL-1α in inflammatory diseases and cancer. *Immunological Reviews* (2018) doi:10.1111/imr.12615.

76. Hickish, T. *et al.* MABp1 as a novel antibody treatment for advanced colorectal cancer: a randomised, double-blind, placebo-controlled, phase 3 study. *Lancet Oncol.* (2017) doi:10.1016/S1470-2045(17)30006-2.

77. Ridker, P. M. *et al.* Effect of interleukin-1β inhibition with canakinumab on incident lung cancer in patients with atherosclerosis: exploratory results from a randomised, double-blind, placebo-controlled trial. *Lancet (London, England)* **390**, 1833–1842 (2017).

78. Kaplanov, I. *et al.* Blocking IL-1β reverses the immunosuppression in mouse breast cancer and synergizes with anti–PD-1 for tumor abrogation. *Proc. Natl. Acad. Sci.* (2019) doi:10.1073/pnas.1812266115.

79. Das, S., Shapiro, B., Vucic, E. A., Vogt, S. & Bar-Sagi, D. Tumor Cell-Derived IL1β Promotes Desmoplasia and Immune Suppression in Pancreatic Cancer. *Cancer Res.* (2020) doi:10.1158/0008-5472.CAN-19-2080.

80. Dinarello, C. A. Interleukin-1 in the pathogenesis and treatment of inflammatory diseases. *Blood* **117**, 3720–3732 (2011).

81. Garlanda, C., Dinarello, C. A. & Mantovani, A. The Interleukin-1 Family: Back to the Future. *Immunity* (2013) doi:10.1016/j.immuni.2013.11.010.

82. Dinarello, C. A. Overview of the IL-1 family in innate inflammation and acquired immunity. *Immunological Reviews* (2018) doi:10.1111/imr.12621.

83. Voronov, E. *et al.* Unique versus redundant functions of IL-1α and IL-1β in the tumor microenvironment. *Frontiers in Immunology* (2013) doi:10.3389/fimmu.2013.00177.

84. Nicolini, A., Ferrari, P., Rossi, G. & Carpi, A. Tumour growth and immune evasion as targets for a new strategy in advanced cancer. *Endocr. Relat. Cancer* (2018) doi:10.1530/ERC-18-0142.

85. Cohen, I. *et al.* Differential release of chromatin-bound IL-1α discriminates between necrotic and apoptotic cell death by the ability to induce sterile inflammation. *Proc. Natl. Acad. Sci. U. S. A.* (2010) doi:10.1073/pnas.0915018107.

86. Werman, A. *et al.* The precursor form of IL-1α is an intracrine proinflammatory activator of transcription. *Proc. Natl. Acad. Sci. U. S. A.* (2004) doi:10.1073/pnas.0308705101.

87. Griffin, B. D. & Moynagh, P. N. In vivo binding of NF-κB to the IκBβ promoter is insufficient for transcriptional activation. *Biochem. J.* (2006) doi:10.1042/BJ20060786.

88. Saccani, S., Pantano, S. & Natoli, G. p38-dependent marking of inflammatory genes for increased NF-κB recruitment. *Nat. Immunol.* (2002) doi:10.1038/ni748.

89. Hoffmann, E., Dittrich-Breiholz, O., Holtmann, H. & Kracht, M. Multiple control of interleukin-8 gene expression. *J. Leukoc. Biol.* (2002) doi:10.1189/jlb.1106655.

90. Winzen, R. *et al.* Functional Analysis of KSRP Interaction with the AU-Rich Element of Interleukin-8 and Identification of Inflammatory mRNA Targets. *Mol. Cell. Biol.* (2007) doi:10.1128/mcb.01493-07.

91. Weber, A., Wasiliew, P. & Kracht, M. Interleukin-1 (IL-1) Pathway. *Sci. Signal.* **3**, 1–7 (2010).

92. Sharma, S. V & Settleman, J. Oncogene addiction: setting the stage for molecularly targeted cancer therapy. *Genes Dev.* **21**, 3214–3231 (2007).

93. Lewis, A. M., Varghese, S., Xu, H. & Alexander, H. R. Interleukin-1 and cancer progression: the emerging role of interleukin-1 receptor antagonist as a novel therapeutic agent in cancer treatment. *J. Transl. Med.* **4**, 48 (2006).

94. Krelin, Y. *et al.* Interleukin-1β-driven inflammation promotes the development and invasiveness of chemical carcinogen-induced tumors. *Cancer Res.* (2007) doi:10.1158/0008-5472.CAN-06-2956.

95. Voronov, E. *et al.* IL-1 is required for tumor invasiveness and angiogenesis. *Proc. Natl. Acad. Sci.* (2003) doi:10.1073/pnas.0437939100.

96. Vidal-Vanaclocha, F., Amézaga, C., Asumendi, A., Kaplanski, G. & Dinarello, C. A. Interleukin-1 Receptor Blockade Reduces the Number and Size of Murine B16 Melanoma Hepatic Metastases. *Cancer Res.* (1994).

97. Kedmi, M. *et al.* EGF induces microRNAs that target suppressors of cell migration: miR-15b targets MTSS1 in breast cancer. *Sci. Signal.* **8**, ra29–ra29 (2015).

98. Lindzen, M. *et al.* A recombinant decoy comprising EGFR and ErbB-4 inhibits tumor growth and metastasis. *Oncogene* (2012) doi:10.1038/onc.2011.518.

99. Solmi, R. *et al.* Displayed correlation between gene expression profiles and submicroscopic alterations in response to cetuximab, gefitinib and EGF in human colon cancer cell lines. *BMC Cancer* **8**, 227 (2008).

100. Straussman, R. *et al.* Tumour micro-environment elicits innate resistance to RAF inhibitors through HGF secretion. *Nature* **487**, 500–4 (2012).

101. Lee, H. J. *et al.* Drug resistance via feedback activation of stat3 in oncogene-addicted cancer cells. *Cancer Cell* (2014) doi:10.1016/j.ccr.2014.05.019.

102. Trusolino, L. & Bertotti, A. Compensatory pathways in oncogenic kinase signaling and resistance to targeted therapies: Six degrees of separation. *Cancer Discov.* **2**, 876–880 (2012).

103. Hobor, S. *et al.* TGFα and amphiregulin paracrine network promotes resistance to EGFR blockade in colorectal cancer cells. *Clin. Cancer Res.* (2014) doi:10.1158/1078-0432.CCR-14-0774.

104. Troiani, T. *et al.* Increased TGF-α as a mechanism of acquired resistance to the anti-EGFR inhibitor cetuximab through EGFR-MET interaction and activation of MET signaling in colon cancer cells. *Clin. Cancer Res.* (2013) doi:10.1158/1078-0432.CCR-13-0423.

105. Frosi, Y. *et al.* A two-tiered mechanism of EGFR inhibition by RALT/MIG6 via kinase suppression and receptor degradation. *J. Cell Biol.* (2010) doi:10.1083/jcb.201002032.

106. Powell, A. E. *et al.* The pan-ErbB negative regulator lrig1 is an intestinal stem cell marker that functions as a tumor suppressor. *Cell* (2012) doi:10.1016/j.cell.2012.02.042.

107. Boumahdi, S. *et al.* SOX2 controls tumour initiation and cancer stem-cell functions in squamous-cell carcinoma. *Nature* **511**, 246–253 (2014).

108. Ciardiello, F. & Normanno, N. HER2 signaling and resistance to the anti-EGFR monoclonal antibody cetuximab: A further step toward personalized medicine for patients with colorectal cancer. *Cancer Discov.* **1**, 472–474 (2011).

109. Mancini, M. *et al.* Combining three antibodies nullifies feedback-mediated resistance to erlotinib in lung cancer. *Sci. Signal.* **8**, ra53–ra53 (2015).

110. Bertotti, A. *et al.* A molecularly annotated platform of patient- derived xenografts ('xenopatients') identifies HER2 as an effective therapeutic target in cetuximab-resistant colorectal cancer. *Cancer Discov.* (2011) doi:10.1158/2159-8290.CD-11-0109.

111. Vallböhmer, D. *et al.* Molecular determinants of cetuximab efficacy. *J. Clin. Oncol.* **23**, 3536–3544 (2005).

112. Stanam, A. *et al.* Interleukin-1 blockade overcomes erlotinib resistance in head and neck squamous cell carcinoma. *Oncotarget* **7**, 76087–76100 (2016).

113. Khambata-Ford, S. *et al.* Expression of epiregulin and amphiregulin and K-ras mutation status predict disease control in metastatic colorectal cancer patients treated with cetuximab. *J. Clin. Oncol.* (2007) doi:10.1200/JCO.2006.10.5437.

114. Jaffe, A. B., Kaji, N., Durgan, J. & Hall, A. Cdc42 controls spindle orientation to position the apical surface during epithelial morphogenesis. *J. Cell Biol.* **183**, 625–633 (2008).

115. Li, C. *et al.* Three-dimensional culture system identifies a new mode of cetuximab resistance and disease-relevant genes in colorectal cancer. *Proc. Natl. Acad. Sci. U. S. A.* **114**, E2852–E2861 (2017).

116. Zwang, Y. & Yarden, Y. p38 MAP kinase mediates stress-induced internalization of EGFR: implications for cancer chemotherapy. *EMBO J.* **25**, 4195–206 (2006).

117. Sztupinszki, Z. & Gyorffy, B. Colon cancer subtypes: Concordance, effect on survival and selection of the most representative preclinical models. *Sci. Rep.* **6**, (2016).

118. Yarden, Y. & Pines, G. The ERBB network: at last, cancer therapy meets systems biology. *Nat. Rev. Cancer* **12**, 553–563 (2012).

119. Hong, D. S. *et al.* MABp1, a first-in-class true human antibody targeting interleukin-1α in refractory cancers: An open-label, phase 1 dose-escalation and expansion study. *Lancet Oncol.* **15**, 656–666 (2014).

120. Ridker, P. M. *et al.* Effect of interleukin-1β inhibition with canakinumab on incident lung cancer in patients with atherosclerosis: exploratory results from a randomised, double-blind, placebo-controlled trial. *Lancet* (2017) doi:10.1016/S0140-6736(17)32247-X.

121. Dienstmann, R. *et al.* Consensus molecular subtypes and the evolution of precision medicine in colorectal cancer. *Nat. Rev. Cancer* (2017) doi:10.1038/nrc.2016.126.

122. Fessler, E. & Medema, J. P. Colorectal Cancer Subtypes: Developmental Origin and Microenvironmental Regulation. *Trends in Cancer* vol. 2 505–518 (2016).

123. Janes, K. A. *et al.* The Response of Human Epithelial Cells to TNF Involves an Inducible Autocrine Cascade. *Cell* **124**, 1225–1239 (2006).

124. Avraham, R. & Yarden, Y. Feedback regulation of EGFR signalling: decision making by early and delayed loops. *Nat. Rev. Mol. Cell Biol.* **12**, 104–117 (2011).

125. Tabernero, J. The role of VEGF and EGFR inhibition: Implications for combining Anti-VEGF and Anti-EGFR Agents. *Molecular Cancer Research* (2007) doi:10.1158/1541-7786.MCR-06-0404.